Flexural testing of rectangular reinforced concrete beams with extruded plastic coarse aggregate replacement

by

Cameron Hicks

B.S., Kansas State University, 2024

A THESIS

submitted in partial fulfillment of the requirements for the degree

MASTER OF SCIENCE

GE Johnson Department of Architectural Engineering and Construction Science
Carl R. Ice College of Engineering

KANSAS STATE UNIVERSITY
Manhattan, Kansas

2024

Approved by:

Major Professor
Kimberly Waggle Kramer P.E., S.E., Ph.D

Copyright

Abstract

Natural aggregates, used in reinforced concrete, are globally recognized as the most valuable non-fuel mineral commodity (Langer, 2002). As the global population continues to rise, the demand for concrete also increases, consequently elevating the need for aggregates. Natural aggregates such as sand, gravel, and crushed stone have passed the rate of renewal, and an aggregate replacement is necessary to meet the ever-increasing demand. Recycled plastic is a possible option for aggregate replacement in reinforced concrete. The utilization of recycled plastics serves the dual purpose of extracting plastic waste from the waste stream and partially replaces the need for natural aggregates.

This research examines the effects of partial coarse aggregate replacement on reinforced concrete beams in four-point bending using a recycled plastic coarse aggregate called Plazrok by Enviroplaz. The reinforced concrete beams had a six-inch (152 mm) by 10-inch (254 mm) cross-section and a clear span of 12 feet (3,658 mm) between supports. Three mix designs were tested including a control, 15 percent, and 30 percent replacement by volume with Plazrok. Prior to the reinforced concrete beam tests, fresh (plastic state) and mechanical property tests such as density, slump, compression, tensile splitting, modulus of rupture, and reinforcement yield strength tests were conducted.

Subsequently, the reinforced concrete beams were subjected to testing, and data on load-deflection were collected using an actuator and linear variable differential transformers (LVDT) along the beam. Crack propagation was monitored and documented throughout the tests. Utilizing the load-deflection data, various parameters including stiffness, modulus of elasticity (MOE), first crack, moment capacity at reinforcement yield, and ultimate strength were

determined. Instantaneous deflection from experimental data was compared with deflection equations from mechanics of materials, specifically employing Bischoff's (2005) and Branson's (1965) effective moment of inertia equations. The objective was to confirm the validity of these equations for lightly reinforced concrete members with partial coarse aggregate replacement with Plazrok. Finally, the experimental flexural capacities were compared to nominal moment capacity equations developed based on the straight-line, parabolic stress, and equivalent stress theories.

The results obtained from the reinforced concrete beam testing displayed promising results for partial coarse aggregate replacement for the 15 and 30 percent replacement members. At 15 and 30 percent replacement by volume there was no significant decrease in member capacity and underwent similar flexural behavior to the control members with a 6.9 and 28.5 percent increase in deflection at failure respectively. ACI 318-19 design method for flexural members was shown to be effective by underestimating the member strength up to 30 percent replacement. A 30 percent replacement was found to reduce stiffness and increase deflection significantly that would pose additional challenges in design.

Table of Contents

List of Figures

List of Tables

List of Equations

Notations

A_c = cross-sectional area, mm^2 (in^2)

A_g = gross area of the cross-section, in^2 (mm^2)

$A_{s,min}$ = minimum tensile steel area, in^2 (mm^2)

A_s = area of tension reinforcement, in^2 (mm^2)

a = depth of equivalent rectangular stress block, in (mm)

b, b_w = width of specimen, in (mm)

C = total compressive force, kip (kN)

D, d = diameter of cylindrical specimen, in (mm)

d = depth from extreme compression fiber to centroid of tension steel, in (mm)

E_c, E = modulus of elasticity of concrete, psi (MPa)

E_{cm} = secant modulus of elasticity of concrete, MPa

E_s = modulus of elasticity of steel, psi (MPa)

F = maximum load, N (lbf)

f_c = concrete compressive strength, psi (MPa)

$f_{c,replacement}$ = compressive strength based on plastic aggregate replacement, psi (MPa)

f_c' = specified (design) compressive strength of concrete, psi (MPa)

f_{ck} = specified compressive strength of concrete, MPa

f_{cm} = mean value of concrete cylinder compressive strength, MPa

f_{cr} = modulus of rupture of concrete, MPa

f_r = modulus of rupture of concrete, psi (MPa)

f_s = modulus of rupture of control mix, psi (MPa)

$f_{s,replacement}$ = modulus of rupture based on plastic aggregate replacement, psi (MPa)

f_t = tensile strength of control mix, psi (MPa)

$f_{t,replacement}$ = tensile strength based on plastic aggregate replacement, psi (MPa)

f_y = yield strength of reinforcement, psi (MPa)

h = height of the beam, in (mm)

I_{cr} = moment of inertia of cracked transformed section

I_e = effective moment of inertia of section

I_g = gross moment of inertia of section

I_t = uncracked transformed moment of inertia, in^4 (mm^4)

jd = internal lever arm between the compression and tensile forces, in (mm)

k = ratio of distance from extreme compressive fiber to neutral axis to the depth d, in (mm)

k_1, k_2, k_3 = coefficients related to magnitude and position of internal compressive force in concrete compression zone

L = span length, mm (in)

l = length, mm (in)

M = bending moment, k-ft (kN-m)

M_a = maximum unfactored moment at the stage which deflections are considered, k-ft (kN-m)

M_{cr} = cracking moment, k-ft (kN-m)

M_n = nominal moment capacity, k-ft (kN-m)

M_{ult} = ultimate resisting moment, k-ft (kN-m)

m = constant exponent

$n = E_s/E_c$ = modular ratio

P = maximum load, N (lbf)

P_{max} = maximum load, lbf (kN)

R = modulus of rupture, MPa (psi)

r = percent of natural aggregate replaced with Plazrok (e.g. 15% = 15)

S_1 = stress corresponding to a longitudinal stress, ε_1, of 50 millionths, MPa (psi)

S_2 = stress corresponding to 40% of ultimate load, MPa (psi)

T = splitting tensile strength, MPa (psi) or total tension force, kip (kN)

w_c = density, unit weight, of normal weight concrete or equilibrium density of lightweight concrete, lb/ft^3 (kg/m^3)

$\bar{y}$ = centroid of transformed section, in (mm)

$\bar{y}_{cr}$ = centroid of the cracked section

y_g = centroid of gross section, in (mm)

y_t = distance from the centroidal axis to the tension face of the member, in (mm)

α = distance from the applied point to nearest support for four-point bending, ft (m)

β_1 = factor relating depth of equivalent rectangular compressive stress block to depth of neutral axis

ε_2 = longitudinal strain produced by stress S_2

ε_{ty} = net tensile strain

$\Delta_{midspan}$ = midspan deflection, in (mm)

λ = modification factor to reflect the reduced mechanical properties of lightweight concrete relative to normal weight concrete of the same compressive strength

Acknowledgements

I would like to thank my advisor, Dr. Kimberly Kramer, for her dedication and guidance over the past two years. I would not be in the position I am today without you. Special thanks to Dr. Christopher Jones for granting me the opportunity to conduct my research in the Kansas State Civil Department Labs and for providing valuable guidance during the experimental setup. I extend my appreciation to Katie Loughmiller for her contribution as a committee member. Lastly, I would like to thank Marissa Ober and Zachary Dillinger for their assistance in creating beam molds, setting up the experiment, and testing all specimens.

Dedication

I dedicate this paper to my family for their support throughout my college experience and everything I strive to achieve in life. I would not be where I am today without your support and assistance.

Chapter 1 - Introduction

1.1 Research Background

Plastics have experienced a surge in usage attributable to their low density, impressive strength-to-weight ratio, durability, and cost-effectiveness. Plastics have found an application in virtually every industry worldwide, spanning packaging, automotive, electronics, agriculture, and construction. However, the increase in plastic production has led to a widespread increase in plastic waste production. For example, plastic production increased from a mere 2 million tons (1.8 million metric tons) in 1950 to a staggering 460 million tons (417 million metric tons) in 2019, marking an astronomical 23,000 percent increase in production (Ritchie et al., 2023). In the United States of America (USA), plastic generation in 2018 reached 35.7 million tons (32.4 million metric tons), which made up 12.2 percent of the total solid waste generated, according to the United States Environmental Protection Agency (EPA) in 2023. Despite this substantial volume, only 3.1 million tons (2.8 million metric tons) of plastic were recycled, while 5.6 million tons (5.1 million metric tons) were incinerated for energy recovery (US EPA, 2023). The remaining 27 million tons (24.5 million metric tons) wound up in landfills, which during rainstorms can contribute to pollution in nearby rivers and ultimately the ocean (US EPA, 2023). Plastic waste requires 20 to 500 years to decompose, yet it never achieves complete decomposition; instead, it only diminishes in size over time (United Nations, 2021).

Natural aggregates hold the distinction of being the most valuable non-fuel mineral commodity globally, primarily due to their indispensable role in the production of concrete, the most widely used manmade material (Langer, 2002). Comprising sand, gravel, and crushed stone, natural aggregates constitute 60 to 75 percent by volume of concrete (Ford & Spiwak, 2017). As concrete usage continues to rise so does aggregate consumption. In 2021, 44.3 billion tons (40.2 billion metric tons) of aggregate were mined with China and Northeast Asia producing 51.8 percent of the 44.3 billion tons (40.2 billion metric tons) (*Growing Global Aggregates Sustainably*, 2021). This extensive production of aggregates for concrete has a significant environmental impact. In proximity to the extraction sites, the qualitative effects are primarily characterized by landscape degradation, noise, dust emissions, potential sedimentation, and contamination of water bodies (De Bortoli, 2023). Additionally, the environmental repercussions extend beyond the immediate vicinity, encompassing broader aspects of land use and change, leading to habitat loss, ecosystem erosion, greenhouse gas emissions, and degradation of air quality (De Bortoli, 2023).

To address the rising demand for aggregates and combat the escalating environmental waste issues, plastic may be used as a partial replacement for natural aggregates. Advantages of plastics in concrete have shown to include versatility and the ability to meet technical requirements, lightweight properties, enhanced durability and longevity, chemical resistance, as well as excellent thermal and electrical insulation properties (Hashmath & Meraj, 2015). Despite the numerous advantages that plastics bring to concrete, certain disadvantages exist. A primary concern is the low bonding properties of plastics, leading to a reduction in the overall strength of the concrete, encompassing compressive, tensile, and flexural strength.

Plastic coarse aggregate partial replacement in concrete research has been limited to mechanical property tests such as compressive, splitting tensile, modulus of rupture, and modulus of elasticity tests (Akram et al., 2015; Ghaly & Gill, 2004; Islam & Shahjalal, 2021; Manjunath, 2016; Narayanan, 2024; Saikia & De Brito, 2012; Shanmugapriya & Santhi, 2017). Plastics, including polyethylene terephthalate (PET) and polypropylene (PP), have been utilized as replacements for fine aggregate in reinforced concrete member tests (Fakhruddin et al., 2021;

Radhi et al., 2022). However, only recently has plastic been explored as a substitute for coarse aggregates in concrete applications. The utilization of plastics as a partial replacement for coarse aggregates not only has the potential to divert more plastic waste from landfills and aid in ocean recycling but also holds the promise of reducing the demand for natural aggregates.

1.2 Thesis Objective

The primary objective of the research outlined in this thesis is to evaluate the feasibility of incorporating recycled waste plastic as a replacement for coarse aggregates in reinforced concrete. This is accomplished through the examination of rectangular reinforced concrete members subjected to 15 and 30 percent replacement of coarse aggregate using Plazrok by Enviroplaz. Plazrok consists of co-mingled waste plastic (grades 1-7), waste colored glass, and fly ash.

Chapter 2 provides a comprehensive background on various types of plastic waste, supplemented by existing studies that investigate the use of recycled/waste plastic as a replacement for coarse aggregates in concrete mixtures. Additionally, the flexural behavior of reinforced concrete beams along with the design standards outlined in ACI 318-19 are introduced. In Chapter 3, the experimental setup and adherence to American Testing Standards (ASTMs) are detailed, providing insight into the methodology followed throughout the experiment. Chapter 4 presents the outcomes of testing concrete with varying replacement percentages (0, 15, and 30 percent by volume) using Plazrok as a coarse aggregate substitute. The load-deflection curves derived from the experimental data are compared to code-based instantaneous deflection calculations and nominal moment capacities. The overarching objective is to determine the applicability of existing ACI 318-19 code equations and theories to members featuring partial coarse aggregate replacement with Plazrok. Lastly, Chapter 5 presents the key findings, recommendations, and future research.

Chapter 2 - Literature Review

2.1 Introduction

A comprehensive review on plastic waste, existing partial coarse aggregate replacement research, and reinforced concrete beam behavior is performed in this chapter. Section 2.2 introduces the escalating issue of plastic waste, presenting types of plastics and their applications. Experimental research is examined in Section 2.3, which explores different replacements of plastic coarse aggregates. Within this section, an analysis of fresh concrete plastic state and mechanical properties of concrete with partial coarse aggregate replacement is undertaken to draw conclusions regarding the influence of recycled-plastic coarse aggregate replacement on the concrete performance. The behavior of reinforced concrete members is detailed in Section 2.4, while Section 2.5 addresses ACI 318-19 design requirements.

2.2 Plastic Waste

The production of plastics has witnessed a continual increase since their inception, driven by factors such as cost-effectiveness, a favorable strength-to-weight ratio, low density, and durability—attributes that surpass those of materials like metal or glass (Gu & Ozbakkaloglu, 2016). In the 1950's, the worldwide plastic production was 1.9 million tons (1.7 million metric tons) but as of 2021 has jumped to a staggering 430.7 million tons (390.7 million metric tons) (Statista, 2021). As of 2021, China produces 32 percent of the world's plastic followed by North America at 18 percent. According to the Organization for Economic Co-operation and Development (OECD) 2022, 50 percent of the plastic waste collects in landfills, 22 percent ends up in the environment through littering and landfill runoff due to rain, and only 9 percent of the plastic is recycled with the rest being incinerated. Over 30 million metric tons of plastic waste have accumulated in the oceans with an additional 120 million tons (109 million metric tons) in rivers (*OECD*, 2022).

2.2.1 Types of Plastic

Two main types of plastic exist: thermoplastics and thermoset plastics. Thermoplastics were first introduced in 1907 followed by thermoset plastics in 1924 (*Thermoplastics vs. Thermosetting*, 2023). The main difference between the two is how the polymers behave during the curing process; thermoset plastic polymers create cross links between other molecules making them impossible to separate while thermoplastics polymers can easily be separated with heat. Thermoset plastics are used in applications where the plastic is required to be highly resistant to chemicals and heat. Thermoplastics can be molded into any shape, are lightweight, and can be easily recycled (*Thermoplastics vs. Thermosetting*, 2023).

Recyclable plastics can be separated into seven categories according to the Resin Identification Codes (RIC): (1) Polyethylene Terephthalate (PET), (2) High-Density Polyethylene (HDPE), (3) Polyvinyl Chloride (PVC), (4) Low-Density Polyethylene (LDPE), (5) Polypropylene (PP), (6) Polystyrene (PS), and (7) Other (*Resin Identification Codes*, 2021). Figure 2-1 illustrates the Resin Identification Codes with one on the left, the easiest to recycle, to seven on the right, the most difficult to recycle. All RIC plastics are thermoplastics.

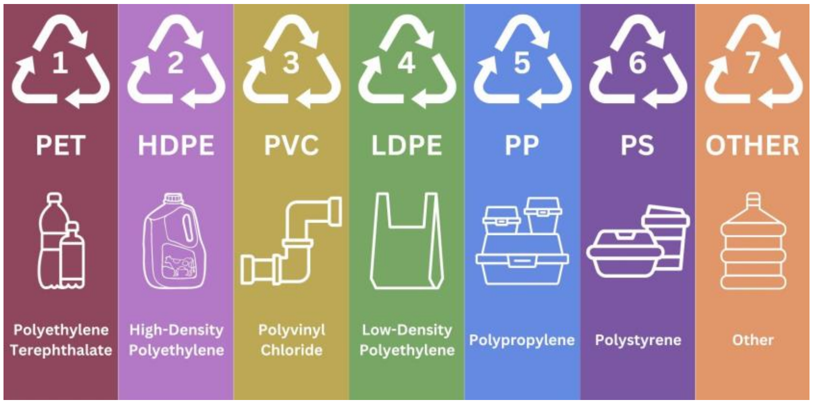

Figure 2-1: Resin Identification Codes (RIC)

Category 1 Polyethylene Terephthalate (PET) is the most common thermoplastic polymer. PET is typically used for single-use clear food and drink containers, such as plastic bottles. PET can be recycled into polyester fabric or filings for carpets and cushion fillings. The second most commonly recycled plastic is Category 2 High Density Polyethylene (HDPE). HDPE plastic is often used for cleaning product bottles, tubs, bottle caps, and milk jugs. HDPE can be colored but the color cannot be removed, and the recycled HDPE must be used in colored plastic products. Category 3 Polyvinyl Chloride plastic (PVC) is not as rigid as PET or HDPE plastics and is typically used for piping, paneling, decking, fencing, and credit cards. PVC contains high levels of hazardous additives to produce desired materials. Most local recycling facilities will not accept PVC for this reason, and it must be separated from other plastics. Category 4 Low Density Polyethylene (LDPE) is a soft flexible plastic used for food and shopping bags. Category 5 Polypropylene (PP) is one of the least recycled post-consumer plastics in the world with a recycled rate of less than one percent (*Plastic by the Numbers*, 2023). PP is not commonly used due to the labor-intensive recycling process which includes collection, sorting, cleaning, melting, and producing new products. The melting process requires melting the plastic to remove contaminants then removing residual molecules under vacuum before solidification (*Plastic by the Numbers*, 2023). Category 6 is Polystyrene (PS) is one of the most difficult plastics to recycle since it is 98 percent air on average. Lastly, Category 7 is for all other recyclable plastics. This category includes electronic equipment, glasses frames, and Legos.

2.2.2 Plazrok

This thesis builds off the research done by Costello et al. (2021) and their use of Plazrok as a partial coarse aggregate replacement in concrete. Plazrok was created by the New Zealand technology company Enviroplaz as a partial coarse aggregate replacement in concrete. Figure 2-2 and Figure 3-1 show the Plazrok received from Enviroplaz. Enviroplaz main driving force behind Plazrok is to reduce the 130,000 tons (143,300 metric tons) of plastic that collects in our waterways and the ocean annually (O'Keane, 2022). Enviroplaz has addressed this concern by creating Plazrok from all seven types of recyclable plastics, including contaminated materials like discolored plastics and residues, colored waste glass, and fly ash. Notably, sorting or washing of the waste plastic is not needed, and the removal of labels and caps is unnecessary. The manufacturing process of Plazrok avoids burning the plastic and instead employs a thermomechanical process (O'Keane, 2022). Enviroplaz asserts Plazrok typically weighs 20 percent less than conventional natural aggregates, while concurrently enhancing the tensile strength of concrete without altering its compressive properties (O'Keane, 2022). Currently, Enviroplaz promotes Plazrok for various applications, branding it as a lightweight solution for tilt-up panels suitable for walls, facades, and noise barriers. Additionally, they recommend Plazrok as a floor topping material and for use in other non-structural elements within a building (*Plazrok*, 2024).

2.3 Existing Recycled Plastic Coarse Aggregate Research

The ensuing subheadings investigate the findings of Alkotami and Kramer (2023), who conducted a comprehensive examination and comparative analysis of twelve studies. Alkotami and Kramer (2023) investigation focused on the partial replacement of coarse aggregate with plastic materials, including Costello et al. (2021) exploration of Plazrok, a study this thesis builds upon. Table 2-1 illustrates eight studies, included in Alkotami and Kramer (2023) investigation, that discussed the impacts of partial coarse aggregate replacement on the mechanical properties of concrete. Included in Table 2-1 is the type of plastic replacements used, water-to-cement ratios (*w/c*), testing standards, and the testing completed within the reference document research (compression, tensile, modulus of rupture, modulus of elasticity). The studies from Table 2-1 used for the comparison of fresh concrete plastic stage properties are listed in Table 2-2. Figure 2-2 shows the coarse aggregate replacement used in Costello et al. (2021), Islam and Shahjalal (2021), Ghaly and Gill (2004), Shanmugapriya and Santhi (2017), Saxena et al. (2016), and Saikia and de Brito (2012).

Table 2-1: Mechanical Concrete Properties in Reference Documents

Reference Document	Plastic	w/c ratio	Standard	Comp.	Tensile	MOR	MOE
Akram et. al. (2015)	E-Plastic	0.50	IS	✓	✓		
Costello et al. (2021)	Plazrok	0.45	ASTM	✓	✓	✓	
Ghaly and Gill (2004)	Variety	0.42-0.69	ASTM	✓			
Islam and Shahjalal (2021)	PP	0.45-0.55	ASTM				✓
Manjunath (2016)	E-Plastic	0.50	IS	✓	✓	✓	
Saikia and de Brito (2012)	PET	0.61-0.74	EN	✓	✓	✓	✓
Saxena et. al. (2016)	PET	0.45	IS				✓
Shanmugapriya and Santhi (2017)	HDPE	0.42	IS	✓	✓	✓	

EN: European National Standard; ASTM: American Society for Testing and Materials; IS: Indian Standard; Comp.: compressive strength; MOR: modulus of rupture; MOE: modulus of elasticity.

Table 2-2: Plastic Concrete Properties in Reference Documents

Reference Document	Plastic	w/c ratio	Standard	Slump	Density
Costello et al. (2021)	Plazrok	0.45	ASTM	✓	✓
Saikia and de Brito (2012)	PET	0.53-0.74	EN	✓	✓
Manjunath (2016)	E-Plastic	0.50	IS	✓	

Costello et al. (2021) **Islam and Shahjalal (2021)**

Ghaly and Gill (2004) **Shanmugapriya and Santhi (2017)**

Saxena et al. (2016) **Saikia and de Brito (2012)**

Figure 2-2: Literature Review Plastic Aggregates

2.3.1 Fresh Concrete Plastic Stage Properties

The plastic stage, also known as the fresh concrete stage, offers valuable insights into the mechanical properties of a concrete mixture. This phase commences from the moment aggregates, water, cementitious materials, and admixtures are combined until the concrete begins to harden. Various tests are conducted on fresh concrete batches during this stage to assess factors such as workability, density, and durability. These various tests are discussed in the following subsections.

2.3.1.1 Slump

The emphasis of this literature review is on conventional concrete mixes rather than self-consolidating concrete. Therefore, the flow test is deemed less optimal for gauging the workability of the mix, and, instead, the commonly utilized method is the slump test. Three main testing standards are used in the previous research with partial aggregate replacement: American Society for Testing and Materials ASTM C143/C143M-15a *Standard Test Method for Slump of Hydraulic-Cement Concrete*, European National Standard EN 12350-2:2019 *Testing Fresh Concrete – Part 2: Slump Test*, and Indian Standard IS 1199-1959 *Methods of Sampling and Analysis of Concrete* (*ASTM C143/C143M-15*, 2015; *EN 12350-2*, 2019; *IS 1199*, 1959).

All three testing standards are virtually identical and share only minor differences with each other. The slump cone size, tamping rod diameter, and the number of strokes per layer are consistent across these standards. The primary distinctions lie in the timeframes for lifting the mold, the number of layers required to fill the cone, and the point at which slump measurements are taken. ASTM C143 mandates a five second timeframe for complete mold removal, with a two-second tolerance. In contrast, EN 12350-2 allows a window of two to five seconds for this action, while IS 1199 does not explicitly address this timeframe. To fill the slump cone ASTM

C143 and EN 12350-2 state to use three layers while IS 1199 specifies four layers. Lastly, ASTM C143 specifies that the slump is measured from the displaced original center while EN 12350-2 and IS 1199 specify measuring from the highest point (*ASTM C143/C143M-15*, 2015; *EN 12350-2*, 2019; *IS 1199*, 1959).

The experimental results of Costello et al. (2021), Manjunath (2016), and Saikia and de Brito (2012) are summarized in Table 2-3. Costello et al. (2021) and Saikia and de Brito (2012) reported an increase in slump with the increase aggregate replacement while Manjunath (2016) found that slump decreased with the increase in replacement. Slump increased with the replacement of coarse aggregate with Plazrok due to the lower absorption rate and additional free water (Costello, 2021). The five and 10 percent replacement for Saikia and de Brito (2012) showed no significant change but at 15 percent replacement with PET plastic the slump increased. This indicates that with higher replacement of coarse aggregate with plastic an increase in slump is expected (Saikia & De Brito, 2012).

Table 2-3: Plastic Aggregate Replacement Effect on Slump

Reference Document	Type of Plastic	Slump Standard	Replacement	w/c	Slump in (cm)
Costello et al. (2021)	Plazrok	ASTM C143	Control	0.45	4.00 (10.2)
			15%	0.45	4.25 (10.8)
			30%	0.45	5.00 (12.7)
			45%	0.45	5.00 (12.7)
Manjunath (2016)	E-Plastic	IS 1199	Control	0.50	5.04 (12.8)
			10%	0.50	4.49 (11.4)
			20%	0.50	3.54 (9.00)
			30%	0.50	2.95 (7.50)
Saikia and de Brito (2012)	PET	EN 12350-2	Control	0.53	5.00 (12.7)
			5%	0.53	4.80 (12.2)
			10%	0.52	4.80 (12.2)
			15%	0.52	5.20 (13.2)

2.3.1.2 Unit Weight and Density

Unit weight and density share similarities, but the distinction lies in the specificity of the terms. Unit weight specifically denotes the weight of the material, while density is a more general term referring to mass per unit volume. The unit weight serves as valuable data for assessing the concrete batch yield and air content, since air contributes volume without adding any weight. Lightweight concrete is defined with a density range of 90 to 135 lb/ft^3 (1,442 to 2,163 kg/m^3) while normal weight is established as 135 lb/ft^3 (2,163 kg/m^3) and above (*ACI 318*, 2019). In older versions of the ACI 318 code, before ACI 318-19, lightweight was defined as 90 to 115 lb/ft^3 (1,442 to 1,842 kg/m^3) leaving a 20 lb/ft^3 (320 kg/m^3) disparity. The upper bound was then changed to 135 lb/ft^3 (2,163 kg/m^3) for lightweight since it was concluded that some amount of lightweight aggregate is required to produce a density under 135 lb/ft^3 (2,163 kg/m^3) (*ACI 318*, 2019).

With the addition of plastics, which are considered lightweight aggregates, the concrete density begins to decrease with increasing coarse aggregate replacement. This is evident in Table 2-4 which shows the densities for Costello et al. (2021) and Saikia and de Brito (2012). At a certain amount of replacement, the concrete transitions from normal-weight to lightweight. Only Costello et al. (2021) included a mix transition to lightweight and that was at 45 percent replacement of coarse aggregate with Plazrok. The only correlation between the aggregate types is the decrease in density. The variances in the density among the different mixtures are influenced by the specific gravities of each plastic replacement and the water-to-cement ratio. Plastics can be used to replace some of the coarse aggregates in a mixture to assist in lowering the unit weight which can be useful in non-loadbearing applications (Ghaly & Gill, 2004).

Table 2-4: Plastic Aggregate Replacement Effect on Density

Reference Document	Type of Plastic	Replacement	w/c	Density lb/ft^3 (kg/m^3)	% Change in Density
Costello et al. (2021)	Plazrok	Control	0.45	146.2 (2342)	0.00%
		15%	0.45	142.1 (2276)	-2.77%
		30%	0.45	136.9 (2193)	-6.36%
		45%	0.45	132.7 (2126)	-9.19%
Saikia and de Brito (2012)	PET	Control	0.53	149.0 (2387)	0.00%
		5%	0.53	146.5 (2347)	-1.68%
		10%	0.52	143.4 (2297)	-3.76%
		15%	0.52	140.7 (2254)	-5.57%

2.3.2 Mechanical Properties

Concrete mechanical properties directly influence the performance and durability of reinforced concrete structures. The mechanical attributes of concrete encompass a range of characteristics, including but not limited to compressive strength, tensile strength, flexural strength, and modulus of elasticity. The compressive strength has the highest impact on the reinforced concrete member size and strength but each of the listed mechanical properties is vital to performance and durability. For this reason, mixtures with partial replacement of coarse aggregates with recycled plastic aggregates must reach the required strength requirements and behave similarly to reinforced concrete members with natural aggregates. Alkotami and Kramer (2023) found that the mechanical properties decreased with increased replacement of aggregate with plastics compared to mixtures containing only natural aggregates. The results are discussed and displayed in Sections 2.3.2.1 through 2.3.2.4.

2.3.2.1 Compressive Strength

Compressive strength is a critical property of concrete that governs the material's ability to withstand axial loads and resist deformation under compressive forces. Concrete is specified based on its 28-day compressive strength. Concrete gains strength as the cementitious material hydrates until the chemical process is complete. The hydration process continues for an unknown time, but most of the compressive strength is gained within the first 28 days. After 28 days, the strength increase is minimal, so test methods and engineers specify 28-day strength.

Compressive strength relates to the mechanical behavior of concrete and alters other properties such as modulus of elasticity, tensile strength, ductility, impermeability, and resistance to ambient conditions (Nemati et al., 2023). The easiest method to increase the compressive strength of a mixture is to decrease the *w/c* ratio. With increasing *w/c* ratios, the workability of the mixtures decreases due to the increased friction between the aggregates and cement with less water. Decreasing the workability of a mixture reduces the mixture's ability to flow, compact, and be finished, but by adding admixtures, such as water reducer, the workability can be increased.

2.3.2.1.1 Testing Methods

There are three main standard testing methods to determine the compressive strength of concrete: American Society for Testing and Materials ASTM C39/C39M cylinder test, European National Standard EN 12390-3 cylinder or cube test, and the Indian Standard IS 516 cube tests.

ASTM C39/C39M-21 *Standard Test Method for Compressive Strength of Cylindrical Concrete Specimens* is primarily used as a compressive test in the United States where 4-inch diameter by 8-inch long (102 mm by 203 mm) cylinders are tested. ASTM C39 states to use Equation 2-1 or Equation 2-2 to calculate the compressive strength of the tested specimens. The procedure for ASTM C39 is described in Section 3.5.1 of this thesis.

Inch-pounds units:

$$f_{cm} = \frac{4\, P_{max}}{\pi\, D^2}$$ **Equation 2-1**

SI Units:

$$f_{cm} = \frac{4000\ P_{max}}{\pi\ D^2} \qquad \textbf{Equation 2-2}$$

European Standard EN 12390 *Testing Hardened Concrete – Part 3 Compressive Strength of Test Specimens* is primarily used as a compressive test in Europe where the test specimens are cubes, cylinders, or cores. Cube specimens are 6 x 6 x 6 inches (150 x 150 x 150 mm) and cylinders have a 6 inch (150 mm) diameter with a 12 inch (300 mm) height that is comparable to ASTM C39 test specimens. The test setup and procedure are similar to ASTM C39 where the specimens are loaded until failure and Equation 2-3 is used to calculate the compressive strength.

IS 516-1959 *Methods of Tests for Strength of Concrete* is primarily used India where the test specimens can be cubes or cylinders. The cube and cylinder specimen size are the exact same as EN 12390-3 specimens. The procedure for making the specimens is similar to ASTM C39 and EN 12390-3 except during the curing process. After filling the molds, test specimens should be stored at 90 percent relative humidity for 24 hours before demolding. Once molds are removed, the specimens are immediately submerged in clean, fresh water until taken out prior to testing (IS 516, 1959). Before testing, excess water is wiped off and then the specimen is loaded until failure. Similarly, to EN 12390-3, the compressive strength is determined by dividing the maximum applied load by the cross-sectional area as shown in Equation 2-3.

$$f_c = \frac{F}{A_c} \qquad \textbf{Equation 2-3}$$

2.3.2.1.2 Cube versus Cylinder Specimens

In North America, France, Japan, Australia, and New Zealand, the standard code specification for assessing compressive strength is cylinder testing. Conversely, in the remaining regions of Europe and Asia, reliance is placed on cube specimens (Narayanan, 2024). Compression stress varies with the slenderness of the testing specimen leading to differing compressive strength when cube sizes vary. Past research has shown that as the specimen size increases the compressive strength decreases.

Many researchers have found the main difference between cube and cylinder testing is the need to cap cylinders. Since cylinders are typically cast in plastic molds, the faces of the cylinders are not usually parallel with the testing faces of the testing machine. Cylinders need to be capped with sulfur, neoprene, or another suitable material to help properly distribute the applied load over the cylinder face (Narayanan, 2024). Cubes are typically cast in rigid molds that have parallel faces which provide an adequate testing surface. Elwell and Fu (1995) special report 119 published by the Transportation Research and Development Bureau of New York State Department of Transportation states the main factors affecting the cylinder and cube strength ratios are: 1) casting, curing, and testing procedures; 2) geometry of specimens; 3) strength levels; 4) direction of loading and characteristics of the machine; and 5) aggregate grading (Elwell & Fu, 1995).

The three main testing standards previously described do not provide any correlation between the cube or cylinder strengths except cubes are commonly assumed 1.25 times stronger than cylinders. Cylinders are deemed to produce more consistent results due to their failure being less affected by the end restraint of the testing machine. Additionally, their strength is less influenced by the properties of the coarse aggregate in the mixture, and the stress distribution on horizontal planes within a cylinder is found to be more uniform compared to cubes (Narayanan, 2024). For these reasons the compressive strengths predicted by cylinders are considered more reliable than those by cubes. However, the strength of a cylinder is generally lower than that of a cube. Higher cube strength is typically attributed to the presence of an overlapped restrained zone in cubes under uniaxial compression, resulting in multi-axial stressed throughout the cube, while cylinders have an unrestrained zone of 0.268*d* in the middle portion (Narayanan, 2024). Moreover, changes in aggregate grading have a more pronounced impact on cube strength than on cylinder strength, and an increase in aggregate coarseness tends to decrease the cylinder or cube strength ratio.

The compressive strengths of different specimen shapes lack a definitive correlation, with only empirical conversions available. When employing these conversion factors, one must consider various parameters such as strength level, concrete type, aggregate size/gradation, capping, mold material, curing conditions, consolidation methods, and specimen age (Narayanan, 2024). This consideration helps in selecting the most appropriate conversion factor. More research is still needed to understand which test is more accurate and there is a debate for whether the size effect is more pronounced in lower or higher strength concrete mixtures.

2.3.2.1.3 Testing Results

The six research documents stated in Table 2-1 are summarized in this section. Except for one mixture, all exhibited a reduction in compressive strength as the partial replacement of coarse aggregate with recycled plastic increased. No large correlation between the studies can be made due to the compressive strength varying depending on the type of plastic aggregate, *w*/*c* ratio, and the shape of the plastic used. Figure 2-3 indicates the effects of recycled plastic replacement on the compressive strength (Akram et al., 2015; Costello et al., 2021; Ghaly & Gill, 2004; Manjunath, 2016; Saikia & De Brito, 2012; Shanmugapriya & Santhi, 2017).

Akram et al. (2015), Manjunath (2016), and Shanmugapriya and Santhi (2017) used the IS 516-1959 cube test while Costello et al. (2021), Ghaly and Gill (2004), and Saikia and de Brito (2012) used cylinders. At a 5 percent replacement level, both cube and cylinder tests yielded comparable results, with approximately a 30 percent and 28 percent reduction in compressive strength, respectively. However, at replacement levels of 10 and 15 percent, the cube tests exhibited an average reduction of only 23 percent in compressive strength, whereas the cylinder tests experienced average reductions of 41 percent and 45 percent, respectively.

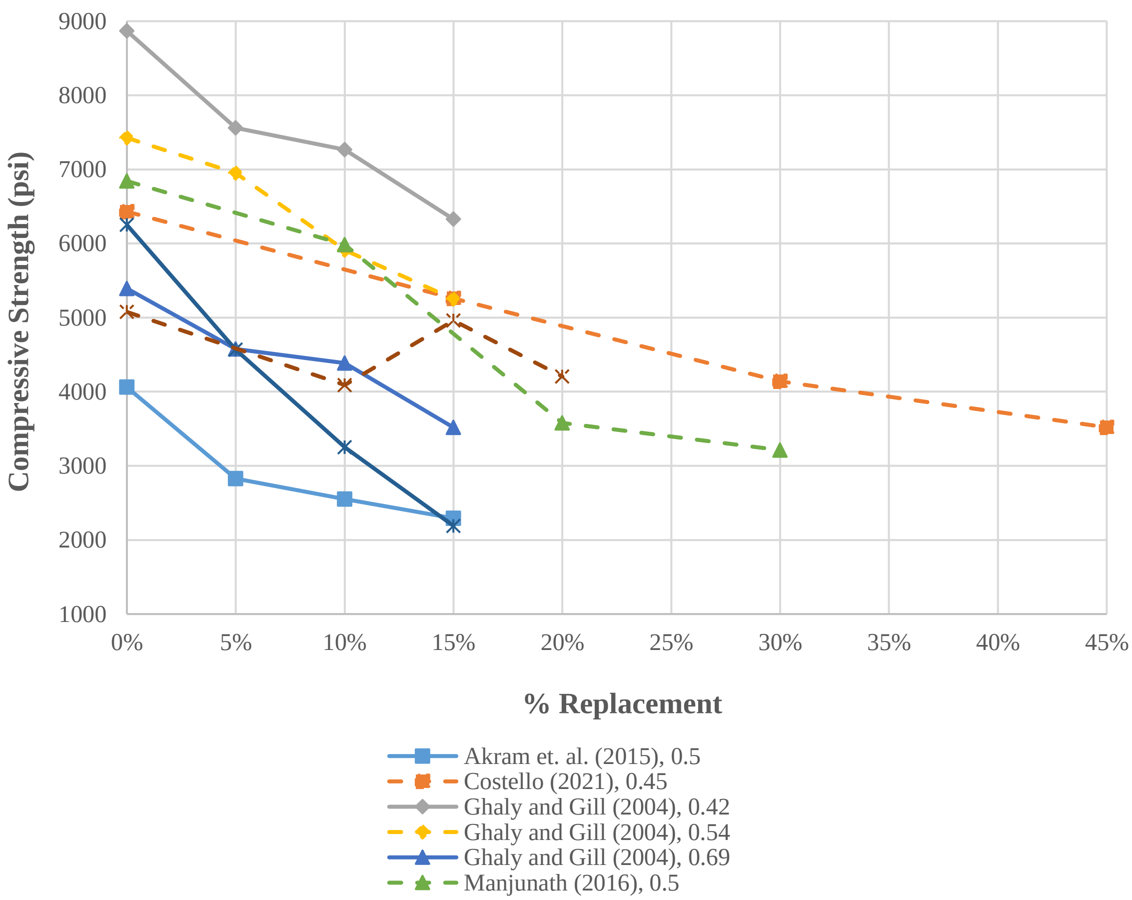

Figure 2-3: Literature Compressive Strength Results

The studies referenced on the compressive strength of concrete with plastic coarse aggregate replacement led to the following four conclusions:

1. When maintaining a constant water-to-cement (w/c) ratio, an increase in the plastic content within the mixture results in a decrease in concrete density, a reduction in compressive strength, and a shift toward less brittle failure.
2. The presence of plastic aggregates diminishes the bond strength within the concrete, leading to concrete failure primarily attributed to the breakdown of the bond between the cement paste and plastic aggregates.
3. Plastic aggregates characterized by sharper edges (non-uniform) as opposed to more uniform plastic aggregates result in an increased water demand to achieve a specified slump in the concrete mixture.
4. Plastic aggregates have high air content and porosity.

Costello et al. (2021) introduced Equation 2-4 for calculating the compressive strength of concrete in Imperial units. This equation is based on the control mixture compressive strength and the percentage of natural aggregates replaced with Plazrok only (Costello et al., 2021). Similarly, Alkotami and Kramer (2023) presented an equation (Equation 2-5) to estimate the compressive strength decrease. The equation from Alkotami and Kramer (2023) is an estimation derived from the research findings presented in the section focusing on PET, E-Plastic, HDPE, PP, and Plazrok coarse aggregate replacement. The equation is designed to provide a close approximation of the extent to which the compressive strength decreases when these materials are used in concrete (Alkotami & Kramer, 2023).

$$f_{c,replacement} = \frac{100 - (r + 5)}{100} f_c \qquad \textbf{Equation 2-4}$$

$$f_{c,replacement} = \frac{100 - (r + 7)}{100} f_c$$ **Equation 2-5**

The effectiveness of Costello et al. (2021) and Alkotami and Kramer (2023) equations are assessed in Section 4.3.1 of the thesis, where it is compared against the ASTM C39 testing results for each percentage of replacement used in the reinforced concrete beams. This comparison will validate the accuracy of Costello et al. (2021) and Alkotami and Kramer (2023) equations against experimental results from additional testing data.

2.3.2.2 Tensile Strength

Splitting tensile testing provides valuable information about the tensile properties of concrete, which is crucial for evaluating its structural behavior. In addition, the test results can be used to determine the suitability of concrete for specific applications, such as assessing its performance in structural elements like beams, slabs, or pavements. Tensile strength reveals concrete's capacity to withstand forces that cause cracking and splitting under tensile stress. Splitting tensile testing is useful in assessing the cracking behavior of concrete. This test offers valuable insights into the initiation and spread of cracks within the specimen when subjected to tensile loading. Furthermore, it aids in understanding the concrete's capability to distribute and resist tensile stresses, a critical factor in managing and preventing crack formation.

Direct tensile testing consists of intricate procedures, induces secondary restraining stresses, and demands expensive equipment in addition to the compression testing machines (Newman, 2003). In addition to the need for supplementary testing machines, the results obtained from direct tensile testing are deemed unreliable. Instead, indirect tensile strength tests such as splitting tensile strength and flexural strength tests are conducted in place of the direct tensile test. The splitting tensile test involves applying a compressive load to a cylinder, generating tensile stresses on the same plane, and leading to tensile failure. This failure precedes compressive failure because the areas of load application experience triaxial compression, enabling the sample to endure higher compressive stresses and undergo tensile failure. The stress distribution is illustrated in Figure 2-4 in Section 2.3.2.2.1.

2.3.2.2.1 Testing Methods

Three main standard testing methods to determine the splitting tensile strength of concrete are: American Society for Testing and Materials ASTM C496/C496M *Standard Test Method for Splitting Tensile Strength of Cylindrical Concrete Specimens*, European National Standard EN 12390-6 *Testing Hardened Concrete Part 6: Tensile Splitting Strength of Test Specimens*, and Indian Standard IS 5816-1999 *Splitting Tensile Strength of Concrete Method of Test*. Each method follows a comparable procedure, applying a diametral compressive load along the length of a cylindrical concrete sample at a continuous rate until failure. During the test setup, an additional bearing bar made of steel is used if the diameter of the largest dimension of the upper bearing face or lower bearing block is less than the length of the cylinder to be tested. The bar is positioned in a way that ensures the load is applied uniformly over the entire length of the specimen. Two bearing strips, each made of nominal 1/8 inch (3.2 mm) thick plywood and measuring an inch (25 mm) in width with a length equal to or slightly longer than the specimen, are used. These bearing strips are inserted between the specimen and both the upper and lower bearing blocks of the testing machine. The cylindrical specimen is then loaded into the testing machine and loaded until failure. Typical specimen sizes for all three methods consist of a 6-inch diameter (150 mm) by 12-inch tall (300 mm) cylinders. The test setup is shown in Figure 2-4.

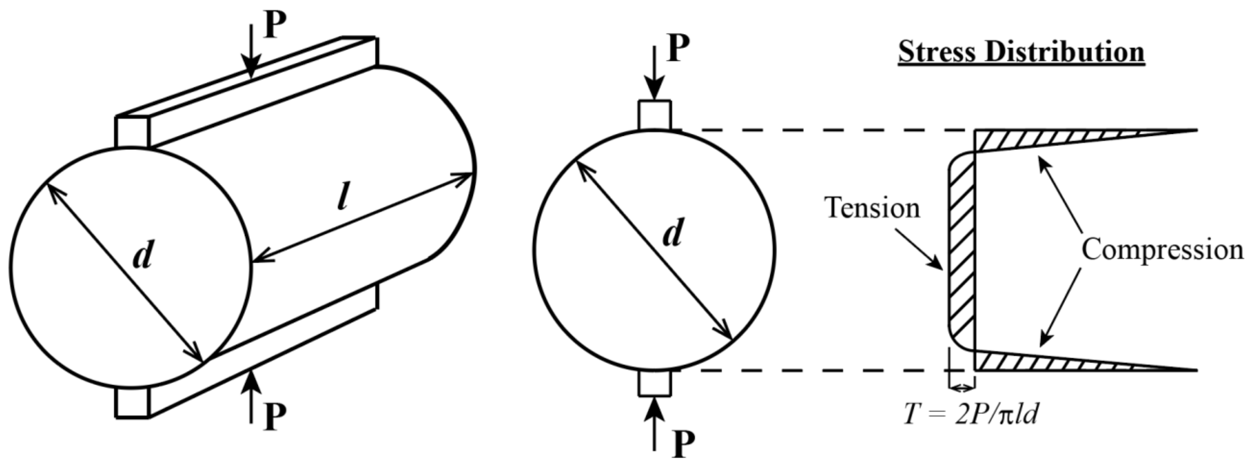

Figure 2-4: Splitting Tensile Test Setup and Stress Distribution

The splitting tensile strength for all three methods is calculated using Equation 2-6 (ASTM C496/C496M, 2017; EN 12390-6, 2023; IS 5816, 1999). The maximum load is recorded for each test, multiplied by two, and divided by the appropriate geometrical factors to determine the splitting tensile strength.

$$T = \frac{2\,P}{\pi\; l\; d} \qquad \textbf{Equation 2-6}$$

2.3.2.2.2 Testing Results

The five research documents stated in Table 2-1 are summarized in this section. Unlike the compression results, which exhibit a clear trend of decreasing compressive strength with higher replacement percentages, the tensile results show a more variable pattern. The tensile strength remains relatively consistent in some cases, increases in others, and decreases in others, depending on factors such as the *w*/*c* ratio and the type of plastic replacement employed. Figure 2-5 illustrates the results of the studies done by Arkam et al. (2015), Costello et al. (2021), Manjunath (2016), Saikia and de Brito (2012), and Shanmugapriya and Santhi (2017).

Shanmugapriya and Santhi (2017) and Manjunath (2016) data exhibited an outlier at 15 and 20 percent replacement, respectively. At these two points the tensile capacity increased instead of remaining constant or decreasing like all of the other samples. For the most part, the figure demonstrates the splitting tensile strength decreases with the increase in plastic replacement. Saikia and de Brito (2012) employed a PET aggregate that differed from the uniform aggregates used by the other four researchers. This non-uniformity resulted in a more pronounced reduction in splitting tensile strength, whereas the data from the other researchers exhibited a more linear trend.

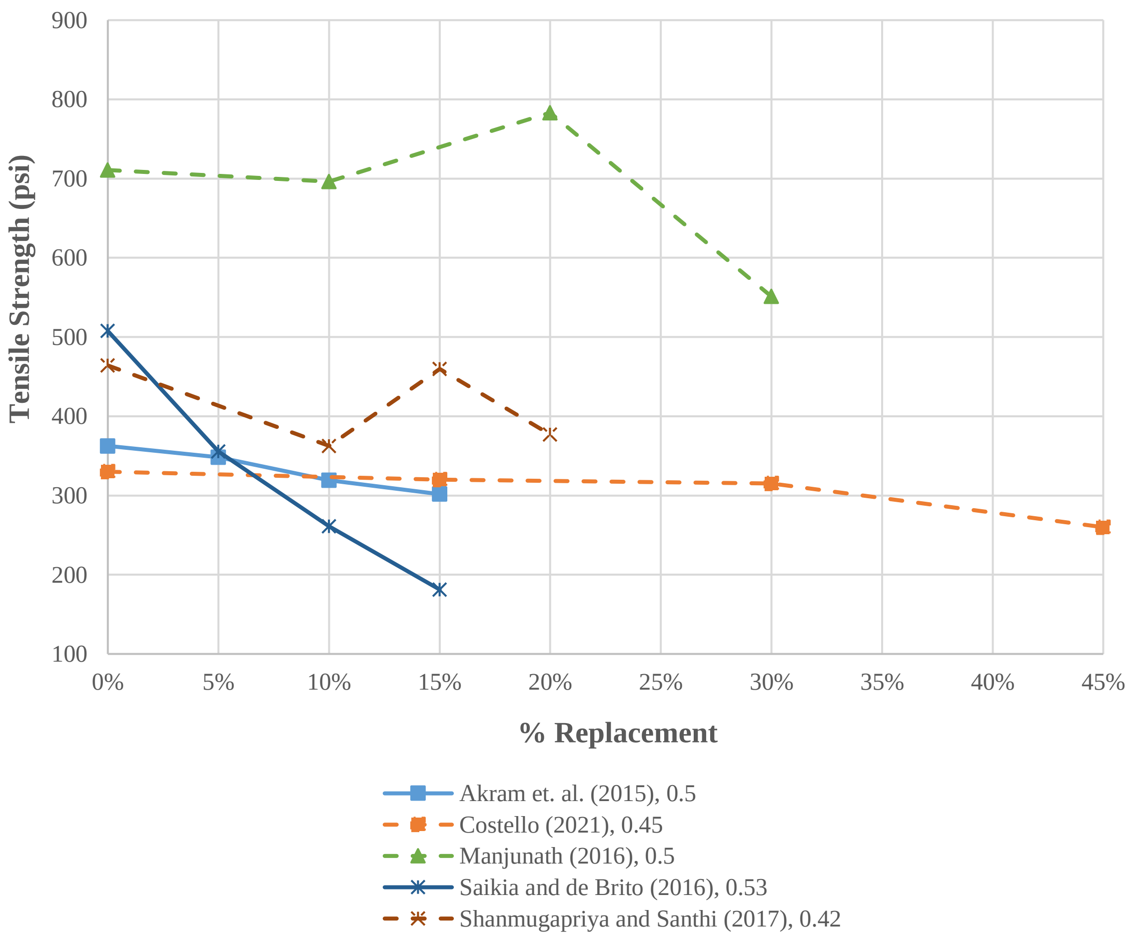

Figure 2-5: Literature Tensile Strength Results

Alkotami and Kramer (2023) presented Equation 2-7 to estimate the splitting tensile strength decrease due to plastic aggregate replacement in Imperial units. The equation from Alkotami and Kramer (2023) is an estimation derived from the research findings presented in the section focusing on PET, E-Plastic, HDPE, PP, and Plazrok coarse aggregate replacement. The equation is designed to provide a close approximation of the extent to which the splitting tensile strength decreases when these materials are used in concrete (Alkotami & Kramer, 2023).

The effectiveness of Alkotami and Kramer (2023) equation is assessed in Section 4.3.2 of the thesis, where it is compared against the ASTM C496 testing results for each percentage of replacement used in the reinforced concrete beams. This comparison will validate the accuracy of Alkotami and Kramer (2023) equations against experimental results from additional testing data.

$$f_{t,replacement} = \frac{100 - (r + 2)}{100} f_t \qquad \textbf{Equation 2-7}$$

2.3.2.3 Modulus of Rupture

The modulus of rupture (MOR) describes the flexural tensile strength of concrete in bending. It represents the maximum tensile stress that a material can withstand without failing under a bending load. The MOR plays a crucial role in designing reinforced concrete members and is used to determine the cracking moment. In design, conducting tests to confirm the MOR for a specific mixture design demands time and resources that are often scarce in many projects. To address this, the American Concrete Institute *ACI 318-19 Building Code Requirements for Structural Concrete* and Indian Standard *IS 456-2000 Plain and Reinforced Concrete Code of Practice* code provides an empirical equation for calculating the MOR. The ACI 318-19 and IS 456-2000 MOR equations are shown in Equation 2-8, Equation 2-9, and Equation 2-10.

<u>ACI 318-19 Section 19.2.3</u>:

Inch-pounds units:

$$f_r = 7.5\lambda\sqrt{f_c'}$$ **Equation 2-8**

SI units:

$$f_r = 0.62\lambda\sqrt{f_c'}$$ **Equation 2-9**

<u>IS 456-2000 Section 6.2.2</u>:

SI units:

$$f_{cr} = 0.7\sqrt{f_{ck}}$$ **Equation 2-10**

2.3.2.3.1 Testing Methods

The modulus of rupture is determined experimentally by a flexural test, commonly known as the "third point bending" test. In this test, a prismatic or cylindrical concrete specimen is subjected to a bending force at midspan until failure. The modulus of rupture can then be calculated based on the applied load, span length, and dimensions of the specimen. Three main standard testing methods to determine the flexural tensile strength of concrete or modulus of rupture are: American Society for Testing and Materials ASTM C78/C78M-22 *Standard Test Method for Flexural Strength of Concrete (Using Simple Beam with Third-Point Loading),* European National Standard EN 12390-5 *Testing Hardened Concrete Part 5: Flexural Strength of Test Specimens*, and Indian Standard IS 516-1959 *Methods of Tests for Strength of Concrete*.

Each method adheres to a similar procedure, wherein a typically rectangular specimen is positioned between two supports and loaded at third points until failure. The application of loads at these third points creates a constant moment region between them, facilitating an accurate calculation of tensile flexural strength when the specimen fails within this region. ASTM C78 test setup is explained in Section 3.5.3 of this thesis. Equation 2-11 is referenced in all of the test methods and is employed to calculate the MOR for a particular specimen, relying on the maximum load observed at the point of failure (ASTM C78/C78M, 2022; EN 12390-5, 2019; IS 516, 1959).

$$R = \frac{P\ L}{b\ d^2}$$ **Equation 2-11**

2.3.2.3.2 Testing Results

The four research documents that performed modulus of rupture testing, stated in Table 2-1 above, are summarized in this section. The flexural strength of each specimen depends on several parameters including: *w*/*c* ratio, replacement of plastic aggregate, the porosity of the plastic, and the transition zone characteristics which refers to the region surrounding the aggregates where the cement paste meets the aggregate. Figure 2-6 illustrates the results of the studies done by Costello et al. (2021), Manjunath (2016), Saikia and de Brito (2012), and Shanmugapriya and Santhi (2017).

Shanmugapriya and Santhi (2017) data exhibited an outlier at 10 and 15 percent replacement. At these two points, the tensile capacity increased instead of remaining constant or decreasing like all other samples. For the most part, the figure illustrates the flexural strength, like the splitting tensile and compression strengths, decreases with the increase in plastic replacement. As stated for the splitting tensile test, Saikia and de Brito (2012) employed a non-uniform PET aggregate. This non-uniformity resulted in a more pronounced reduction in flexural tensile strength. The data demonstrates that there is no correlation in the decline of strength among the various aggregate types; instead, it indicates that the overall modulus of rupture decreases as the replacement level increases.

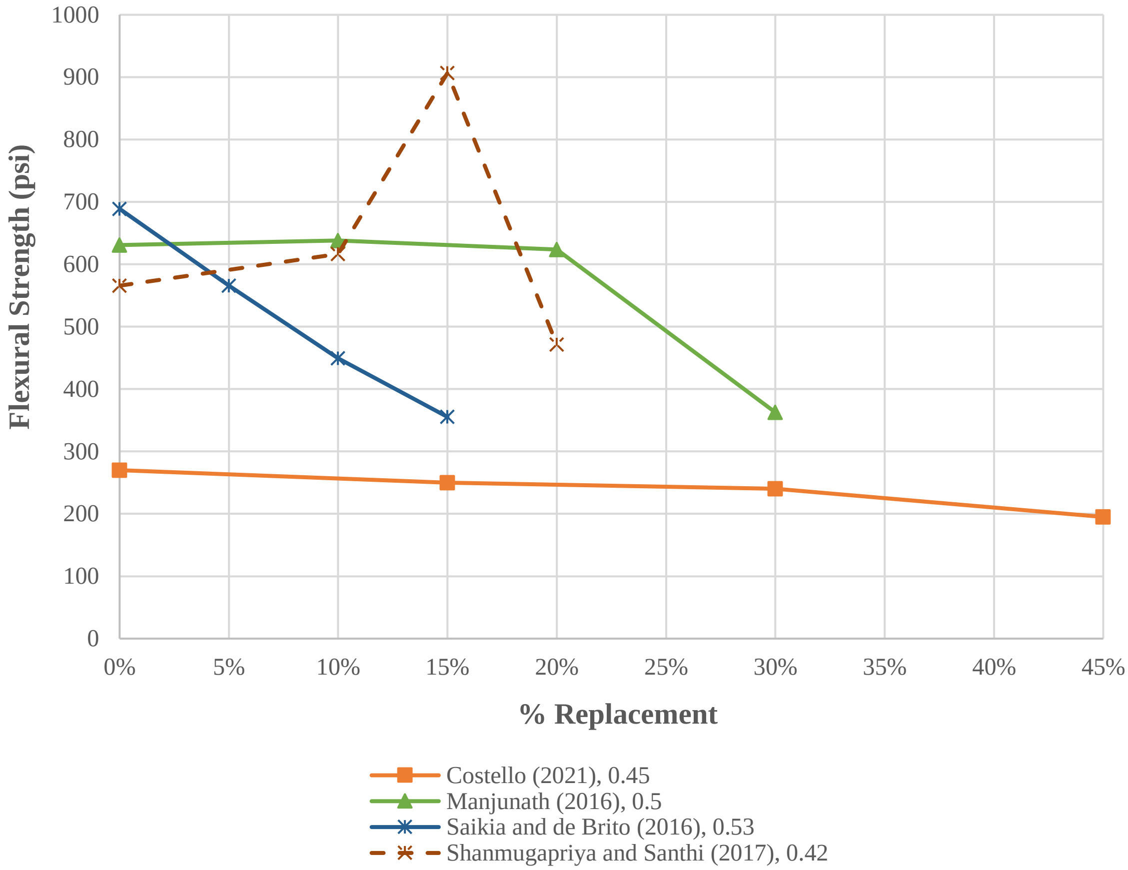

Figure 2-6: Literature MOR Results

Alkotami and Kramer (2023) presented Equation 2-12 to estimate the modulus of rupture decrease due to plastic aggregate replacement in Imperial units. The equation is designed to provide a close approximation of the extent to which the modulus of rupture decreases when plastic replacement is used in concrete (Alkotami & Kramer, 2023). The effectiveness of Alkotami and Kramer (2023) equation is assessed in Section 4.3.3 of the thesis, where it is compared against the ASTM C496 testing results for each percentage of replacement used in the reinforced concrete beams.

$$f_{s,replacement} = \frac{100 - (r + 4)}{100} f_s \quad \textbf{Equation 2-12}$$

2.3.2.4 Modulus of Elasticity

The modulus of elasticity in concrete is characterized as the ratio of the applied stress to the corresponding strain. This parameter not only signifies the concrete's capacity to resist deformation under applied stress but also indicates its stiffness. The overall modulus of elasticity mirrors the concrete's ability to deform elastically, and it is influenced by factors such as the type of aggregates and the *w*/*c* ratio used in the mixture design. The modulus of elasticity can be determined experimentally based on the slope of linear portion of the stress-strain curve or through specific testing or through analytical equations developed in code books around the world. Popular experimental methods are explained in Section 2.3.2.4.1.

Equation 2-13 through Equation 2-19 illustrate the analytical equations presented by common codes around the world such as the American Concrete Institute (ACI), Indian Standard (IS), European National Standard (EN), and the Canadian Standard Association (CSA). Equation 2-13, Equation 2-14, Equation 2-15, and Equation 2-16 are ACI 318-19 Section 19.2.2.1 code equations to determine the modulus of elasticity based on density and compressive strength of concrete. These equations provide an estimate of the modulus of elasticity for general design use based on studies summarized in Adrian Pauw (1960) paper titled *Static Modulus of Elasticity of Concrete as Affected by Density* (*ACI 318*, 2019). The modulus of elasticity equations obtained are compared to the experimental results in Chapter 4 of this thesis to verify their accuracy with plastic aggregate replacement.

ACI 318-19 Section 19.2.2:

Inch-pounds units:

$$E = w_c^{1.5} 33\sqrt{f_c'}$$ **Equation 2-13**

$$E = 57{,}000\sqrt{f_c'}$$ **Equation 2-14**

SI units:

$$E = w_c^{1.5} 0.043\sqrt{f_c'}$$ **Equation 2-15**

$$E = 4{,}700\sqrt{f_c'}$$ **Equation 2-16**

<u>IS 456-2000</u>:

SI units:

$$E = 5000\sqrt{f_{ck}}$$ **Equation 2-17**

<u>EN 1992-1-1:2004</u>:

SI units:

$$E_{cm} = 22\left[\frac{f_{cm}}{10}\right]^{0.3}$$ **Equation 2-18**

<u>CAN/CSA A23.3-04</u>:

SI units:

$$E = 4{,}500\sqrt{f_c'}$$ **Equation 2-19**

2.3.2.4.1 Testing Methods

The precise value of the modulus of elasticity in concrete is established through a laboratory test using the *ASTM C469/C469M Standard Test Method for Static Modulus of Elasticity and Poisson's Ratio of Concrete in Compression*. This test involves analyzing the deformation of the specimen under various load variations. The observations are then used to generate a stress-strain graph (load-deflection graph) from which the modulus of elasticity of concrete is derived. The modulus is determined by drawing a line on the stress-strain curve, specifically from a stress value of zero to 45 percent of the compressive stress and measuring the slope of this line.

The testing setup for ASTM C469 closely resembles the setup and loading procedures outlined in ASTM C39, as previously described. ASTM C469 uses compressometers to determine displacement during loading at different points along the specimens. One compressometers is attached rigidly to the specimen while the other is attached at two diametrically opposite points so that it is free to rotate. The testing procedure requires the specimen to undergo loading at least three times, with data from the first loading not being recorded. In the initial loading, the performance of the gauges is observed, and any necessary corrections to the attachments are made before proceeding to the second loading. The load is then applied continuously and without shock until it reaches 40 percent of the average ultimate load of companion specimens. This maximum load is utilized in Equation 2-20 to calculate the modulus of elasticity (ASTM C469/C469M, 2022).

$$E = \frac{S_2 - S_1}{\varepsilon_2 - 0.00005}$$ **Equation 2-20**

2.3.2.4.2 Testing Results

The results from the three studies by Islam and Shahjalal (2021), Saikia and de Brito (2012), and Saxena et al. (2020) is presented in Figure 2-7. All studies concluded that the MOE is dependent on the density of the concrete, the amount of plastic aggregate replacement, and the compressive strength of the mixture. In the study conducted by Islam and Shahjalal (2021), it was discovered that for a mixture with a *w/c* of 0.45, the MOE experienced a decrease of 1.3, 29.7, and 37.5 percent with 10, 20, and 30 percent plastic coarse aggregate replacement, respectively. Similarly, for a *w/c* of 0.55, the MOE decreased by 4.8, 34.5, and 47.5 percent for 10, 20, and 30 percent plastic coarse aggregate replacement, respectively (Islam & Shahjalal, 2021). Islam and Shahjalal (2021) reached the conclusion that the *w/c* significantly influences the overall reduction of the MOE as plastic content decreases. This finding aligns with similar conclusions reported by Saikia and de Brito (2012) as well as Saxena et al. (2020).

The ability of each plastic to deform easily and its lower stiffness in comparison to concrete are key factors contributing to the decrease in MOE. This reduced stiffness is a primary reason for the observed decline in MOE. Additionally, the decreased density of the mixture, attributed to the increased porosity introduced by the plastic components, also plays a role in this phenomenon.

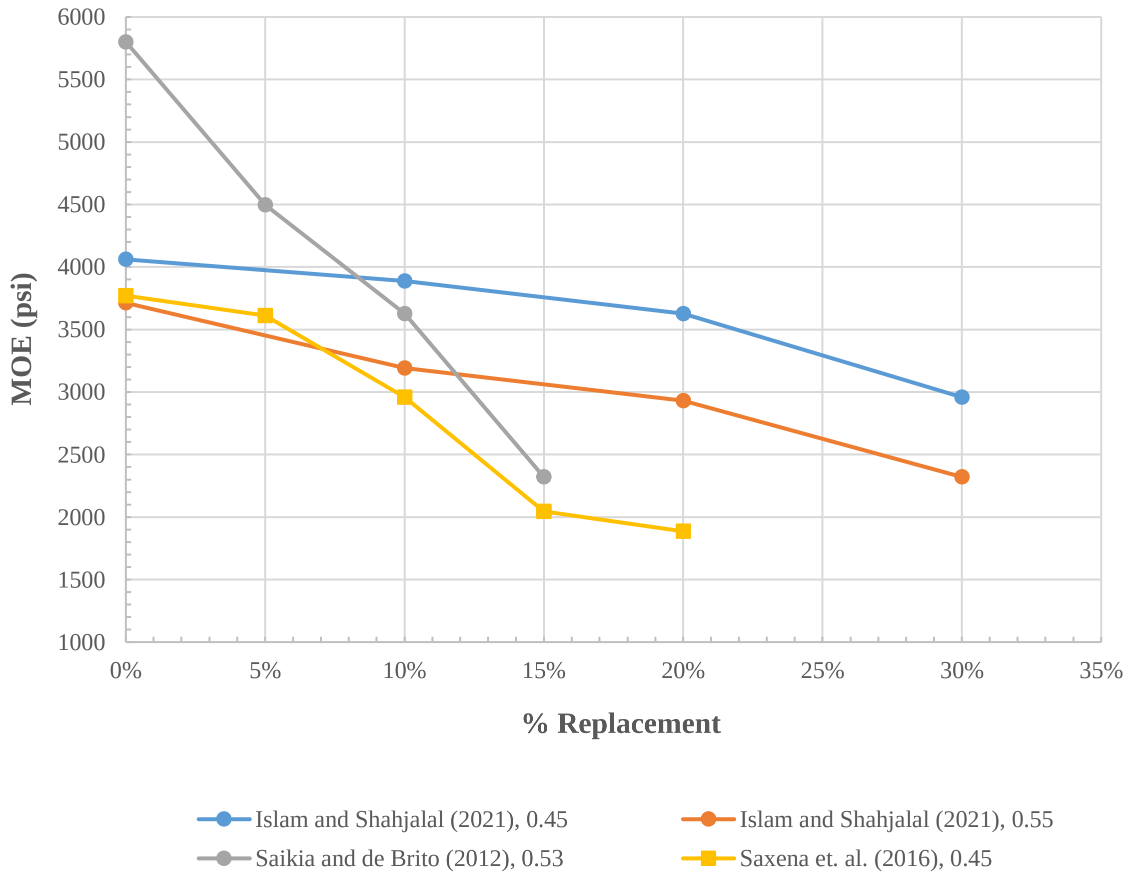

Figure 2-7: Literature MOE Results

2.4 Existing Coarse Aggregate Replacement Beam Tests

This section explores two existing studies on coarse aggregate replacement conducted by Fakhruddin (2021) and Radhi (2022). Notably, limited studies have explored the use of plastic as a coarse aggregate replacement, primarily due to the reductions in mechanical and plastic stage properties introduced by plastic materials.

Fakhruddin (2021) conducted a study specifically examining the effects of PET plastic as a coarse aggregate replacement. The focus of this study was on a 10 percent replacement by volume. Radhi's (2022) study, on the other hand, concentrated on the use of HDPE plastic waste as a replacement for coarse aggregate at varying percentages—10, 20, and 30 percent by volume. These studies contribute valuable insights into the potential applications and effects of incorporating plastic materials as coarse aggregate replacements in concrete mixtures.

2.4.1 Experimental Setup

Figure 2-8 depicts the replacement of coarse aggregate with plastic in the studies conducted by Fakhruddin (2021) and Radhi (2022). Fakhruddin (2021) utilized PET plastic obtained from plastic bottles cut in a specialized machine, with the plastic particles ranging in size from 3/4 of an inch to 0.187 inches (No. 4 sieve) (19 to 5 mm) (Fakhruddin et al., 2021). Radhi (2022) used HDPE plastic derived from vegetable crates, and the plastic particles varied in size from 3/4 of an inch to 0.079 inches (19 to 2 mm). Radhi (2022) gave more insight into their concrete mix design than Fakhruddin (2021).

Fakhruddin (2021) **Radhi (2022)**

Figure 2-8: Beam Specimen Coarse Aggregate Replacements

Fakhruddin (2021) used a control concrete mix design comprising of an unspecified type of cement, sand, gravel, Dramix 3D 80/60 steel fiber reinforcing, and a superplasticizer. The mix design has a *w/c* of 0.40. The beams in Fakhruddin's (2021) study had a width of 3.94 inches (100 mm), a depth of 5.91 inches (150 mm), and a clear span length of 43.31 inches (1100 mm). These beams were intentionally designed to fail in flexure. For tensile flexural reinforcement, 13 mm reinforcing bars were utilized, equivalent to a #4 bar size in the Imperial system. The top bars and shear stirrups were 8 mm, which is roughly a #3 bar size. The beam geometry is shown in Figure 2-9. The reinforcement ratio for Fakhruddin’s (2021) beams is 0.033 or 3.3 percent.

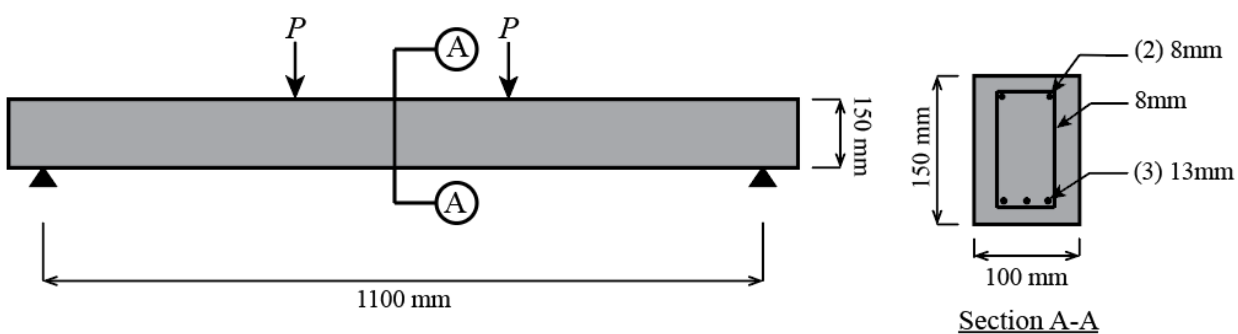

Figure 2-9: Fakhruddin (2021) Beam Geometry

Radhi (2022) utilized a control concrete mix composed of Type 1 Portland cement, silica fume, locally sourced natural sand and gravel, and Visco Crete-5930 superplasticizer with a water-cement ratio of 0.29. The addition of superplasticizer aimed to enhance the workability of the mix (Radhi et al., 2022). The beams in their study were designed to undergo tension-induced failure (flexural failure) in accordance with the specifications of ACI 318-14.

The beam specimens had dimensions of 7.09 inches (180 mm) in width, 11.02 inches (280 mm) in depth, and a length of 78.74 inches (2000 mm). For the bottom tensile reinforcement, two bars with a diameter of 16 mm were utilized, equivalent to #5 bars in Imperial standards. Additionally, two bars with a diameter of 10 mm (#4 bar) were employed as compression steel to provide support for the 10 mm (#4 bar) diameter stirrups, which were crucial for preventing shear failure. The overall geometry of the beams is illustrated in Figure 2-10. The reinforcement ratio for Radhi's (2022) beams is 0.011 or 1.1 percent.

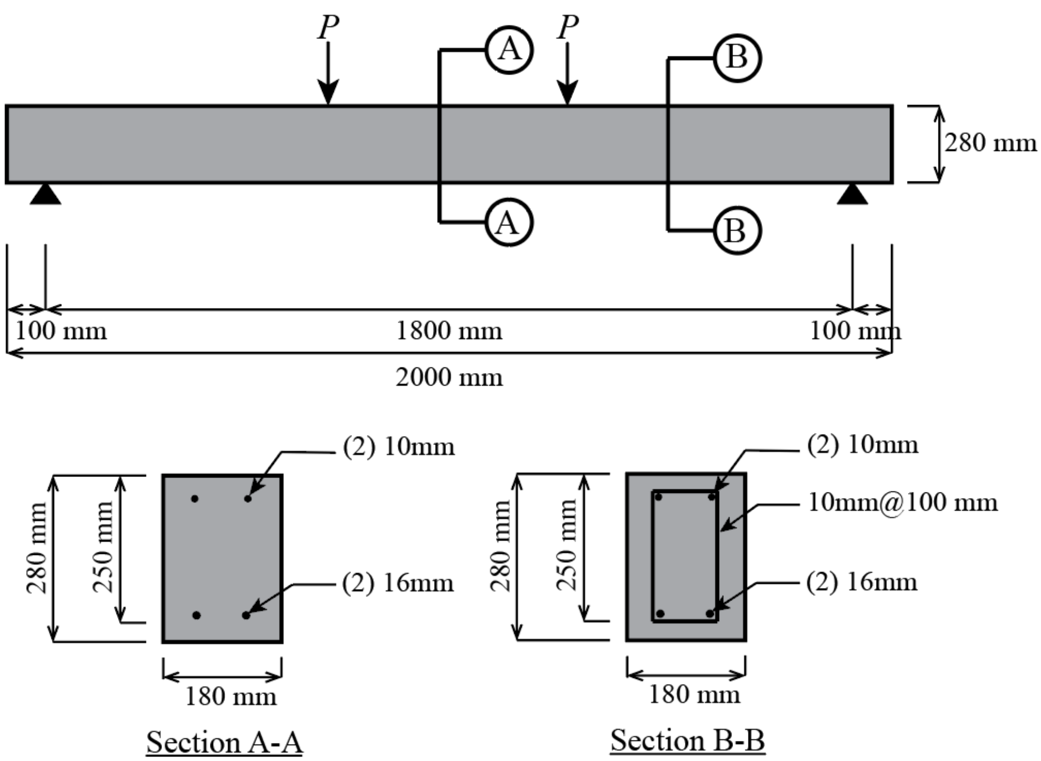

Figure 2-10: Radhi (2022) Beam Geometry

2.4.2 Specimen Results

In the initial testing phase, Fakhruddin (2021) observed an average compressive strength of 4,354 lb/in^2 (30.02 MPa) for the control mix and 2,666 lb/in^2 (18.38 MPa) for the 10 percent replacement mix. This results in a compressive strength reduction of 38.7 percent. The hypothesis proposed was that the smooth texture of the PET plastic resulted in diminished bond strength between the aggregate and the cement paste, aligning with the conclusions drawn in Section 2.3.2.1 of the thesis.

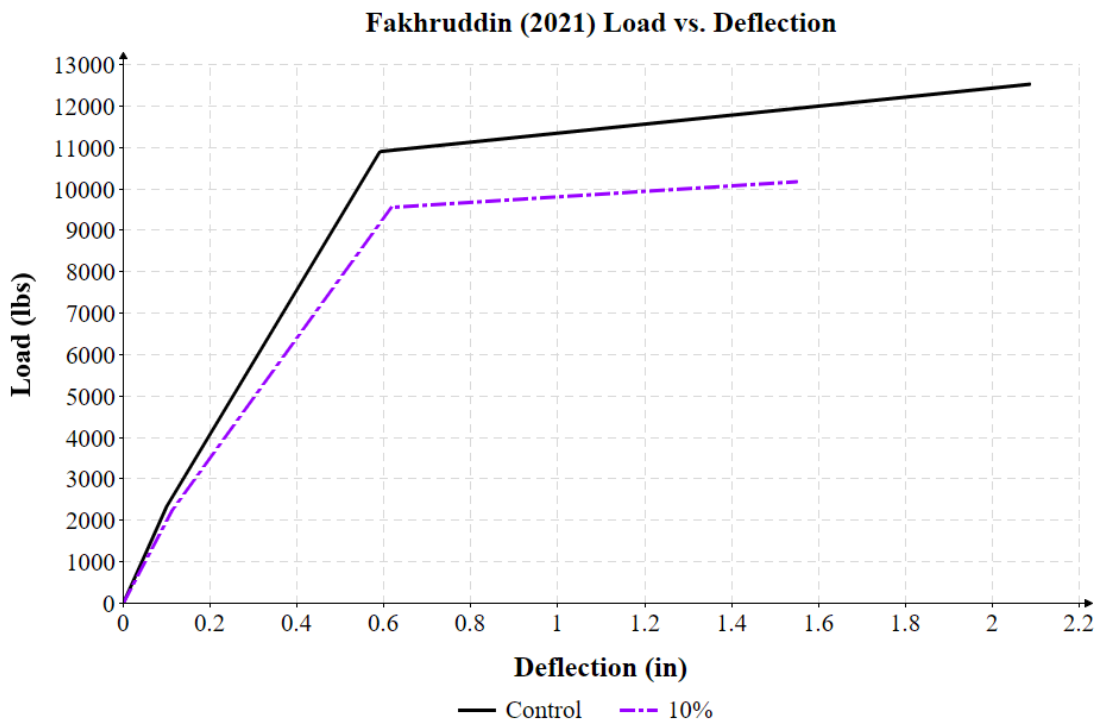

Figure 2-11: Fakhruddin (2022) Beam Specimen Load-Deflection Results

Figure 2-11 illustrates the averaged load-deflection behavior for Fakhruddin's (2022) beams. Analysis of the load-deflection curve revealed a 14.7 percent reduction in stiffness for the 10 percent replacement beam, decreasing from 23.4 kip/in (4.1 kN/mm) to 19.9 kip/in (3.5 kN/mm). Fakhruddin (2022) noted a higher occurrence of cracks in the 10 percent replacement beam, and these cracks propagated more rapidly throughout the member. As the applied load increased, the 10 percent replacement beams exhibited a quicker decrease in stiffness compared to the control beams, evident in the slope of the line up to yield.

The yield point for the control beams was 18.8 percent higher (2.4 kips or 10.46 kN) than that of the 10 percent replacement beams. Notably, no significant difference in deflection between the control and replacement beams at the onset of first cracking and at the point of reinforcement yield occurred; only a change in load was observed. Figure 2-11 visually indicates the control beam exhibiting greater ductility than the 10 percent replacement beams, attributable to the reduced bond capabilities of the mix. The ultimate load of the 10 percent replacement beam decreased by 18.8 percent compared to the control beam.

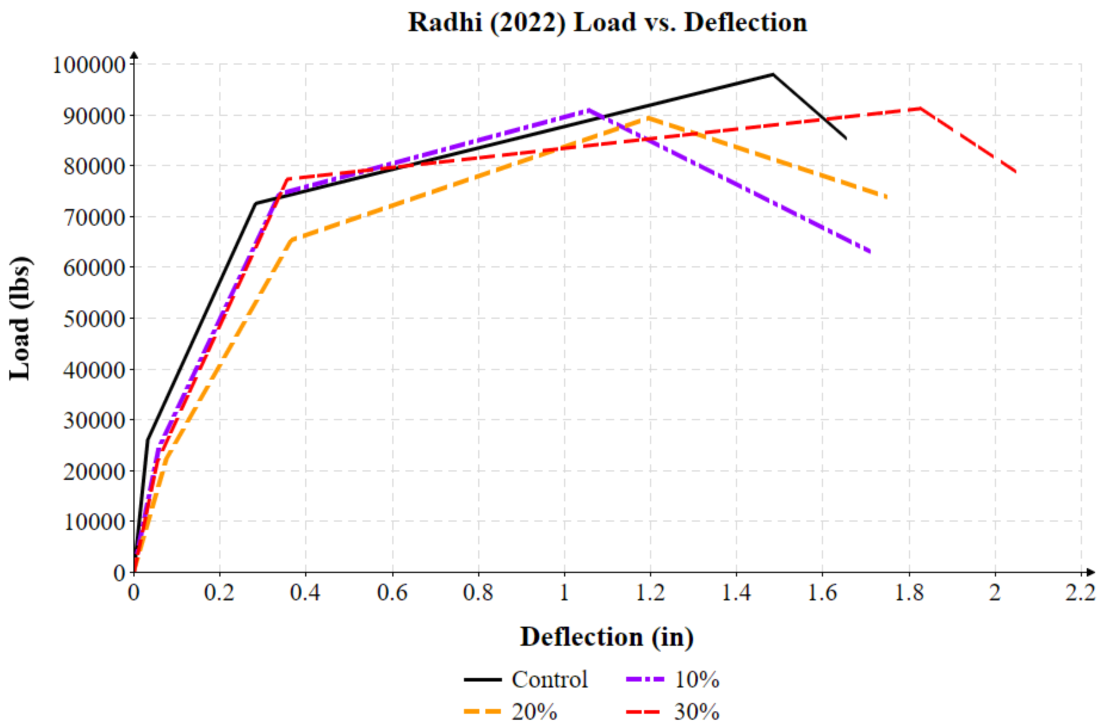

Figure 2-12: Radhi (2022) Beam Specimen Load-Deflection Results

Figure 2-12 illustrates the load-deflection results for Radhi's (2022) beam specimens. Each beam exhibited a linear or semi-linear increase in deflection with the growing load until reaching the first cracking point. At this point, a local drop in load was observed, followed by a subsequent close rise in load. The control beam first cracked at a load of approximately 26.1 kips (116 kN), while the aggregate replacement beams cracked between 21.8 and 24.5 kips (97 and 109 kN).

The tensile steel yielded between 65.2 and 77.3 kips (290 and 344 kN) for all beam types, marking a noticeable change in the slope of the load-deflection curve. A distinguishing factor between the beams lies in their ultimate loads. The control and 30 percent replacement beams steadily increased to their peak loads, at which point the load suddenly dropped, leading to specimen failure. In contrast, the 10 and 20 percent replacement beams experienced a steady decrease in load after reaching their peak loads before eventually failing.

For both Fakhruddin (2022) and Radhi (2022) the following conclusions were made based on the beam tests with plastic coarse aggregate replacement:

1. An increase in plastic aggregate replacement results in a reduction in the stiffness and modulus of elasticity of the concrete, leading to a decrease in the cracking load, yield load, and ultimate load.
2. When designing a member for flexural failure, replacing up to 30 percent of coarse aggregate with plastic does not alter the beam failure mode.

2.5 Flexural Behavior of Reinforced Concrete Beams

Since the beginning of the 1900's, a consistent evolution in the theory of reinforced concrete has occurred. A deeper understanding and significant improvements in the properties of materials have been achieved. Extensive theoretical and experimental investigations have been conducted on the stresses and modes of failure in the common range of reinforced concrete structural elements and assemblies. This thorough exploration has led to increased confidence in calculations, both within the service load range using elastic theory and at the ultimate load of the structure employing ultimate strength theory (Park, 2003). Progress in comprehending material properties and failure mechanisms has facilitated more accurate and reliable assessments in the field of reinforced concrete structures.

Concrete exhibits considerable strength in compression but lacks strength in tension. Typically, the compressive strength of concrete in structures ranges from 3000 to 9000 psi (20–60 MPa), while its tensile strength is usually around 10–15 percent of the compressive strength (Park, 2003). The effectiveness of concrete in structures is achieved by introducing steel reinforcement to provide tensile resistance after concrete cracking. With proper reinforcement, concrete transforms from a relatively brittle material into a composite material with predictable strength in compression, tension, flexure, and shear. The beam flexural capacity depends on several strength parameters including the concrete and reinforcement strengths, the beam cross sectional dimensions, and the tension and compression reinforcements (Arafah, 2000). Currently, two main theories are used to model a beam in flexure, and each has a different design procedure. The theories are working stress design and ultimate strength design or limit state design.

Working stress design, or allowable stress design (ASD), was the earliest method used in the design of reinforced concrete and steel. This design method operates under the assumption that concrete behaves elastically, and elastic interaction between the steel and concrete exists. The key premise is the relationship between loads and stresses remains linear, allowing for a simplified and linear correlation between applied loads and resulting stresses (Rathi, 1964).

Working stress design encounters challenges when closely examining the fundamental structural necessities of strength and serviceability (Allen, 1981). Section 2.5.1 introduces the straight-line theory which is the basis for working stress design.

In engineering today, limit state design is synonymous with ultimate strength design. In practice, ultimate strength theories emerged after the working stress theory to provide a more precise prediction of the behavior of a fixed cross-section under both elastic and inelastic material actions. Then came limit state design which encompasses both ultimate strength and serviceability considerations, offering a comprehensive approach to structural design that addresses various potential failure modes and performance criteria (Allen, 1981). The ultimate strength theories are described in Sections 2.5.2 and 2.5.3.

2.5.1 Straight-Line Theory

The triangular stress distribution is known as the ‘straight-line theory’ or ‘standard theory’ and was one of the earliest working stress theories. The first theoretical analysis of the behavior of reinforced concrete beams was published by Matthias Koenen in 1886. Koenen assumed that the steel alone took the tensile stresses, the neutral axis was at mid-depth of the section, and the concrete above the neutral axis had a straight-line distribution of compressive stress (Park, 2003). In 1894, Edmund Coignet and N. de Tedesco presented the first elastic theory for flexure in a form similar to that used today. Their theory assumed that reinforced concrete obeyed Hooke’s law (Park, 2003). During the 1890s and early 1900s, many rival theories were used to explain reinforced concrete behavior after cracking concrete since it does not strictly obey Hooke’s law. Additionally, a consensus to neglect the tensile resistance of concrete in the engineering community had not occurred. A few of the rival theories to Coignet and Tedesco are shown in Figure 2-13. The linear distribution of concrete stress was advanced by Koenen (1886), Neumann (1890), Coignet and Tedesco (1894), and Melan (1896). Later theories by Thullie (1897), Ritter (1899), Ostenfeld (1902), Talbot (1904), Withey (1907), and Mensh (1914) introduced a non-linear distribution of concrete stress were the basis for ultimate strength design (Hognestad, 1951).

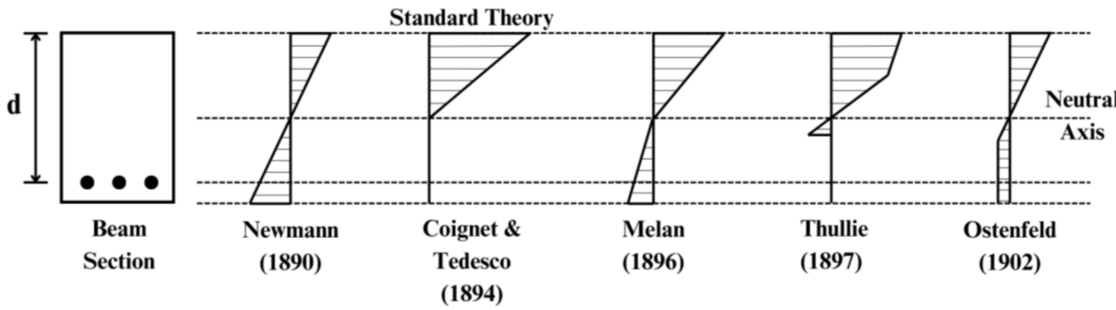

Figure 2-13: Rival Stress Distribution Theories Around 1900

Coignet and Tedesco's straight-line theory obtained general acceptance around 1900 due to its mathematical simplicity (Rathi, 1964). The working stress design methodology uses the straight-line theory where concrete and steel behave as linear-elastic materials with their stresses proportional to the strains. The working stress design assumes that concrete can only resist compression and is ineffective in tension. The assumption is that the stress-strain relation for concrete is a straight line under service loads within the allowable working stresses. The straight-line stress distribution and its parameters are shown in Figure 2-14.

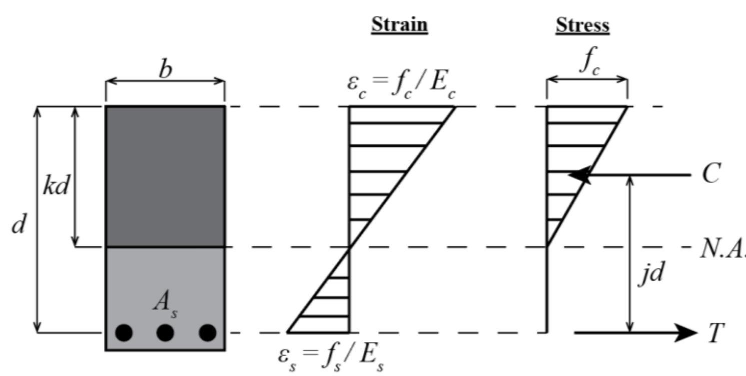

Figure 2-14: Stress-Strain Diagram for a Reinforced Concrete Beam

Figure 2-14 specifies the parameters for the straight-line theory. Using the parameters in Figure 2-14, Equation 2-21 provides the nominal moment capacity when considering the moment about the tension force, while Equation 2-22 presents the nominal moment capacity when taking the moment about the compression force.

$$M = Cjd = \frac{1}{2} f_c k j b_w d^2 \qquad \textbf{Equation 2-21}$$

$$M = Tjd = A_s f_s jd \qquad \textbf{Equation 2-22}$$

where,

$$jd = d - \frac{kd}{3} \quad \rightarrow \quad j = 1 - \frac{1}{3}k \qquad \textbf{Equation 2-23}$$

$$k = \sqrt{2\rho n - (\rho n)^2} - \rho n \qquad \textbf{Equation 2-24}$$

2.5.2 Parabolic Stress Theory

The first introduction of parabolic compression stress blocks for reinforced concrete was in the 1890's with R. M. von Thullie's flexural theory in 1897 and W. Ritter's theory in 1899. These early theories had a goal of explaining and predicting the ultimate strengths of concrete flexural members as viewed in tests (Hognestad et al., 1955). These studies were the discontinued around 1900 when the elastic straight-line theory became accepted in design. Ultimate strength theories began to rise again in the 1930's when it was determined the straight-line theory was not satisfactory for estimating the ultimate strength of reinforced concrete members (Hognestad, 1952).

The performance of reinforced concrete components under high loads is largely determined by whether the initiation of failure is caused by general yielding of the reinforcement. When yielding occurs, failures tend to exhibit substantial ductility, whereas crushing failures tend to be brittle. The ultimate strength of components that fail in this manner is primarily influenced by the properties of the reinforcement, which are well controlled by the manufacturer (Hognestad, 1952). ASTMs establish the minimum reinforcement strength, resulting in no issues with lower than specified strength.

The ultimate strength equations for flexural design are developed based on assumed properties of the materials, equilibrium equations, and compatibility (Hognestad, 1952). Figure 2-15 displays the parameters of the parabolic stress block for a singly reinforced member.

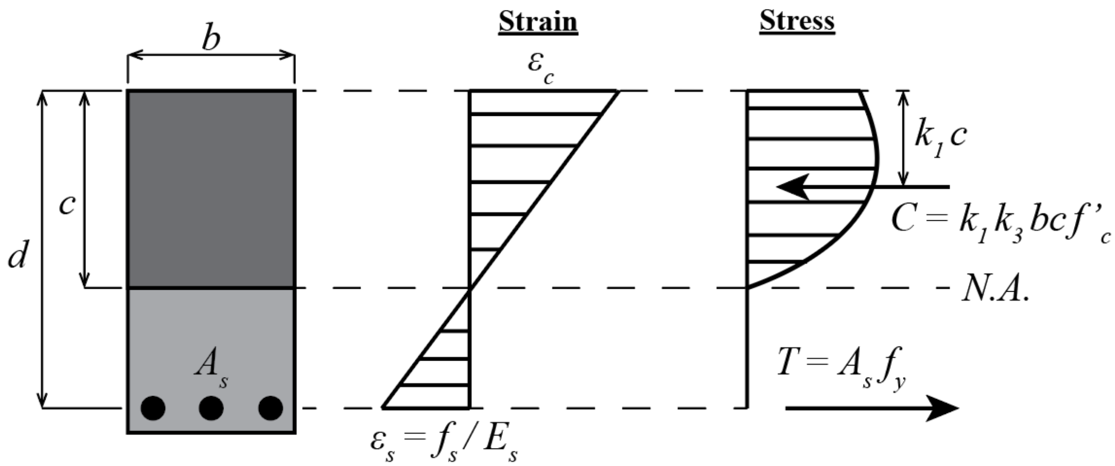

Figure 2-15: Parabolic Stress Design Parameters recreated from Hognestad (1952)

The ultimate moment capacity based on the parabolic stress distribution is expressed as,

$$M_{ult} = A_s\, f_y \left(d - \frac{k_2}{k_1\, k_3} \frac{A_s\, f_y}{b_w\, f_c'} \right)$$ **Equation 2-25**

Measuring stresses at high loads is difficult because the stress is not proportional to the strains. This makes it difficult to predict the stress block. Different methods have been examined such as concentric compression tests, bending-simulation machine, photo elastic methods, stress meters, and testing reinforced concrete members (Hognestad et al., 1955). The

k_1, k_2, and k_3 factors have been studied extensively. These are "coefficients related to the magnitude and position of the internal compressive force in the concrete compression zone" (Hognestad et al., 1955). From reinforced concrete member testing the ultimate moment can be determined and then plugged into Equation 2-25 where the ratio of k_2 to k_1k_3 can be found. Based on reinforced concrete member testing the ratio of k_2 to k_1k_3 has been suggested to be taken as 0.5 to 0.6 (Hognestad et al., 1955). As more testing has been done different equations have been developed based on the age of the concrete and its strength.

2.5.3 Equivalent Stress Theory

To greatly simplify the work required to design rectangular reinforced concrete beams Charles S. Whitney proposed a complete revision of the methods currently used in 1937. The prevailing methods at that time resulted in unnecessarily large and inefficient member sizes. These methods did not accurately represent the compressive strength of concrete, and provide a higher factor of safety against concrete failure than steel failure (Whitney, 1937). The formulas employed in these methods assumed a cracked section and linear variation of stress, which were inadequate for predicting ultimate strength and conditions under working loads (Whitney, 1937).

The usual parabolic formulas are based on the stress variation in the beam followed the shape of the first part of the stress-strain curve for the concrete cylinder up to the point of maximum load. Whitney proposed an equivalent stress block taking the shape of a rectangle, as shown in Figure 2-16, to represent the parabolic area of stress. The stress block has a depth of a and does not extend to the neutral axis as shown for the parabolic and triangular stress blocks. Similarly, to the parabolic stress block, the concrete is assumed to take zero tensile load. ACI 318-19 has adopted this method for determining the design strength of reinforced concrete members.

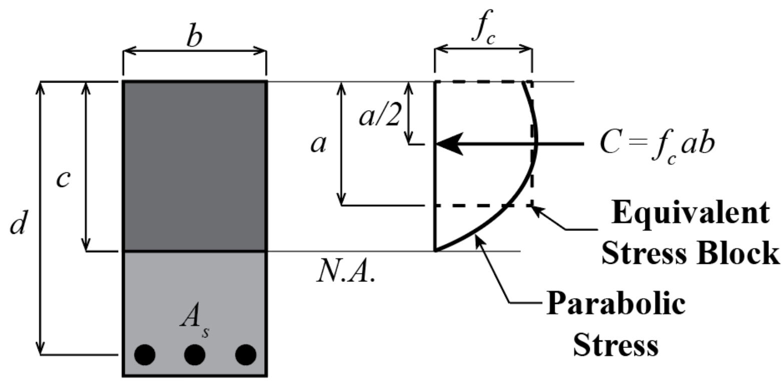

Figure 2-16: Beam Equivalent Stress Block recreated from Whitney (1937)

The equivalent stress block can be used to determine the ultimate capacity of doubly reinforced and singly reinforced sections. The yielding of the tension reinforcement controls the ultimate strength, and the tensile steel stress (f_s) is equal to the yield stress (f_y) at ultimate strength. Figure 2-17 below shows the assumed relations for a rectangular beam under simple flexure.

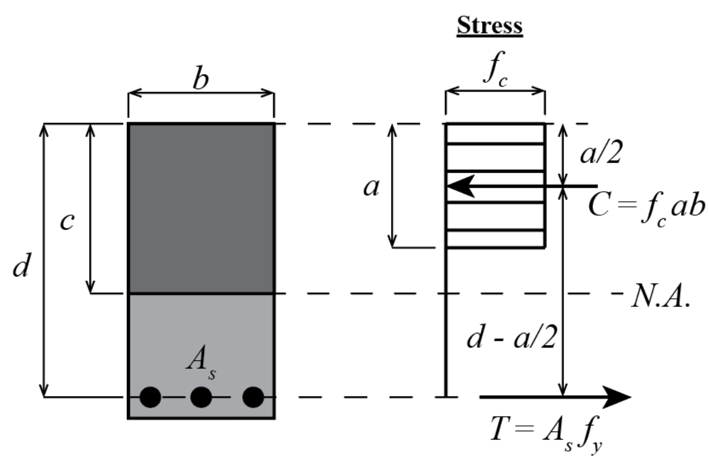

Figure 2-17: Whitney Stress Block Parameters recreated from Whitney (1937)

As the beam is loaded, the concrete will crack starting in the tensile region, and the steel will begin to elongate. As the steel elongates, the depth of the beam in compression, *a*, will decrease until the concrete's unit stress reaches ultimate or *a* equals its limiting value per

Equation 2-27 (Whitney, 1937). Whitney assumed that the ultimate strength of the concrete, f_c, is equal to 85 percent of the corresponding cylinder strength. The bending moment can be calculated as shown in Equation 2-26 at any concrete stress and stress block depth. The ultimate moment capacity is calculated by setting f_c equal to $0.85f'_c$.

$$M = f_c a b_w \left(d - \frac{a}{2}\right) = 0.85 f_c' a b_w \left(d - \frac{a}{2}\right)$$ **Equation 2-26**

where,

$$a = \frac{A_s\, f_y}{0.85 f_c'\, b_w}$$ **Equation 2-27**

$$f_c = 0.85 f_c'$$ **Equation 2-28**

2.5.4 Four-Point Bending Load-Deflection Response

In the experimental phase of this thesis, a four-point simply supported bending test was chosen as the optimal method, particularly suitable for composite materials like reinforced concrete. The key benefit of utilizing a four-point bending test lies in its ability to establish a constant moment region between the point loads. This design ensures that the maximum flexural stress is distributed across the beam section between the two-point loads, mitigating the risk of premature failure caused by stress concentration at a single point. This test produces predictable and easily repeatable results.

Figure 2-18 illustrates the typical load-deflection behavior of a beam in four-point bending. The beam members typically undergo both bending and shear forces. In the pure bending region (between the point loads), only flexural deformation takes place. On the other hand, between the point loads and the supports both flexure and shear coexist, and deformations include both flexural and shear components. Following the initiation of cracks due to external loads, the behavior of reinforced concrete members deviates from that predicted by elastic theory.

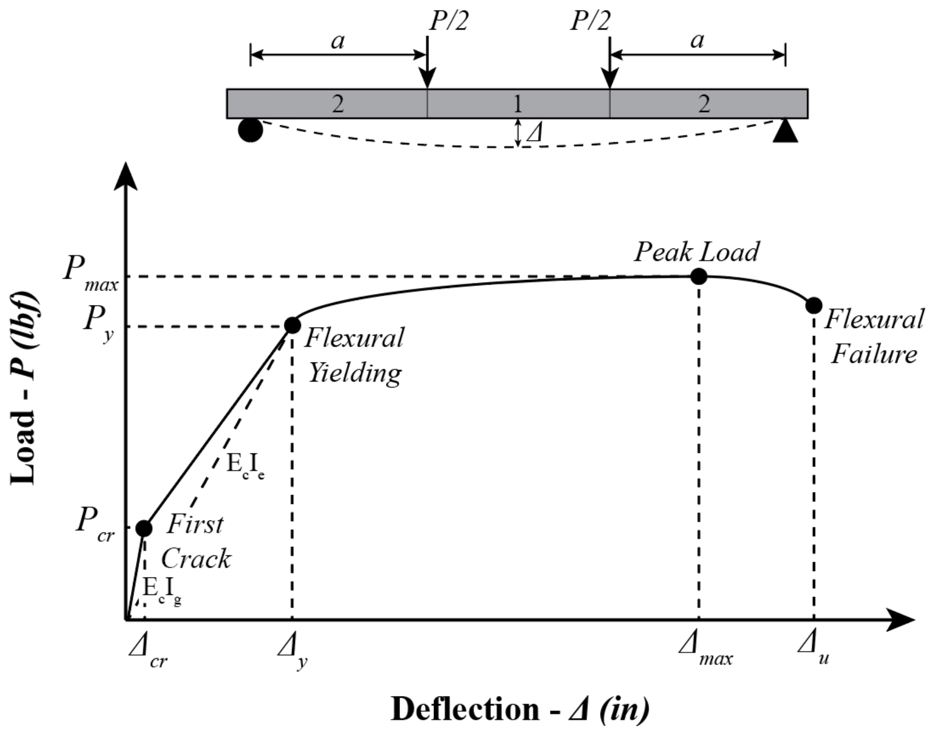

Figure 2-18: Four-Point Bending Typical Load-Deflection Behavior

In many structures, deflection takes precedence over strength as the decisive factor. The stiffness of a member is influenced by both short- and long-term mechanical properties of the concrete, as well as the degree of flexural cracking (ACI 435R, 2020). Consequently, expressions defining parameters such as the modulus of rupture, modulus of elasticity, creep, shrinkage, and temperature effects become essential in predicting the deflection of reinforced concrete members. Furthermore, the stiffness and quantity of reinforcement exert control over the member's stiffness after the occurrence of cracking.

2.5.4.1 Experimental Stiffness and Modulus of Elasticity

During the loading phase, the beam undergoes variations in stiffness attributed to the deterioration of the concrete section. As the beam deflects, the center of the beam will yield at ultimate load, the sections on either side of this region will crack but the steel will not yield, and the ends of the member will be uncracked. The flexural stiffness regions are shown in Figure 2-19. The stiffness was determined based on the elastic portion of the load-deflection curve and used to determine the modulus of elasticity.

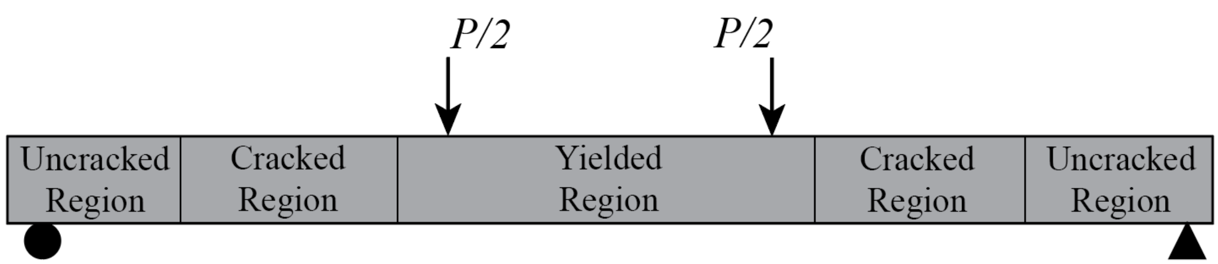

Figure 2-19: Flexural Stiffness Regions in Four-Point Bending

The secant modulus of elasticity was used as the modulus of elasticity of concrete (ACI 435R, 2020). The secant modulus is the slope of a line from the origin to a specified point along the stress-strain or load-deflection curve. The second point is typically taken at $0.45f_c'$ which results in a secant modulus of 4×10^6 psi (28,000 MPa) for normal weight concrete at 28 days (ACI 435R, 2020). For higher-strength concretes boasting compressive strengths surpassing 8000 psi (56 MPa), reported values have been as high as 8×10^6 psi (56,000 MPa) (ACI 435R, 2020). ACI 318 (2019) recommends using Equation 2-13 to compute the secant modulus based on the density of the concrete. According to ACI 435R (2020) and ACI 318 (2019) commentary, a notable level of variation, potentially up to 20 percent, can be anticipated when using a predicted value based on Equation 2-13 or Equation 2-14 in comparison to experimental values.

In utilizing a load-deflection plot to calculate the secant modulus, the stiffness (E_cI_g) can be obtained by measuring the slope of a line from the origin to the first crack, as depicted in Figure 2-18. As E_cI_g is defined as the ratio of force to elastic deformation, Equation 2-29 can be substituted and rearranged to find the secant modulus, as presented in Equation 2-30. Equation 2-29 shows the equation for the deflection between the point loads.

$$\Delta_{midspan} = \frac{P_u\,\alpha}{24E_c\,I}(3L^2 - 4\alpha^2) \qquad \textbf{Equation 2-29}$$

$$E_c = \frac{k\,\alpha}{24I_t}(3L^2 - 4\alpha^2) \qquad \textbf{Equation 2-30}$$

2.5.4.2 Pre-Cracking Region

When the maximum flexural moment under service load in a beam result in a tensile stress lower than the modulus of rupture (f_r) (Equation 2-8), no flexural tension cracks emerge on the tension side of the concrete element, provided the member is unrestrained, and shrinkage and temperature tensile stresses are insignificant. In such scenarios, the effective moment of inertia of the uncracked transformed section (I_t) is applicable for deflection calculations (ACI 435R, 2020). For design purposes, the gross moment of inertia (I_g), disregarding the contribution of reinforcement, can also be utilized with minimal loss of accuracy.

To determine the uncracked transformed moment of inertia the centroid ($\bar{y}$) needs to be determine using Equation 2-31. Then using the parallel axis theorem, the uncracked transformed moment of inertia can be determined by Equation 2-32 (Ugural & Fenster, 2003).

$$\bar{y} = \frac{\sum A_i \bar{y}_i}{\sum A_i} = \frac{A_g\,y_g + (n-1)A_s d}{A_g + (n-1)A_s} \qquad \textbf{Equation 2-31}$$

$$I_t = \sum\left(I_i + A_i(y_i - \bar{y})\right)$$

$$= \frac{1}{12} b_w\, h^3 + A_g\left(y_g - \bar{y}\right)^2 + (n-1)A_s(d - \bar{y})^2$$ **Equation 2-32**

2.5.4.3 Post-Cracking Region

Once the applied loads cause a bending moment resulting in a tensile stress larger than the modulus of rupture the section cracks. The cracking moment is computed using Equation 2-33.

$$M_{cr} = \frac{f_r\, I_t}{y_t}$$ **Equation 2-33**

For four-point bending, cracks begin to develop at the center of the beam and propagate outwards. The cracked moment of inertia (I_{cr}) applies to these cracked sections, while the gross moment of inertia (I_g) pertains to the uncracked sections. As the load increases, more sections of the beam become cracked, leading to a reduction in stiffness. Given that the stiffness of the member changes over time, several methods have been developed to estimate the variations in stiffness caused by cracking along the span. These approaches may involve modifying the flexural rigidity of the member using an average or effective moment of inertia, adjusting the curvature along the span and at critical sections, computing an average curvature or the ratio *M/EI* at each location along the member span, or employing an incremental evaluation of section-curvature (ACI 435R, 2020). Conservatively estimating deflection can be achieved by using the effective stiffness or curvature at the critical section where the member stiffness is at its lowest.

ACI 318-19 presently employs an effective moment of inertia (I_e) approximation formulated by Bischoff (2005). However, before the release of ACI 318-19, Branson's equation from 1965 was the original method utilized by ACI. The effective moment of inertia provides a practical solution that takes into account the random distribution of cracks for all cases including non-uniform members (Branson & Trost, 1982). At crack locations, the concrete essentially carries zero tension. However, between cracks, the concrete actively contributes to resisting tensile stress due to the bond between the reinforcement and concrete. This phenomenon, commonly known as tension stiffening, is considered in the analysis by incorporating the effective moment of inertia (Bischoff & Scanlon, 2007). Tension stiffening has an effect on a members stiffness, deflection, and crack widths under service load conditions (Bischoff, 2005).

Branson's experimental investigation in 1965 lead to the development of Equation 2-34. The exponent, *m*, is some unknown power that varies with the cross-section of the element. By changing the value of *m*, the model can account for the permanent deflection sustained by reinforced concrete members. Branson's experiment consisted of simply supported rectangular beams with a reinforced ratio of 1.65 percent and a stiffness ratio I_g/I_{cr} of about 2.2 (Branson, 1965).

$$I_e = I_g \left(\frac{M_{cr}}{M_a}\right)^m + I_{cr}\left[1 - \left(\frac{M_{cr}}{M_a}\right)^m\right] \leq I_g$$ **Equation 2-34**

Branson (1965) suggested that *m* should equal a value of 4 for a single section of a rectangular or T-beam. Due to the varying stiffness along the beam, 4 was not adequate to describe the average effective moment of the entire span. Branson (1965) then suggested that *m* should be taken a 3 to account for tension stiffening and variation of flexural stiffness along the member. The average effective moment of inertia over the span of a simple reinforced concrete beam is shown in Equation 2-35 (Branson, 1965). The values of I_e is applicable to the transition zone between I_g and I_{cr} as a function of the level of cracking, expressed as M_{cr}/M_a (ACI 435R, 2020).

$$I_e = I_g \left(\frac{M_{cr}}{M_a}\right)^3 + I_{cr}\left[1 - \left(\frac{M_{cr}}{M_a}\right)^3\right] \leq I_g \qquad \textbf{Equation 2-35}$$

Branson's effective moment of inertia method is adequate when calculating immediate deflections for members with reinforcement ratios (ρ) greater than 1 percent (Bischoff, 2005). Once the reinforcement ratio dropped below 1 percent, which is typical for slabs and lightly reinforced concrete beams, issues with Branson's effective moment of inertia equation arise. Along with lightly reinforced members, Branson's equation also underpredicts the immediate deflections for beams with fiber reinforced polymer (FRP) bars. In 2005, Peter Bischoff presented a new effective moment of inertia equation to accurately predict the immediate deflections of beams of all reinforcement ratios and beams with FRP bars.

To derive the new I_e equation, Bischoff used a simple spring model to accurately demonstrate the effect of stiffness variation along a member. From a springs in a series model, where the series is consist of cracked and uncracked springs, the effective stiffness can be determined by taking the average of the inverse stiffness (*1/EI*) and not *EI* (Bischoff, 2005). This discovery led to the change in Branson's equation shown in Equation 2-36.

$$\frac{1}{I_e} = \frac{1}{I_g}\left(\frac{M_{cr}}{M_a}\right)^m + \frac{1}{I_{cr}}\left[1 - \left(\frac{M_{cr}}{M_a}\right)^m\right] \geq \frac{1}{I_g} \qquad \textbf{Equation 2-36}$$

Bischoff (2007) found that m = 2 in Equation 2-36 correlates to Branson's (1965) use of m = 4 in Equation 2-35. Rearranging Equation 2-36 yields Equation 2-37 (Bischoff & Scanlon, 2007).

$$I_e = \frac{I_{cr}}{1-\left(\frac{M_{cr}}{M_a}\right)^2\left(1-\frac{I_{cr}}{I_g}\right)} \leq I_g$$ **Equation 2-37**

Equation 2-37 is not the final ACI 318-19 code equation which includes two-thirds multiplied by M_{cr} (shown in Equation 2-38). M_{cr} is multiplied by two-thirds to account for restraint factors that can diminish the effective cracking moment. Additionally, this adjustment considers the reduced tensile strength of concrete during construction, which may lead to cracking affecting service deflections at a later stage (Scanlon & Bischoff, 2008).

$$I_e = \frac{I_{cr}}{1-\left(\frac{\frac{2}{3}M_{cr}}{M_a}\right)^2\left(1-\frac{I_{cr}}{I_g}\right)} \leq I_g$$ **Equation 2-38**

The cracked moment of inertia used in the effective moment of inertia calculations can be calculated as follows:

$$I_{cr} = \frac{1}{3} b_w \, \bar{y}_{cr} + n \, A_s (d - \bar{y}_{cr})^2$$ **Equation 2-39**

2.5.4.4 Post-Yield Region

Once the tensile steel yields, the section is considered to be fully cracked, and I_{cr} (per Equation 2-39) is utilized. This assumption has been verified for accuracy, as the effective moment of inertia, I_e, of the section beyond yielding, obtained through nonlinear analysis considering tension stiffening, is found to be comparable to or less than that of I_{cr}. In accordance with ACI 318-19, the yield point is regarded as the failure point for reinforced concrete members in flexure. Consequently, the moment equations employed in design are formulated to achieve tensile yielding of the steel within the member. This design approach recognizes that the yield point marks a critical condition, and the equations are tailored to ensure the structural integrity and safety of the reinforced concrete elements, considering the behavior of the steel reinforcement under tensile loading.

2.6 ACI 318-19 Beam Design

The following section outlines the flexural design steps and equations specified in ACI 318-19, which were employed for the preliminary sizing of reinforced concrete beams in this thesis. Additionally, the process of checking the flexural capacity predictions against the American standard is addressed. While the beams were primarily controlled by flexure, the shear strength of the members was also assessed in accordance with ACI 318-19. Based on ACI 318-19 Section 22.5, it was determined that the shear strength of the concrete beam was adequate. All safety factors were excluded from preliminary and final strength calculations.

2.6.1 Flexural Design

In reinforced concrete, flexural tension failure occurs when a structural element, beam or slab, undergoes bending forces. Flexural tension is experienced on the lower side of the element, tension face, for simply supported members. In reinforced concrete structures, steel reinforcement is utilized to counteract tensile forces, particularly those induced by flexural tension. The process of flexural tension failure generally unfolds in distinct stages: cracking, propagation of cracks, and ultimate failure.

The reinforcement plays a crucial role in resisting tensile forces and preventing catastrophic failure. The flexural strength, or modulus of rupture, serves as a vital parameter for comprehending and designing for flexural tension in reinforced concrete members alongside the compressive strength of the mixture.

The strain in the extreme compression fiber strain limit (ε_u) is assumed to be 0.003 per ACI 318-19 Section 22.2.2.1. The strain limit is the corresponding *x*-axis value to Whitney's (1937) assumed uniformly distributed equivalent compression stress of $0.85f_c'$ (Wang & Quayyum, 2023). The strain in the tensile reinforcing steel can be determined by Equation 2-40 as stated in ACI 318-19 Section 21.2.2.1. The modulus of elasticity in the steel (E_s) is the theoretical value of 29,000 ksi (200 GPa) and the yield strength of the reinforcement is based on the grade of the steel. For grades 60, 70, and 80 of deformed reinforcement the equivalent yield strains are 0.00207, 0.00241, and 0.00276 respectively.

$$\varepsilon_{ty} = \frac{f_y}{E_s} \qquad \textbf{Equation 2-40}$$

The value of the net tensile strain (ε_{ty}) determines the safety factors used in the design of axial and flexural reinforced concrete members. A tension-controlled section is more ductile than a compression controlled or transition section which provides a warning of failure by excessive cracking and deflection. A compression-controlled section is a brittle failure, due to the concrete crushing before the steel yields, giving little warning before failure. ACI 318 defines a section as tension-controlled when the strain the tension reinforcement is greater than $\varepsilon_{ty} + 0.003$, a section is compression controlled when the strain is less than ε_{ty}, and for any value between the two condition is considered the transition zone (*ACI 318*, 2019). Since tension-controlled sections have a ductile failure the safety factor (ϕ) used in design is 0.9 while a compression-controlled section has a safety factor (ϕ) of 0.65. The correlation between the safety factors used in design and the net tensile strain in the steel is shown in Figure 2-20.

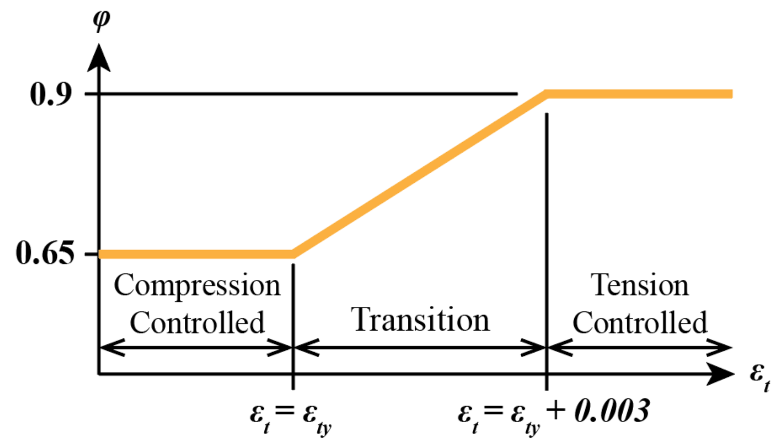

Figure 2-20: Variation of Strength Reduction Factors with Net Tensile Strain in Steel recreated from ACI 318-19

ACI 318-19 Section 22.2.2.4 allows for the use of the equivalent rectangular concrete stress distribution, providing a simplified approach for parabolic stress design. Section 2.5.2 highlights the suitability of the parabolic stress block, especially in high-strain scenarios where stress and strain are not proportional. Given ACI's focus on designing to steel yielding and the non-linear stress-strain relationship not being considered, the equivalent stress block emerges as a suitable method of analysis. A reinforced concrete beam section’s strain, stress, and internal force diagram with ACI 318-19 parameters is shown in Figure 2-21.

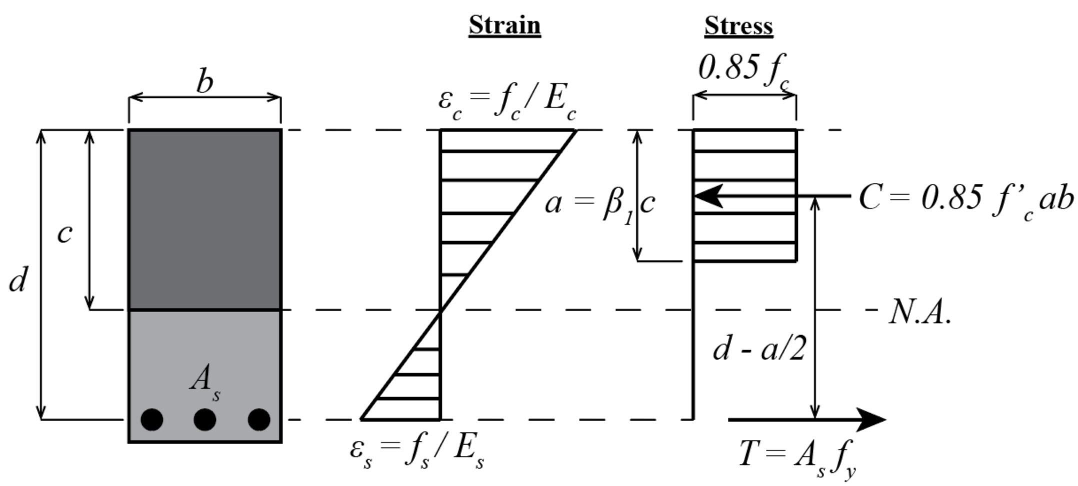

Figure 2-21: ACI 318-19 Beam Section Parameters

The depth of the equivalent stress block (a) is defined in Equation 2-41 and is ACI 318-19 Equation 22.2.2.4.1. The neutral axis depth can be determined by solving Equation 2-41 for c. The β_1 factor is defined in Equation 2-42 which is an adjustment factor for the equivalent stress distribution based on the design strength of the concrete to account for the variates in the parabolic shape for higher strength concrete. When $f_c' \leq 4000$ psi then $\beta_1 = 0.85$ and for mixes greater than 8000 psi $\beta_1 = 0.65$ (Darwin et al., 2015).

$$a = \beta_1 c = \frac{A_s f_y}{0.85 f_c' b_w} \qquad \textbf{Equation 2-41}$$

β_1 according to Table 22.2.2.4.3:

$$\beta_1 = 0.85 - \frac{0.05(f_c' - 4000)}{1000} \quad \text{and} \quad 0.65 \leq \beta_1 \leq 0.85 \qquad \textbf{Equation 2-42}$$

The nominal moment capacity is obtained by summing the moments about the centroid of the compression force (Equation 2-43).

$$M_n = A_s f_y \left(d - {}^{a}/_{2}\right) \qquad \textbf{Equation 2-43}$$

ACI 318-19 Section 9.6.1 outlines minimum reinforcement requirements aiming to create a beam capable of sustaining loading even after flexural cracking, allowing for visible cracking and deflection (*ACI 318*, 2019). This provision serves as an early warning of potential overload conditions. The minimum reinforcement required per ACI 318-19 is shown in Equation 2-44.

$$A_{s,min} = \frac{3\sqrt{f_c'}}{f_y} b_w d \geq \frac{200 b_w d}{f_y} \qquad \textbf{Equation 2-44}$$

Chapter 3 - Test Setup and Procedure

3.1 Introduction

This chapter covers the formulation of the concrete mixture, design of specimens, their fabrication, and the test setup. The results of these tests are analyzed and expounded upon in Chapter 4. Specimen fabrication, curing, and material strength testing all conform with the guidelines in ASTM C31 Standard Practice for Making and Curing Concrete Test Specimens in the Field.

3.2 Mix Design

Two distinct replacement amounts were investigated to collect data on the effects of increasing the amount of recycled coarse aggregate replacement. The control mixture design was formulated upon a conventional commercial 4000 psi (27.6 MPa) normal-weight interior mix by Midwest Concrete Materials (MCM). In Table 3-1, the material classifications, quantities, specific gravities, and the individual volumes for the baseline mixture are detailed. The control mixture incorporated natural river rock as the coarse aggregate and was tailored to yield one cubic yard of concrete. In contrast, the replacement mixtures employed Plazrok at two different rates: 15 percent and 30 percent as replacements for the coarse aggregate by volume.

Table 3-1: Control Mix Design

CONTROL MIX					
Material Type	**Description**	**Quantity**		**Specific Gravity**	**Volume (ft^3)**
Cement	Ashgrove Type I/II Cement	564	lbs	3.15	2.87
Fine Aggregate	MCM KP Fine Aggregate	2054	lbs	2.63	12.52
Coarse Aggregate	Bayer Zeandale ASTM 57/67 - CA5	1094	lbs	2.60	6.74
Water	Water	30.4	gal	1.00	4.06
Replacement Aggregate	**Plazrok by Enviroplaz**	**0**	**lbs**	**0.70**	**0.00**
Admixture	Grace Mid-Range Water Reducer	25	lq. oz.	-	-
	Air Content	3.00%			0.81
	Total:	**3966**	lbs		**27.00**

Initial mixture quantities were determined according to the mixture design specifications outlined by MCM. Table 3-2 exhibits the preliminary quantities for each component of the mixture. These mixture quantities facilitated the preparation of the Plazrok prior to the arrival of the concrete truck on-site, where the Plazrok was subsequently introduced into the truck. Upon arrival, the truck incorporated the coarse aggregate replacement into the batched mixture through 70 rotations and added water until achieving a six-inch slump. Each mixture was mixed in a concrete truck and yielded one cubic yard of concrete.

Table 3-2: Preliminary Mix Designs

Mix		Cement		Fine		Coarse		Plazrok		Water		Admixture		Total	
Control	Quantity	564	lbs	2054	lbs	1094	lbs	0	lbs	30.4	gal	25	lq. Oz.	**3966**	**lbs**
	Volume	2.87	ft^3	12.52	ft^3	6.74	ft^3	0	ft^3	4.06	ft^3	-		**27**	**ft^3**
15% Replacement	Quantity	564	lbs	2054	lbs	929.9	lbs	44.2	lbs	30.4	gal	25	lq. Oz.	**3846**	**lbs**
	Volume	2.87	ft^3	12.52	ft^3	5.73	ft^3	1.01	ft^3	4.06	ft^3	-		**27**	**ft^3**
30% Replacement	Quantity	564	lbs	2054	lbs	765.8	lbs	88.4	lbs	30.4	gal	25	lq. Oz.	**3726**	**lbs**
	Volume	2.87	ft^3	12.52	ft^3	4.72	ft^3	2.02	ft^3	4.06	ft^3	-		**27**	**ft^3**

MCM's batching process does not precisely replicate the designated mixture design, resulting in a deviation from the intended 15 or 30 percent coarse aggregate replacement. The actual batched mixtures are provided in Appendix A and summarized in Table 3-3. Upon analysis, it was determined that for the 15 percent and 30 percent replacement mixtures, the actual coarse aggregate replacement rates based on the batching process were still accurate to a hundred of a percent.

Table 3-3: Actual Batched Mix

Mix		Cement		Fine		Coarse		Plazrok		Water		Admixture		Total	
Control	Quantity	590	lbs	2120	lbs	1120	lbs	0	lbs	26.4	gal	24	lq. Oz.	**4050**	**lbs**
	Volume	3	ft^3	12.91	ft^3	6.9	ft^3	0	ft^3	3.53	ft^3	-		**27.15**	**ft^3**
15% Replacement	Quantity	570	lbs	2120	lbs	940	lbs	44.2	lbs	23.3	gal	25	lq. Oz.	**3869**	**lbs**
	Volume	2.9	ft^3	12.91	ft^3	5.79	ft^3	1.01	ft^3	3.11	ft^3	-		**26.53**	**ft^3**
30% Replacement	Quantity	560	lbs	2140	lbs	760	lbs	88.4	lbs	23.2	gal	24	lq. Oz.	**3742**	**lbs**
	Volume	2.85	ft^3	13.03	ft^3	4.68	ft^3	2.02	ft^3	3.1	ft^3	-		**26.49**	**ft^3**

3.2.1 Materials

MCM utilizes Type I/II cement, locally sourced fine and coarse aggregates, and mid-range water reducer for components for their interior mixture design. Collaborating with the Civil Engineering Department at Kansas State University, MCM obtained the control mixture and determined the replacement ratio for coarse aggregates. Once the truck was on-site, water was introduced to achieve a mixture with a six-inch (152 mm) slump enhancing its workability. This increased workability facilitated the flow of the mixture around the rebar upon placing it into the beam molds. Figure 3-1 displays the Plazrok, used as coarse aggregate replacement, contained within the bags received from Enviroplaz. Further details regarding the coarse aggregate gradation can be found in Section 3.2.2.

Figure 3-1: Plazrok (Coarse Aggregate Replacement)

In each beam, two #3 ASTM A615 Grade 60 bars were employed as flexural reinforcement. These bars were positioned with a two-inch (51 mm) cover at the bottom and 1-1/2 inches (38 mm) of cover on the sides. The decision to utilize a two-inch (51 mm) cover at the bottom was influenced by the availability of reinforcement chairs. To ensure precision in determining the yield strength of reinforcement, rebar testing was conducted in accordance with the procedures outlined in ASTM E8/E8M-16a, as described in Section 3.5.4 of this report.

3.2.2 Aggregate Gradation (ASTM C136/C136M, 2019)

MCM procures ASTM 57/67 stone material from a local supplier. The natural stone meets the grading specifications outlined in ASTM C33/C33M-18 Standard Specifications for Concrete Aggregates Table 3 (ASTM C136/C136M, 2019). Both the natural and Plazrok coarse aggregate underwent sieving processes and passed through a 1-1/2-inch (38 mm) and 1-inch (25 mm) sieves, as detailed in Table 3-4. The natural coarse aggregate exhibited a size range from 3/4 of an inch (19 mm) to a number 8 mesh size, which is 0.0937 inches (2.4 mm). Conversely, the Plazrok was uniform and ranged in size from 3/4 of an inch (19 mm) to 3/8 of an inch (9.5 mm).

Table 3-4: Percent of Coarse Aggregate Passing through Sieve

Coarse Agg. Type	Size of Sieve							
	1-1/2 in	1 in	3/4 in	1/2 in	3/8 in	No. 4	No. 8	No. 16
Natural	100.0%	100.0%	90.5%	49.5%	28.0%	4.0%	0.5%	0.0%
Plazrok	100.0%	100.0%	100.0%	65.8%	0.0%	0.0%	0.0%	0.0%

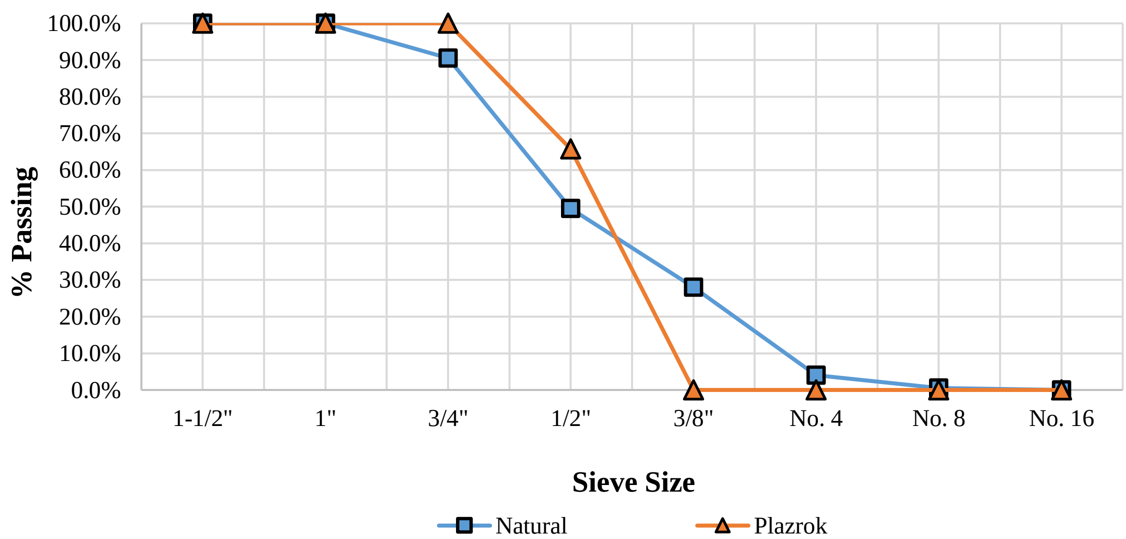

Figure 3-2: Coarse Aggregate Average Grading

3.3 Specimen Design

The specimens were designed to adhere to the stipulations outlined in the ACI 318-19 code requirements. Design assumptions were established concerning both the concrete and reinforcement strengths. A series of iterations were conducted to determine the optimal dimensions for the members to be tested, ensuring that the specimens met the necessary criteria outlined in the code.

3.3.1 Design Assumptions and Preliminary Computations

Several design assumptions were established to configure the experiment. A typical 4000 psi (27.6 MPa) interior mix was obtained from MCM and employed for initial beam sizing calculations. The reinforcement was assumed to be ASTM A615 Grade 60 steel, possessing a yield strength of 60 ksi (414 MPa). Considering the increased use of higher strength recycled steel when producing reinforcement, a yield strength of 60 ksi (414 MPa) is conservative for predicting the ultimate capacity of the beams since the yield strength will be higher than 60 ksi (414 MPa). The bottom cover was assumed to be 1-1/2 inches (38 mm) in accordance with ACI 318-19 Table 20.5.1.3.1 (*ACI 318*, 2019). The selection of a 4-foot (1.2 m) bar was based on the availability of spreader bars in the laboratory, which was used to determine the required loading.

Preliminary computations were done to ascertain the optimal length and cross-section of the flexural members. Utilizing the assumed properties described earlier, cross-sections were determined for clear span lengths of 18-foot (5.5 m), 15-foot (4.6 m), and 12-foot (3.7 m). ACI 318-19 Table 9.3.1.1 provided a minimum depth for simply supported non-prestressed beams. Upon establishing the height of the members, the depth of the reinforcement was computed by subtracting the cover from the overall height of the member. A depth-to-width ratio of 1.75 was employed to determine the minimum beam width.

Conforming to the minimum flexural requirements outlined in ACI 318-19 Section 9.6.1.2, Equation 2-44 was used in designing the beams with minimal flexural steel (*ACI 318*, 2019). Given that each specimen adhered to minimum steel requirements, the sections were categorized as tension-controlled, signifying that the bars will yield before the concrete crushes.

3.3.2 Specimen Geometry and Reinforcement

Following trials involving the three clear span lengths, a clear span of 12 feet (3.7 m) was selected based on various factors including available space in the lab, beams maneuverability, material quantities, and the force required to attain the ultimate capacity of the members. The beams were designed to be 6 inches (152 mm) wide and 10 inches (254 mm) deep, with an effective depth of 8 inches (203 mm), as depicted in Figure 3-3. Tensile reinforcement at the bottom of the members consisted of two number three bars.

After finalizing the member size, the shear strength was checked per ACI 318-19 Section 9.6.3 (*ACI 318,* 2019). This evaluation concluded that shear stirrups were not necessary to prevent a shear failure.

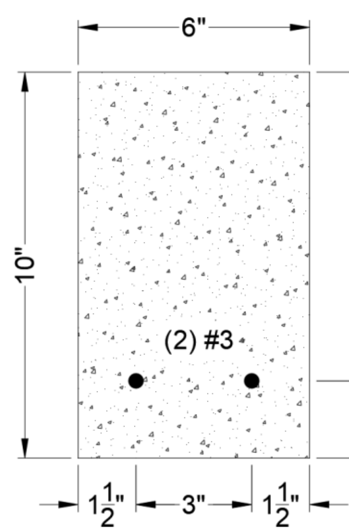

Figure 3-3: Beam Cross-Section

3.4 Specimen Fabrication

3.4.1 Beam Molds

Molds were designed and constructed to achieve the desired 6-inch (152 mm) by 10-inch (254 mm) cross-section. To facilitate ease of reuse after each pour, these molds were constructed from three-quarter-inch melamine sheets, which are particle boards coated in durable thermosetting plastic. The choice of these sheets was intentional to enable efficient cleaning and multiple reuses. Each mold was planned for three usages, once for each mix.

To counter the pressure exerted by the fresh concrete and prevent the sides from bowing out, external braces were incorporated onto the molds. Additionally, thin waterproof tape was applied to prevent any leakage or loss of water, preserving the integrity of the particle board, and ensuring the molds' reusability. The setup for the specimen molds was positioned in a location where they could remain stationary for 24 hours, complying with the guidelines outlined in ASTM C31/C31M-22 Standard (ASTM C31/C31M, 2022).

Before installing the flexural rebar, the molds were cleaned and coated with a concrete formwork release agent per ASTM C31 Section 5.1 (ASTM C31/C31M, 2022). Once cleaned, the cut-to-length flexural reinforcement was positioned on two-inch (51 mm) rebar stands (chairs) providing a 1-1/2-inch (38 mm) cover from each perpendicular face. The 1-1/2-inch (38 mm) cover was used on the sides per ACI 318-19-member cover requirements. The assembled and cleaned molds, along with the prepared flexural reinforcement, are depicted in Figure 3-4.

Figure 3-4: Constructed Molds

3.4.2 Pouring Specimens

The concrete delivery from MCM was received on-site and, upon arrival, underwent the necessary addition of coarse aggregate replacement as required. The pouring process commenced following the *ASTM C31 Standard Practice for Making and Curing Concrete Test Specimens in the Field*. To achieve the desired slump of 6 to 8 inches (152 to 203 mm), careful monitoring and adjustments were made during the pouring process.

The slump test, conducted in accordance with *ASTM C143/C134M-15a Standard Test Method for Slump of Hydraulic-Cement Concrete*, used a one-foot-tall (305 mm) slump cone A samples were taken at the beginning of and after the pour to provide an accurate representation of the entire batch (ASTM C143/C143M, 2015). The slump cone was filled in three sections and each layer was rodded 25 times each (ASTM C143/C143M, 2015). Figure 3-5 illustrates an example of the slump tests performed.

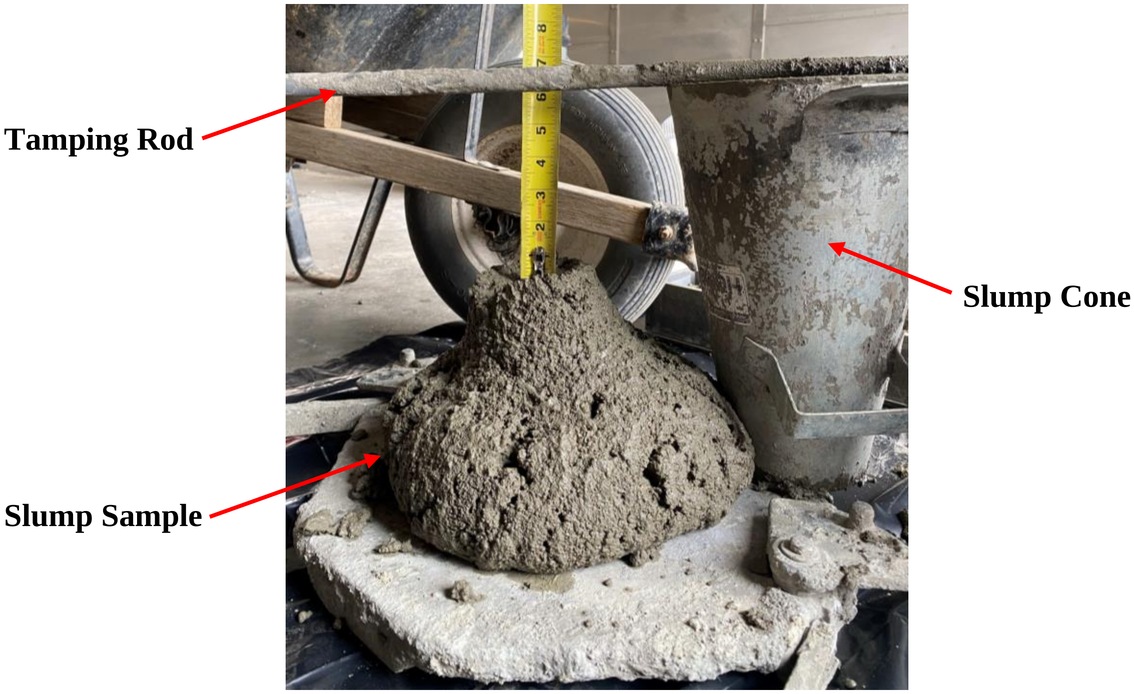

Figure 3-5: Control Mix Slump Test

The concrete for the beams was placed in layers to allow the distribution of concrete using a tamping rod prior to consolidation with the vibrator (ASTM C31/C31M, 2022). The utilization of a Milwaukee 2910-20 M18 internal vibrator facilitated the consolidation of each of the beams after pouring, followed by the finishing of the beam surfaces with a trowel. The Plazrok made the top surface of the beam difficult to finish due to it wanting to float on the surface of the member. Figure 3-6 visually depicts the sequential process: layer pouring (on the left), consolidation via vibration, and surface finishing.

Figure 3-6: Pouring & Consolidating the Beams

Three samples were extracted from each mix to assess the hardened concrete properties as required in ASTM C31. Hardened concrete testing conformed to ASTM C39, ASTM C496, and ASTM C78. The molds required for the hardened properties tests are shown in Figure 3-7 below. The concrete samples were mixed, poured, and cured in the same environment as the beams to mitigate potential environmental variations that could impact the test outcomes.

Figure 3-7: Concrete Molds for Hardened Concrete Testing

3.4.3 Specimen Curing

Given the size of the beams, the use of a moist room for regulating the moisture levels during the curing process was not feasible. All specimens, including additional samples, were cured according to ASTM C31. As the concrete pouring of the specimens occurred during the winter season, measures were taken to maintain the curing temperature within the optimal range of 60°F and 80°F [16°C and 27°C]. This was achieved by pouring concrete within a heated metal building (ASTM C31/C31M, 2022).

Following the concrete placement, the specimens were immediately covered with black plastic sheets to effectively manage moisture loss, a process visually depicted in Figure 3-8. To accommodate the constraints of laboratory timeframes, the beams were cured for two to three days before removing the molds in preparation for subsequent pours, as illustrated in Figure 3-9.

After a minimum curing period of three weeks, all specimens were transported on a flatbed trailer three miles to the laboratory for further evaluation. The specimens were cured for at least 28 days, ensuring compliance with standard curing durations, and were tested prior to reaching a maximum of 56 days to maintain the integrity of the results. The control specimens were 35 days old; 15 percent replacement specimens were 43 days old, and 30 percent were 39 days old at the time of testing.

Figure 3-8: Curing of Samples

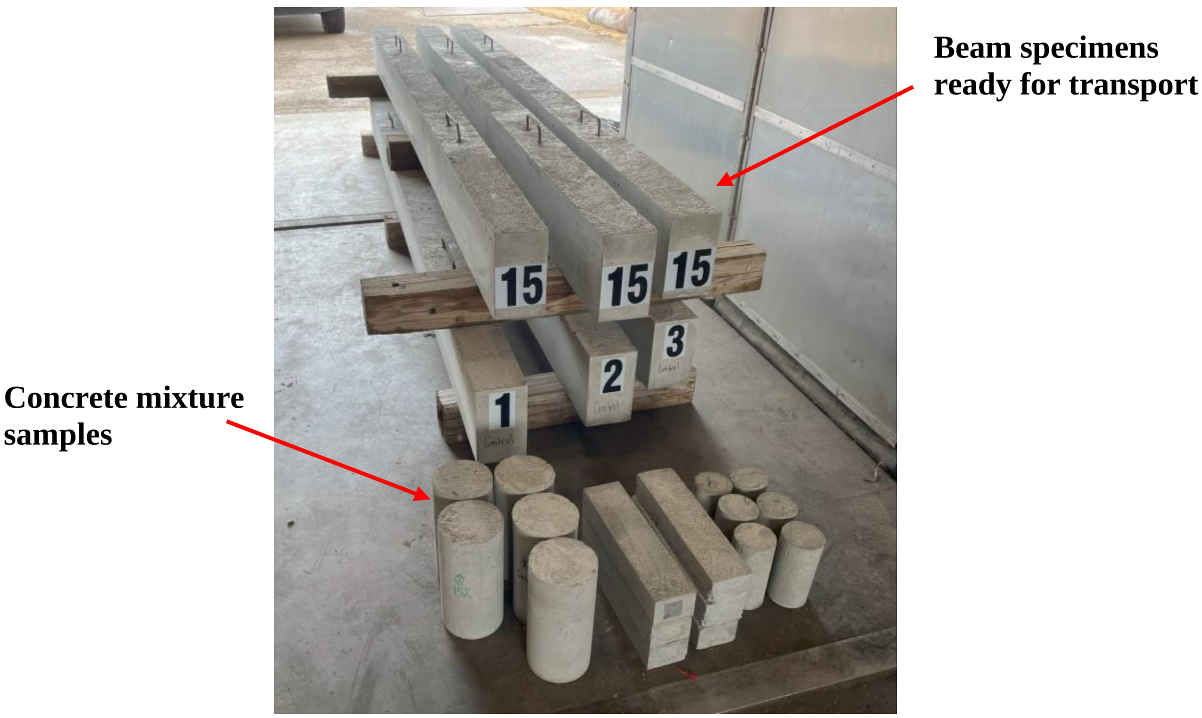

Figure 3-9: Specimen Storage

3.5 Material Strength Test Setup

This section outlines the prerequisites and experimental configurations essential for conducting four distinct tests: the ASTM C39 compression test, ASTM C496 tensile splitting test, ASTM C78 modulus of rupture test, and ASTM C370 reinforcement ultimate strength test. Each test was designed to predict and assess the anticipated behavior of the concrete beams. The compression, tensile splitting, and modulus of rupture, and reinforcement ultimate strength tests were conducted prior to the initial beam testing to facilitate accurately predicting the concrete beams' behavior at the time of testing to failure.

3.5.1 Compressive Test Setup (ASTM C39/C39M, 2021)

Compressive strength testing was performed using a Forney 250 Series Compression Machine equipped with Automatic Controls and Standard Frame adhering to the procedures stipulated in the ASTM C39/C39M-21 Standard Test Method for Compressive Strength of Cylindrical Concrete Specimens. The Forney machine applied a stress rate ranging from 35 psi/s ± 7 psi/s [241 kPa/s ± 48 kPa/s] applied to the 4 inch (102 mm) diameter by 8 inch (203 mm) tall cylinders (ASTM C39/C39M, 2021). Test specimens were prepared and cured per ASTM C31, as detailed in Section 3.4. Metal caps were affixed to both ends of the cylinders before placing and alignment in the testing machine. For each mix, three cylinders were subjected to testing to derive an average compressive strength representative of the respective concrete mixes. A visual representation of the test setup, including pre and post-test images, is illustrated in Figure 3-10.

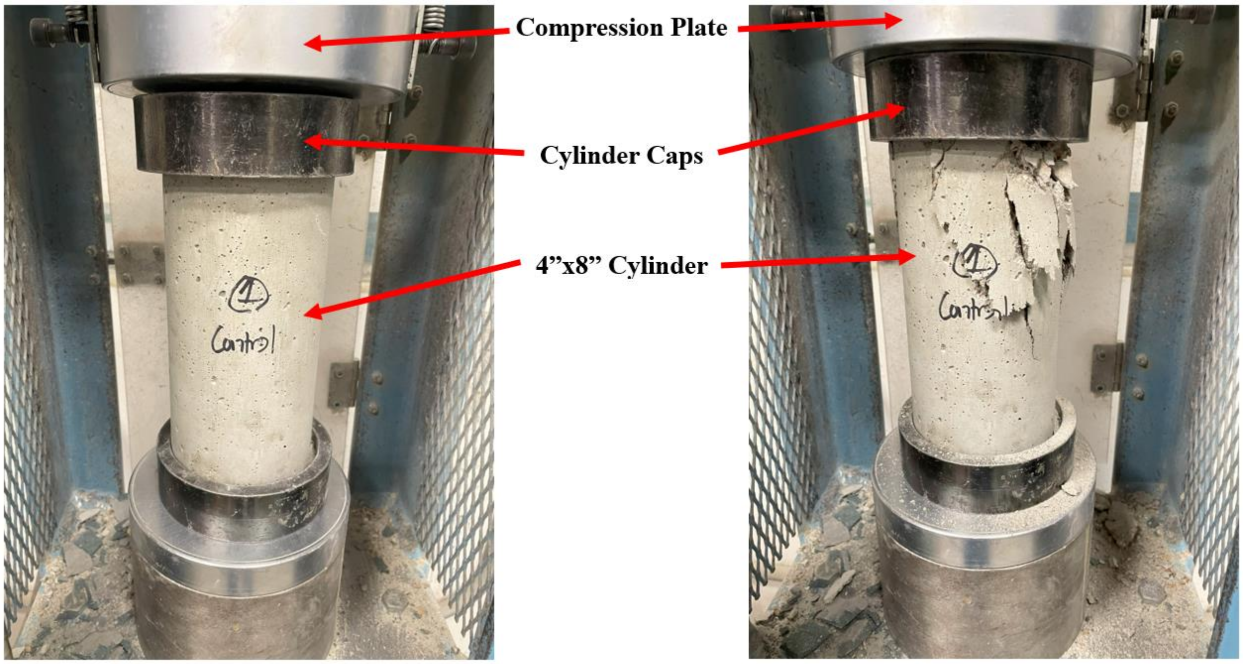

Before **After**

Figure 3-10: Compression Test Setup and Failure

3.5.2 Tensile Splitting Test Setup (ASTM C496/C496M, 2017)

The tensile splitting tests were conducted utilizing a Baldwin Southwark Tate-Emery Universal Tensile/Compression Tester as stipulated in ASTM C496/C496M-17 Standard Test Method for Splitting Tensile Strength of Cylindrical Concrete Specimens. For each of the three concrete mixtures, three specimens, 6-inch (152 mm) diameter by 12-inch (305 mm) tall cylinders, were prepared and cured, as described in Section 3.4. The tensile splitting tests consisted of applying a compressive force along the length of the cylinders until failure occurred (ASTM C496/C496M, 2017). Figure 3-11 depicts the testing apparatus utilized, meeting the prescribed criteria in the ASTM C496 standard. The cylinders were aligned in the center of the load cell. The load was subsequently applied at a consistent rate, maintained between 100 to 200 psi/min (289 to 1,379 kPa/min) (ASTM C496/C496M, 2017). The failures observed during the testing exhibited a consistent pattern resembling the failure mode portrayed in Figure 3-12.

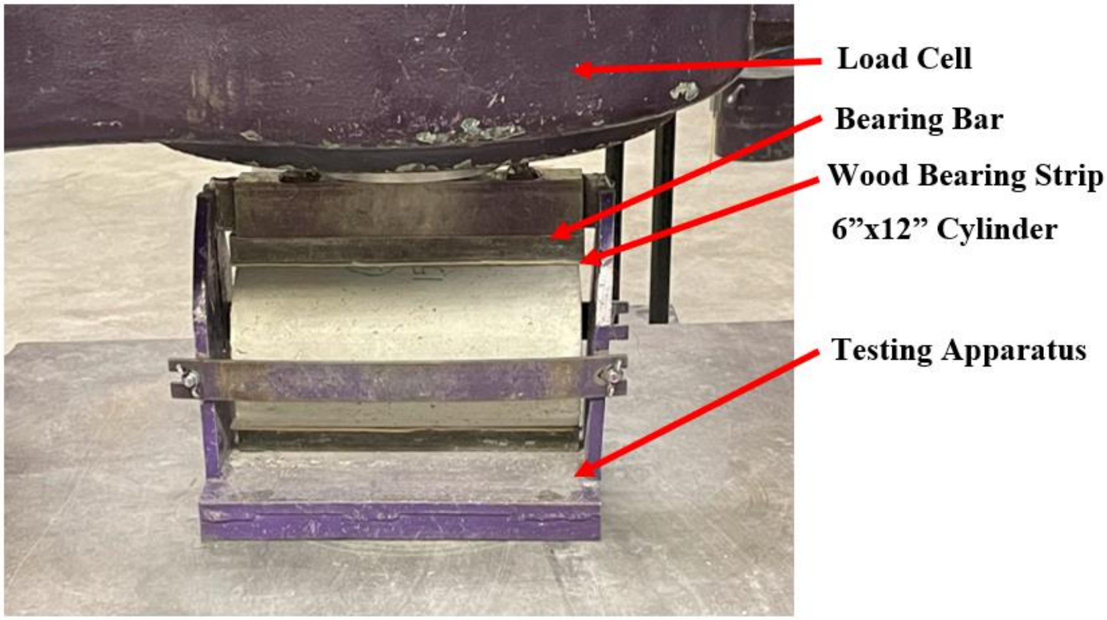

Figure 3-11: Tensile Splitting Test Setup

Figure 3-12: Tensile Splitting Failure

3.5.3 Modulus of Rupture Test Setup (ASTM C78/C78M, 2022)

The Modulus of Rupture tests were performed on a Forney LA-270 Series Beam Tester Compression Machine with Manual Controls and Standard Frame following the guidelines outlined in ASTM C78/C78M-22 Standard Test Method for Flexural Strength of Concrete (Using Simple Beam with Third-Point Loading). Three, 4-inch (102 mm) by 3-inch (76 mm) by 16-inch (406 mm), prisms were prepared for each mix (ASTM C78/C78M, 2022).

For the testing setup, the prisms were positioned on supports 15 inches (381 mm) apart from the centerline of the load cell, as shown in Figure 3-13. The force was applied by the load cell to the spreader bar with a spacing of 5 inches (127 mm) between point loading on the beam (ASTM C78/C78M, 2022). The load was applied at a consistent rate ranging between 125 to 175 psi/min [0.9 to 1.2 MPa/min] per ASTM C78, aiding in the determination of the modulus of rupture.

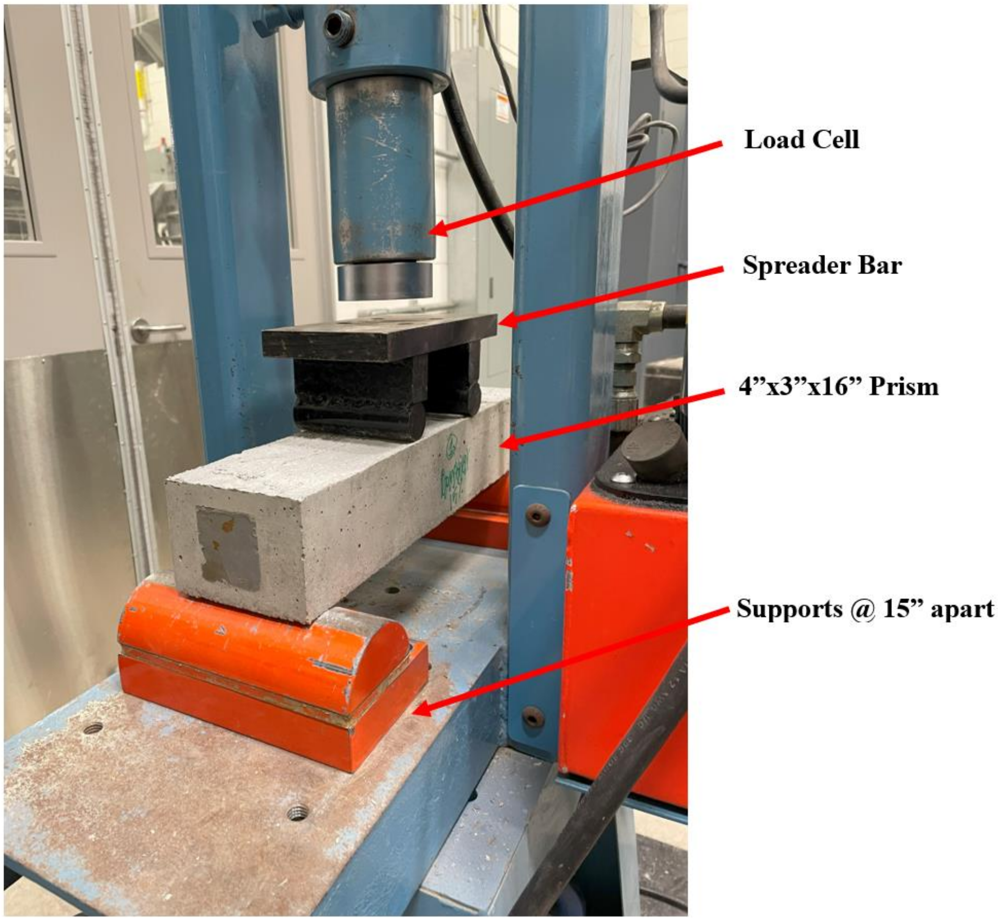

Figure 3-13: Modulus of Rupture Test Setup

Figure 3-14: Modulus of Rupture Tested Specimens

3.5.4 Reinforcement Strength Test (ASTM A370, 2022)

The assessment of the ultimate strength of the flexural reinforcement involved the utilization of an MTS Axial Test System, aligned with guidelines specified in ASTM A370-22 Standard Test Methods and Definitions for Mechanical Testing of Steel Products as referenced in ASTM A615/A615M-22 Standard Specification for Deformed and Plain Carbon-Steel Bars for Concrete Reinforcement.

The flexural reinforcement consisted of grade 60 number 3 bars conforming to ASTM A615. Each reinforcement sample subjected to testing measured 12 inches (305 mm) in length and featured 4 inches (102 mm) in the grips on either side, as visually demonstrated in Figure 3-15. A Micro-Measurements 120 ohms strain gauge was attached at the midpoint of the test specimen to monitor and record strain measurements. Suring the testing procedure, the MTS System tracked time, axial force, and axial displacement. Simultaneously, the System 7000 tracked the strain gauge readings until the reinforcement yielded.

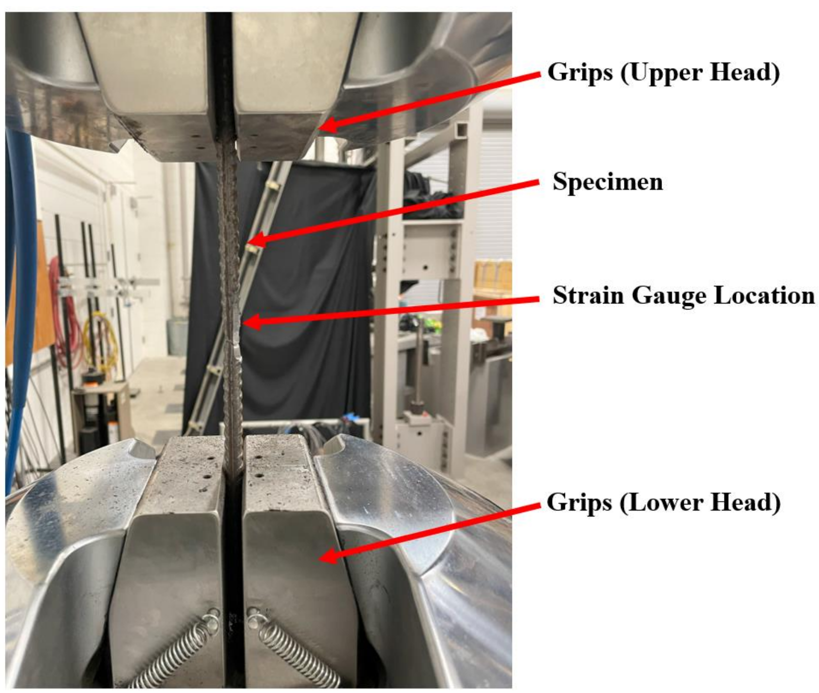

Figure 3-15: Reinforcement Strength Test Setup

3.6 Beam Specimen Test Setup

3.6.1 Testing Apparatus

The experimental testing setup for this study was designed around the utilization of the 100-kip (445 kN) capacity MTS Hydraulic Actuator in Kansas State University's Civil Department Structures Lab. A four-foot (3.7 m) spreader bar was employed to apply the point loads at quarter points along the beam. This methodology aimed to establish a constant moment region with no shear between the applied loads. For accurate measurement and tracking of beam deflection, linear variable differential transformers (LVDTs) were securely held in position using stands and placed on smooth metal plates affixed to the top of the beam with hydrocal gypsum cement. The metal plates provided a smooth surface for the LVDTs to slide on preventing them from snagging on the rough surface of the beam as it deflects. Figure 3-16 shows the detailed configuration of the testing apparatus.

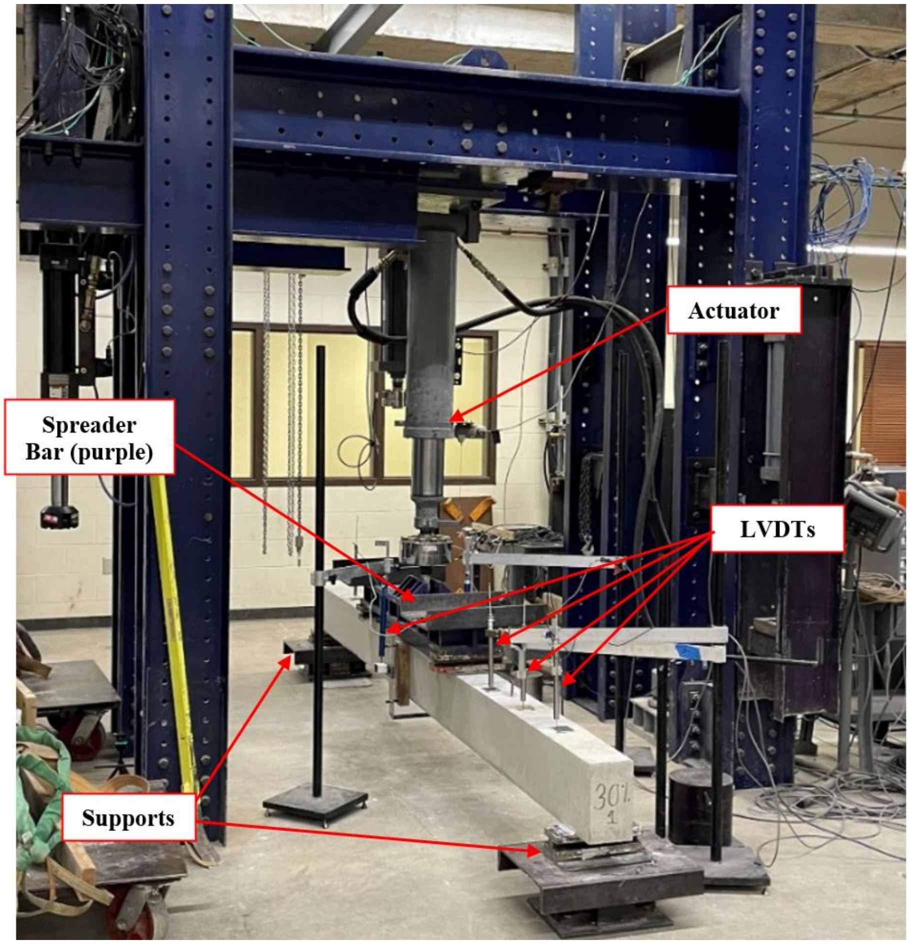

Figure 3-16: Testing Apparatus

The experimental setup was designed to replicate a roller and pinned connections. The pinned support, illustrated on the right side of Figure 3-17, comprises two steel plates interconnected by a steel rod. These steel plates have a grove allowing rotational movement around the steel rod while the beam undergoes deflection, restricting horizontal translation. The roller support, as shown on the left side of Figure 3-17, comprises two flat steel plates enabling rotational movement at horizontal translation of the beam. To secure these connections during the experiment, each top steel plate was attached to the beam with hydrocal to prevent the connection from slipping during the test.

Figure 3-17: Support Conditions (Right: Pin, Left: Roller)

3.6.2 Data Collection & Instrumentation

Data collection involved two distinct systems: the MTS Hydraulic Actuator System and the Micro-Measurements System 7000 Data Acquisition System. The MTS Hydraulic Actuator System tracked actuator stroke, applied load, and time elapsed. While the System 7000 collected actuator force, time, and displacements of all the LVDTs displacements. The MTS System gave a more accurate reading of the force progression over time while the System 7000 provided more accurate deflection readings along the beam by utilizing the LVDTs instead of the actuator stroke.

The actuator system recorded deflection at midspan of the beam, and the force applied to the spreader bar, shown as P_u in Figure 3-18. A total of six LVDTs were used to record beam deflection during a force application. On the left side of the beam, a single 8-inch (203 mm) LVDT was positioned halfway between the applied point load and the roller support. On the right side, three LVDTs spaced one foot (305 mm) apart, were situated to provide comprehensive understanding of the beam's curvature. Additionally, two ten-inch (254 mm) LVDTs were positioned at midspan to provide more accurate displacement measurements compared to the actuator system. Figure 3-18 shows the testing apparatus used to perform the tests.

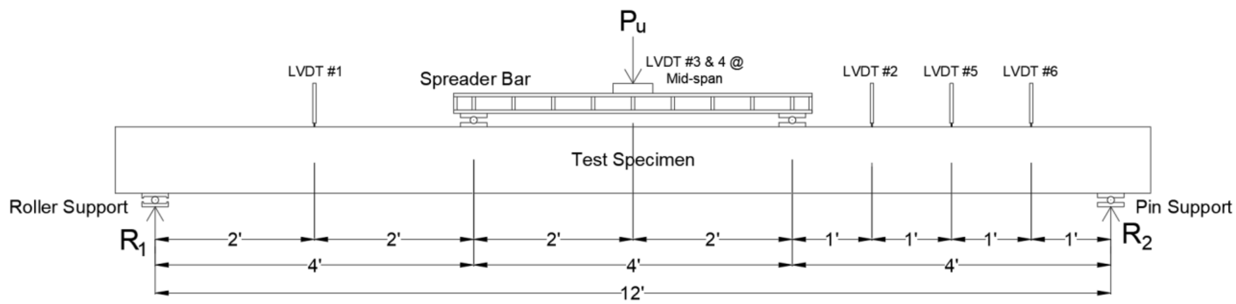

Figure 3-18: Flexural Test Setup

3.7 Design & Setup Limitations

The lab was shared with another experiment using similar sized beams and more tests to run. For this reason, the height of the beam off the ground was not changed which produced issues when testing the coarse aggregate replacement beams. The beams deflected more than expected and tests were limited to 9 inches (229 mm) of deflection at midspan.

Chapter 4 - Test Results and Discussion

4.1 Introduction

This chapter provides the experimental testing results for fresh and hardened concrete properties, tensile testing result of reinforcement, and, ultimately, the testing results for the concrete beam specimens. As stated in Chapter 3, three specimens were tested for each material strength test and beam test to obtain an average. Throughout this section the control, 15 percent replacement, and 30 percent replacement data are colored orange, green, and blue respectively.

4.2 Fresh Concrete Properties

The initial mix design provided by MCM had a *w/c* ratio of 0.45. Upon the arrival of the concrete truck, water adjustments were made to achieve a 6-inch slump (15 cm), resulting in a *w/c* ratio ranging from 0.34 to 0.37 based on the truck batched mixtures shown in Appendix A. Final batched mix designs are shown in Section 3.2 Table 3-3 and the concrete fresh properties are outlined in Table 4-1.

Table 4-1: Fresh Concrete Properties

Mix	*w/c*	Density		Change in Density
		lb/ft^3	kg/m^3	
Control	0.37	149.1	2388	0.00%
15% Replacement	0.34	145.8	2335	-2.21%
30% Replacement	0.35	141.2	2262	-5.30%

A *w/c* ratio below 0.40 indicates a stiff mixture, with an expected slump of three inches or less. A mid-range water reducing admixture was used in each mix of 24 to 25 ounces depending on the mixture which is on the lower end. Based on these two observations and achieving a 6-inch slump for each mixture implies a *w/c* ratio higher than the documented 0.34 to 0.37. To estimate the *w/c* ratio more accurately, Duff Abrams' 1918 equation, illustrating the relationship between compressive strength and *w/c* ratio, was used (Abrams, 1918). Using this equation and considering the parameters based on cement type, content, and curing conditions, the approximate *w/c* ratio for the control mixture was determined to be 0.55.

However, Abrams' equation cannot reliably estimate the *w/c* ratio for replacement mixtures due to the introduction of numerous unknown variables resulting from the use of plastic coarse aggregate replacement. The higher-than-recorded *w/c* ratio can be attributed to additional water left in the truck after washing out from previous pours. Pouring the specimens at midday implies that concrete trucks had already made deliveries and the trucks were washed out, leaving residual water. According to Abrams' equation, it is suggested that 10 gallons or more of water might have remained in the truck before batching the one cubic yard of concrete for each experimental mixture. While this additional water might not be as noticeable if the truck were full, its effect was significant with the smaller batched amounts, noticeably affecting the mixtures slump and strength.

Even with sources of error in calculating the *w/c* ratio there was still a noticeable increase in workability for the 15 and 30 percent replacement mixes. The replacement mixtures required less water to be added on site to reach the 6-inch (15 cm) slump. This suggests that Plazrok increased the workability of the mix and reduced water demand.

The density of the mixtures decreased with increasing plastic aggregate replacement. As per Section 2.3.2.2, lightweight concrete density ranges from 90 to 135 lb/ft^3 (1442 to 2162 kg/m^3) per ACI 318-19, but neither the 15 nor 30 percent replacements are classified as lightweight concrete, as indicated in Table 4-1.

4.3 Material Strength Testing Results

This section presents experimental testing results for concrete compression, tensile splitting, and modulus of rupture tests for each concrete mixture design, along with reinforcement tensile testing. Verifying assumed material strengths is crucial for ensuring structural integrity, durability, and safety. These material strengths not only contribute to formulating new equations but also assist in predicting the behavior of concrete members before actual testing.

All concrete specimens were fractured one day before the beam specimens were tested. The control specimens were 35 days old; the 15 percent replacement specimens were 43 days old; and the 30 percent replacement specimens were 39 days old at the time of fracture for each respective category.

4.3.1 Cylinder Compression Results

Testing was conducted in accordance with ASTM C39, as outlined in Section 3.5.1. Equation 2-1 was applied to calculate the compressive strength of each mix based on the load at failure for each cylinder. The testing results for cylinder compressive strength are presented in Table 4-2 displays the averaged compressive strength for each cylinder and mix. The average control compressive strength was used to calculate the percentage decrease for each replacement cylinder.

The compressive strength of the concrete decreased with an increase in the replacement of coarse aggregate with Plazrok. On average, the control mix demonstrated a strength 400 psi (2.76 MPa) greater than the mix design, owing to the reduced batched *w/c* of 0.37 instead of 0.45. Upon replacing the natural river rock coarse aggregate with Plazrok, a 7.8 percent decrease in compressive strength occurred with a 15 percent replacement, and a 20.0 percent decrease was observed with a 30 percent replacement. The decrease in compressive strength with the increase in replacement can be contributed to the reduced bond strength between the cement paste and Plazrok.

Table 4-2: Experimental Cylinder Compressive Test Results

Cylinder	Control			15%			30%		
	Compressive Strength f_c		Decrease from Control	Compressive Strength f_c		Decrease from Control	Compressive Strength f_c		Decrease from Control
	psi	MPa		psi	MPa		psi	MPa	
#1	4,361	30.07	0.00%	4,021	27.72	9.00%	3,529	24.33	20.1%
#2	4,571	31.52	0.00%	4,113	28.36	6.92%	3,818	26.32	13.6%
#3	4,324	29.81	0.00%	4,085	28.17	7.55%	3,267	22.53	26.1%
Average	**4,419**	**30.47**	**0.00%**	**4,073**	**28.08**	**7.82%**	**3,538**	**24.39**	**20.0%**

Table 4-3 presents a comparison between the experimental outcomes detailed in Table 4-2 and the research conducted by Costello et al. (2021). Costello et al. compressive strength results showed variations of 28.7, 18.8, and 11.1 percent when compared to the results presented in Table 4-2 for the control, 15, and 30 percent replacement mixes, respectively. Costello et al. study employed the same 4000 lbs/in^2 (27.58 MPa) interior mix design by MCM as utilized in this thesis, but with notable variations that resulted in a higher compressive strength.

Table 4-3: Average Cylinder Compressive Strength Comparison with Costello et al. (2021)

Mix	Experimental f_c		Decrease from Control	Costello et al. f_c		Decrease from Control
	psi	MPa		psi	MPa	
Control	4,419	30.47	0.00%	6,197	42.73	0.00%
15%	4,073	38.08	7.82%	5,013	34.56	19.1%
30%	3,538	24.39	20.0%	3,979	27.43	35.9%

One difference pertains to the coarse aggregate used. Costello et al. (2021) utilized a CA-4 coarse aggregate, commonly employed in various concrete types and comprising siliceous gravel or crushed stone. In contrast, the specimens tested in this thesis employed a CA-5 type coarse aggregate, suitable for all concrete except concrete in contact with soil and is also composed of siliceous gravel or crushed stone. The distinction between CA-4 and CA-5 lies in the grading requirements. According to the Kansas Department of Transportation, CA-4 aggregates are allowed to range in size from a 1/2-inch (12.5 mm) mesh to a number 8 (2.36 mm) mesh, while CA-5 aggregates can range from a ¾-inch (19 mm) mesh to a number 8 (2.36 mm) mesh (*Kansas Department of Transportation Special Provision to the Standard Specifications*, 1990).

Another significant difference is the methods of batching and mixing the concrete. In Costello et al. (2021) study, the mixing process took place in a laboratory setting, where each material was meticulously measured to the weights and volumes specified in the mix design received from MCM. This method of weighing out each of the material led to a very accurate w/c ratio whereas the unknown amount of additional water left in the truck after washout led to an increased *w/c* ratio (outlined Section 4.2) and decreased compressive strength. The batched mix design was then mixed following the guidelines outlined in *ASTM C192/C192M-19 Standard Practice for Making and Curing Concrete Test Specimens in the Laboratory*.

In contrast, for this thesis, concrete trucks and a batching plant were utilized to measure out the materials. Batching plants inherently introduce sources of error during material measurement, which is why acceptable tolerances are defined for the scales to ensure that the batch mix attains the designated strength. For instance, recommended tolerances by weight for cement, aggregates, water, and admixtures are ±1, ±2, ±1, and ±3 percent, respectively (*Recommended Guide Specifications for Batching Equipment and Control Systems in Concrete Batch Plants*, 1977). Costello et al. (2021) was able to keep a consistent *w/c* ratio of 0.45 while the *w/c* ratio varied for the results shown in Table 4-2.

The equations introduced by Alkotami and Kramer (2023), and Costello et al. (2021) are compared with the average experimental testing outcomes in Table 4-2. Costello et al. (2021) proposed Equation 2-4 to estimate the decrease in compressive strength linked to Plazrok replacement. Alkotami and Kramer (2023) put forth Equation 2-5 as a near approximation for compressive strength reduction across various plastic replacements. Costello et al. (2021) Equation 2-4 resulted in a 13.2 and 18.8 percent error while Alkotami and Kramer (2023) Equation 2-5 resulted in a 15.4 and 21.3 percent error for the 15 and 30 percent replacements, respectively, in this study.

Table 4-4: Experimental Compressive Test Comparison to Proposed Equations

Mix	Experimental		Equation 2-4		% Error	Equation 2-5		% Error
	psi	MPa	psi	MPa		psi	MPa	
Control	4,419	30.47	4,419	30.47	0.00%	4,419	30.47	0.00%
15%	4,073	38.08	3,535	24.37	13.2%	3,447	23.77	15.4%
30%	3,538	24.39	2,872	19.80	18.8%	2,784	19.20	21.3%

The findings in Table 4-2 suggest that various types of plastics, each with a different impact on compressive strength, cannot be adequately captured by a single equation unless additional variables are considered. The percent replacement with plastic aggregate does not exhibit a linear relationship, owing to factors like *w/c*, which significantly influences concrete compressive strength. Additionally, the shape of the aggregate contributes to the bond strength between plastic and cement paste, impacting compressive strength. For a more accurate approximation, an equation must account for adjustments based on aggregate type, *w/c*, and percentage replacement.

4.3.2 Cylinder Tensile Splitting Results

Testing was conducted in accordance with ASTM C496, as outlined in Section 3.5.2. Equation 2-6 was applied to calculate the tensile splitting strength of each mix based on the load at failure for each cylinder. The testing results for cylinder tensile splitting strength are presented in Table 4-5. The results in Table 4-5 display the averaged tensile splitting strength for each cylinder and mix. The average control tensile splitting strength was used to calculate the percentage decrease for each replacement cylinder.

The tensile splitting strength exhibited a notable increase with the incorporation of plastic coarse aggregate. Specifically, at 15 percent replacement, the splitting tensile strength increased by 38.5 percent, and at 30 percent replacement, it increased by 17.7 percent, both in comparison to the average control strength. These trends were consistent with those depicted in Figure 2-5 for various other plastic replacements, although the strength increase observed in other types of plastic replacement was not as pronounced as the results outlined in Table 4-5.

Several contributing factors may account for the significant increase in strength, including alterations in the *w/c*, the structural integrity of the specimens, and, most crucially, the type of aggregate used. The data strongly suggests that Plazrok has the potential to increase the splitting tensile strength of concrete.

Table 4-5: Experimental Tensile Splitting Test Results

Cylinder	Control			15%			30%		
	Strength		Decrease from Control	Strength		Decrease from Control	Strength		Decrease from Control
	psi	MPa		psi	MPa		psi	MPa	
#1	275	1.90	0.00%	377	2.60	-37.4%	381	2.63	-38.6%
#2	315	2.17	0.00%	435	3.00	-38.2%	321	2.21	-2.10%
#3	246	1.70	0.00%	345	2.38	-39.9%	277	1.91	-12.5%
Average	**279**	**1.92**	**0.00%**	**386**	**2.66**	**-38.5%**	**326**	**2.25**	**-17.7%**

Note: Negative percentages indicate increase in strength instead of decrease.

Table 4-6 presents a comparison between the experimental outcomes detailed in Table 4-5 and the research conducted by Costello et al. (2021). In Costello et al. (2021) study, a decrease of 3.2 and 4.2 percent in tensile splitting strength was observed in comparison to their control. Consistent with both studies, the tensile splitting strength exhibited a decline following the 15 percent replacement, suggesting a general trend towards a reduction in tensile strength with higher replacements of coarse aggregates.

Table 4-6: Average Tensile Splitting Strength Comparison with Costello et al. (2021)

Mix	Experimental f_t		Decrease from Control	Costello et al. f_t		Decrease from Control
	psi	MPa		psi	MPa	
Control	279	1.92	0.00%	331	2.28	0.00%
15%	386	2.66	-38.5%	320	2.21	3.20%
30%	326	2.25	-17.7%	270	1.86	4.20%

Note: Negative percentages indicate increase in strength instead of decrease.

The equation proposed by Alkotami and Kramer (2023), expressed as Equation 2-7, is assessed against the average experimental testing results outlined in Table 4-7. Alkotami' and Kramer equation aimed to provide a close approximation for the reduction in splitting tensile strength across different plastic replacements. However, this equation yielded a 40.0 and 41.8 percent error for the 15 and 30 percent replacements, respectively, in this study.

The observed error is attributed to Equation 2-7 assuming a linear relationship between all mix designs and percent replacements with different types of plastic aggregate. As revealed by the results in Table 4-5, such a relationship cannot always be assumed to be linear due to variations in the *w/c* in each mix, the types of aggregate used, and the specific characteristics of the plastic coarse aggregate replacement. More research is needed to derive an accurate equation that consists of factors that change based on the types of coarse aggregate used.

Table 4-7: Experimental Splitting Tensile Strength Comparison to Proposed Equation

Mix	Experimental		Equation 2-7		% Error
	psi	MPa	psi	MPa	
Control	279	1.92	279	1.92	0.00%
15%	386	2.66	232	1.60	40.0%
30%	326	2.25	190	1.31	41.8%

4.3.3 Modulus of Rupture Results

Testing procedures adhered to ASTM C78, detailed in Section 3.5.3, where Equation 2-12 was used to calculate the MOR, or flexural strength, for each mix based on the load at failure for each specimen. The MOR testing results are presented in Table 4-8, displaying the averaged MOR for each specimen and mix. The average control MOR served as the baseline for calculating the percentage decrease for each replacement specimen.

Table 4-8 reveals the modulus of rupture testing outcomes from material testing, indicating an overall decline in concrete flexural strength with an increase in Plazrok replacement. The reduction in flexural strength follows a nearly linear trend, with a 17.5 and 26.5 percent decrease in strength observed with 15 percent and 30 percent replacement, respectively. Notably, the results in Table 4-8 are 64, 38.8, and 42.6 percent higher than the tensile splitting results presented in Table 4-5. This aligns with the anticipated relationship where MOR is expected to be larger than the splitting tensile strength by 60 to 80 percent (Olanike, 2014).

Table 4-8: Experimental Modulus of Rupture Test Results

Cylinder	Control			15%			30%		
	Flexural Strength f_r		Decrease from Control	Flexural Strength f_r		Decrease from Control	Flexural Strength f_r		Decrease from Control
	psi	MPa		psi	MPa		psi	MPa	
#1	685	4.72	0.00%	696	4.80	-1.61%	527	3.63	23.1%
#2	821	5.66	0.00%	610	4.21	25.6%	581	4.01	29.2%
#3	819	5.65	0.00%	588	4.05	28.2%	596	4.11	27.2%
Average	**775**	**5.34**	**0.00%**	**631**	**4.35**	**17.5%**	**568**	**3.92**	**26.5%**

Note: Negative percentages indicate increase in strength instead of decrease.

Table 4-9 provides a comparison between the experimental results in Table 4-8 and Costello et al. (2021) MOR data. In both datasets, a decrease in concrete flexural strength is observed with an increase in Plazrok replacement. Costello et al. results exhibited reductions of

65.2, 60.4, and 57.7 percent for the control, 15, and 30 percent replacement specimens, respectively. Notably, Costello et al. testing produced higher splitting tensile strengths (as shown in Table 4-6) than MOR (shown in Table 4-9), which is unexpected. Typically, the modulus of rupture is larger than the splitting tensile strength, as mentioned previously (Olanike, 2014).

Several factors could contribute to Costello et al. (2021) lower flexural strength, including variations in the *w/c*, the type of aggregate used, and the bond between the cement paste and coarse aggregates. These factors can impact the overall integrity and mechanical properties of the concrete, influencing the observed differences in MOR between the two sets of data.

Table 4-9: Average Modulus of Rupture Comparison with Costello et al. (2021)

Mix	Experimental f_r		Decrease from Control	Costello et al. f_r		Decrease from Control
	psi	MPa		psi	MPa	
Control	775	5.34	0.00%	270	1.86	0.00%
15%	631	4.35	17.5%	250	1.72	19.1%
30%	568	3.92	26.5%	240	1.66	35.9%

Table 4-10 provides a comparison between Equation 2-8, the ACI 318-19 code equation for MOR, Equation 2-10, the IS 456 code equation for MOR, and Alkotami and Kramer (2023) suggested equation for the change in MOR with plastic coarse aggregate replacement. The ACI 318-19 and IS 456 code equations yield tensile strength values significantly lower than the experimental values. According to the ACI 318-19 Commentary, MOR is more variable than compressive strength and is typically 10 to 15 percent of the compressive strength. The code equations tend to be cautious, resulting in a value that is approximately 10 percent of the compressive strength of the mix. With the experimental control value being 17.5 percent of the compressive strength, there is a 35.6 and 27.7 percent error for the ACI 318-19 and IS 456 code equations, respectively. On the other hand, Alkotami and Kramer (2023) suggested Equation 2-12 produces values similar to the experimental results. The equation indicates that as the percentage of coarse aggregate replacement increases, the accuracy of the equation decreases.

Table 4-10: Experimental MOR Comparison to Proposed Equations

Mix	Thesis Results	Equation 2-8	% Error	Equation 2-10	% Error	Equation 2-12	% Error
	psi (MPa)	psi (MPa)		psi (MPa)		psi (MPa)	
Control	775 (5.34)	499 (3.44)	35.6%	560 (3.86)	27.7%	775 (5.34)	0.00%
15%	631 (4.35)	478 (3.30)	24.3%	538 (3.71)	14.7%	628 (4.33)	0.52%
30%	568 (3.92)	446 (3.08)	21.5%	501 (3.46)	11.8%	512 (3.53)	9.95%

4.3.4 Reinforcement Tensile Results

Testing procedures were conducted in accordance with ASTM A370, as detailed in Section 3.5.4. Table 4-11 presents the results of steel reinforcement tensile testing for the three specimens, along with their average. Additionally, Figure 4-1 illustrates a stress-strain curve, where the strain gage readings are depicted in a solid red line, and data acquired from the actuator is shown in a dotted blue line.

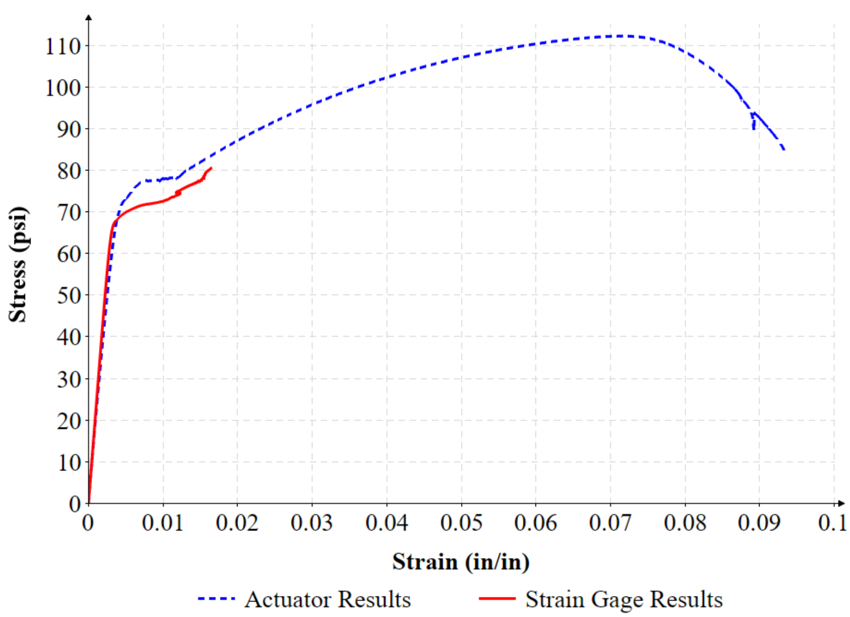

Figure 4-1: Reinforcement Stress vs. Strain Test Results

Table 4-11: Steel Reinforcement Test Results

Specimen Properties		Bar #1	Bar #2	Bar #3	Average
Bar Diameter, d_b	in.	0.3610	0.3475	0.3570	0.3555
	mm	9.17	8.83	9.09	9.03
MOE, E_s	ksi	20,918	22,767	20,050	21,245
	GPa	144.2	157.0	138.2	146.5
Yield Strength, F_y	ksi	69.63	72.40	67.35	69.79
	MPa	480.1	499.2	464.4	481.2
Yield Strength, ε_y	-	0.00482	0.00489	0.00493	0.00488
Ultimate Strength, F_u	ksi	109.3	117.0	110.4	112.2
	MPa	753.6	806.7	761.2	773.6
Ultimate Strain, ε_y	-	0.08938	0.08745	0.08919	0.08867

From the slope of the elastic portion of the strain gage readings, the modulus of elasticity was determined. The strain gages delaminated from the specimens after the reinforcement yielded, resulting in the loss of readings. Beyond the yield point, data collected from the actuator was utilized to determine the yield stress/strain and ultimate stress/strain. The values of stress and strain were determined based on the definitions of normal stress ($\sigma = P/A$) and normal strain ($\varepsilon = \delta/L$).

The theoretical modulus of elasticity for steel is well-established at 29,000 kip/in² (200 GPa). However, the modulus of elasticity obtained from the strain gages in this study indicates a value of 21,245 kip/in² (147 GPa), resulting in a 36.5 percent error. The decision to use strain gages was influenced by their perceived accuracy, cost-effectiveness, and ease of use. However, this choice introduced sources of error, including transverse sensitivity of the strain gage, temperature variations, strain gage misalignment, and error associated with the non-linearity of the Wheatstone bridge (Motra et al., 2014).

The strain gage's reliability depends on proper attachment to the specimen with sufficient contact area, and any contamination can lead to misreadings. Additionally, the strain gage values are only reliable in the elastic region. Beyond that point, after the yield point (as shown in Figure 4-1), the strain gage loses contact with the specimen and either shows no value or an inaccurate value due to bonding issues (Motra et al., 2014). For more precise readings, an extensometer, which is designed to measure changes in length accurately, should have been used. Considering the sources of error associated with the strain gage readings, the theoretical modulus of elasticity was used in Section 4.4 calculations to ensure the accuracy and reliability of the results.

The specified reinforcement used was ASTM 615 Grade 60, characterized by a minimum tensile strength of 60 kip/in² (414 MPa) and an ultimate strength of 80 kip/in² (552 MPa) (ASTM A615, 2022). As indicated in Table 4-11, the average yield stress was determined to be 69.8 kip/in² (481 MPa), while the average ultimate stress was found to be 112.2 kip/in² (774 MPa). This trend is becoming more prevalent due to the increasing utilization of recycled steel in the production of deformed bars. While the ultimate and yield strengths see an increase, it's important to note that this shift may result in a decrease in the overall ductility of the specimen.

4.4 Flexural Beam Testing

The following section explores the outcomes of the beam specimen testing. Load-deflection diagrams for the control, 15, and 30 percent replacement beams are presented first, accompanied by a discussion of their respective results in Section 4.4.1 through 4.4.3. Followed by discussion on the determination of the stiffness and secant modulus in Section 4.4.4. Section 4.4.5 focuses on the flexural capacity, drawing comparisons with the equations outlined in Section 2.5 and 2.6. Finally, Section 4.4.6 addresses the distribution of plastic aggregate throughout each of the beam specimens.

Figure 4-2 illustrates the displacement data collected by the Linear Variable Differential Transformers (LVDTs) along the beam. LVDTs 3 and 4, positioned at mid-span, were averaged for each beam in the subsequent calculations. The LVDT layout is shown in Figure 3-18.

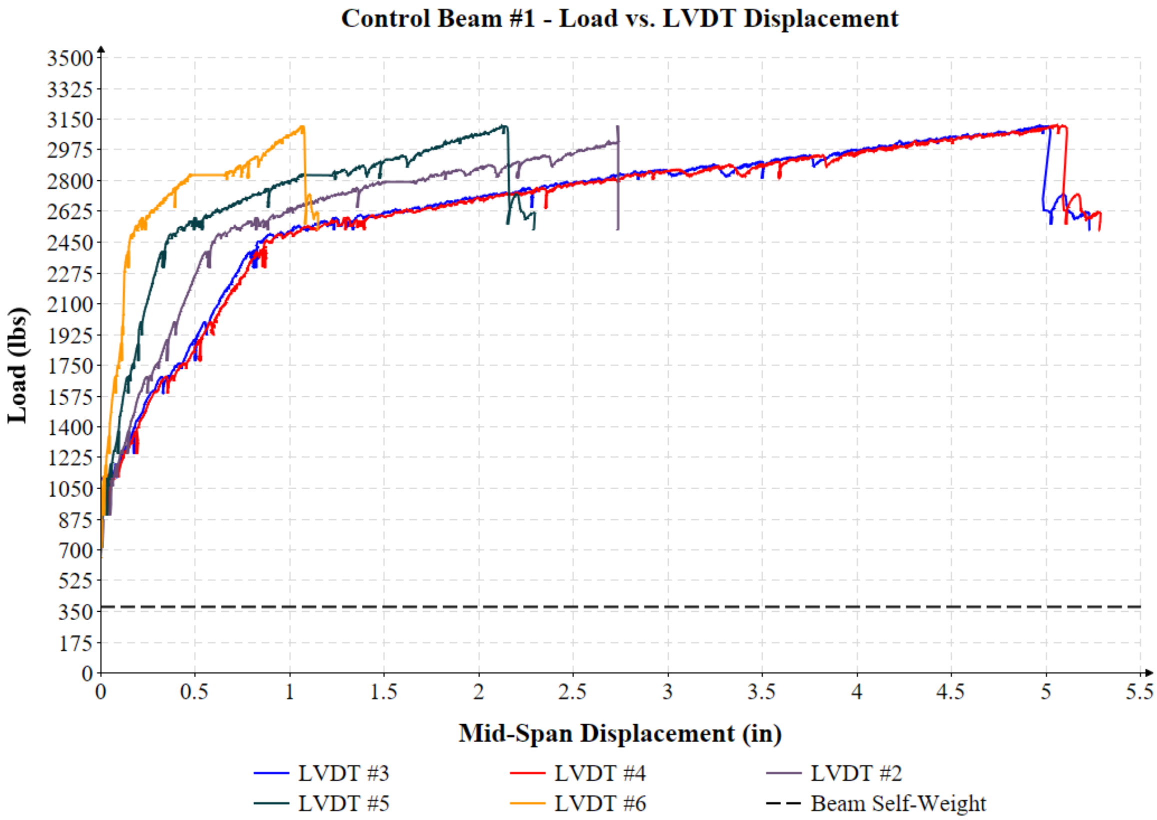

Figure 4-2: Example of LVDT Displacement along Control Beam #1

The load-deflection curves presented in Sections 4.4.1, 4.4.2, and 4.4.3 adopt the notation depicted in Figure 4-3. These curves illustrate the load-deflection behavior for half the span of the beam, resulting in the applied load being halved. To accommodate this idealization, all calculated cracking moments are adjusted by a factor of two. Load-deflection results in Table 4-12, Table 4-13, and Table 4-14 are presented using the notation from Figure 4-3.

The slope of the load-deflection curves up to cracking is considered as the uncracked stiffness (E_cI_{gt}), where E_c represents the secant modulus of concrete, and I_{gt} is the transformed gross moment of inertia derived from Equation 2-32. The slope of the load-deflection curve between the first crack and flexural yielding represents the stiffness after cracking (E_cI_e), where I_e denotes the effective moment of inertia.

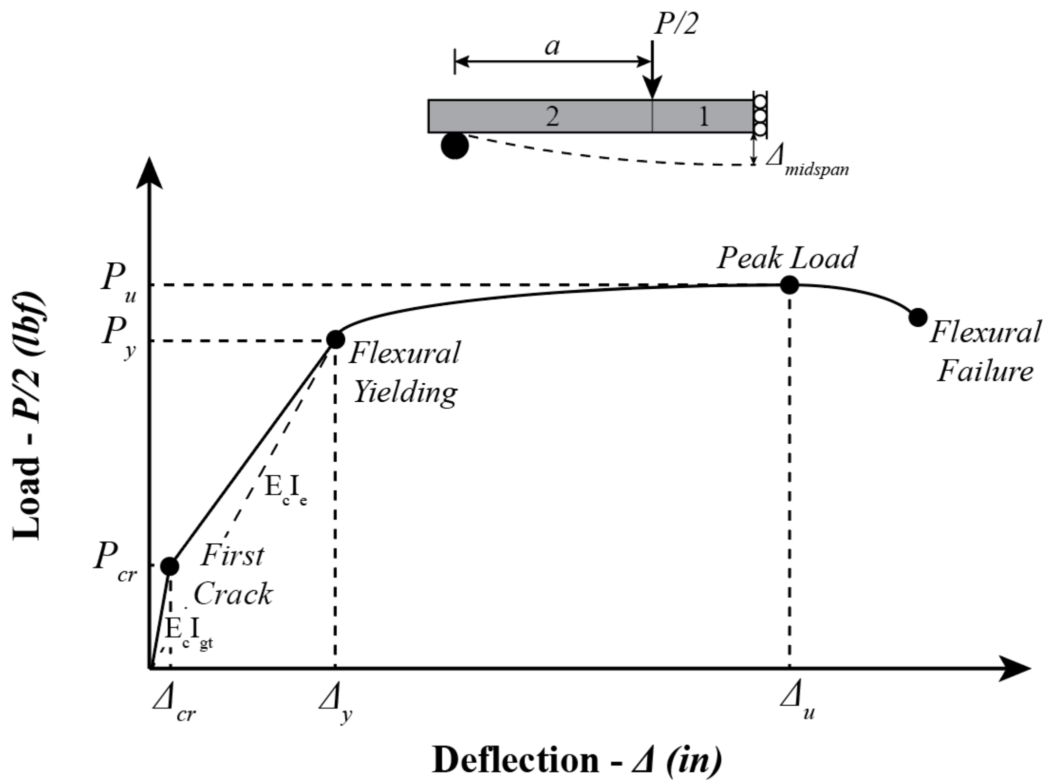

Figure 4-3: Load-Deflection Thesis Notation

The load-deflection curves shown in Sections 4.4.1, 4.4.2, and 4.4.3 required the self-weight of the member to be added to the loads obtained from the actuator system. The actuator was zeroed with the 542-pound (246 kg) spreader bar attached prior to contacting the beams. The initial deflection due to the self-weight of the member was not accurately measured and a accurate stiffness could not be obtained from a secant line from the origin to first crack. Instead, the stiffness was determined based on a secant line from the load due to the self-weight to the location of first crack. An example of the secant line is shown in Figure 4-19 in Section 4.4.4.

4.4.1 Control Beam Load-Deflection Results

The control beams underwent testing prior to the examination of the 15 and 30 percent replacement beams. The results obtained from testing the three control beam specimens are summarized in Table 4-12, and the corresponding load-deflection data is presented in Figure 4-4. Table 4-12 provides details on the stiffness, MOE, and load and deflection at crack, yield, and ultimate stages for each control beam, along with the average values. The determination of the stiffness and MOE for each member is detailed in Section 4.4.4.

Table 4-12: Control Beam Testing Results Obtained from Load-Deflection

Specimen Properties		Beam #1	Beam #2	Beam #3	Average
Stiffness, EI	kip/in	18.99	19.03	19.99	19.34
	kN/m	3,325	3,333	3,501	3,387
MOE, E_c	ksi	3,941	3,951	3,943	3,945
	GPa	27.17	27.24	27.19	27.20
Load @ Crack, P_{cr}	lbs.	1,123	1,018	1,060	1,067
	N	4,993	4,528	4,715	4,745
Deflection @ P_{cr}, Δ_{cr}	in.	0.039	0.034	0.036	0.036
	mm	0.991	0.864	0.919	0.925
Load @ Yield, P_y	lbs.	2,429	2,494	2,655	2,526
	N	10,806	11,092	11,810	11,236
Deflection @ P_y, Δ_y	in.	0.844	0.844	0.825	0.838
	mm	21.44	21.44	20.96	21.28
Peak Load, P_u	lbs.	3,115	3,239	3,219	3191
	N	13,855	14,406	14,319	14,193
Deflection @ P_u, Δ_u	in.	5.02	6.21	5.63	5.62
	mm	127.5	157.7	142.9	142.7

Each specimen exhibited a load-deflection response similar to Figure 4-3, as illustrated in Figure 4-4. The first crack in each beam was prominent, marked by a notable jump in displacement without a significant change in load. The control beams, on average, experienced cracking at 1,067 lbs (4,745 N) with a deflection of 0.036 inches (0.925 mm). Using Equation 2-33, the theoretical cracking moment was calculated to be 6.458 kip-ft (8.756 kN-m), corresponding to a theoretical point load of 1,615 lbs (7,182 N). The control beams, on average, cracked 548 lbs (2,438 N) below the theoretical cracking load. The reason the theoretical cracking load is higher than the average experimental cracking load is due to the abnormally high experimental MOR obtained in Section 4.3.3. Based on the beam results the actual tensile strength aligns more with the splitting tensile strength testing results presented in Section 4.3.2.

Post-cracking, the specimens exhibited linear deflection with the load until the reinforcement yielded. At the yield point, a sharp change in slope toward a flatter line occurred. After the tension steel yielded, a significant increase in deflection and a decrease in the member's stiffness occurred as more of the member's cross-section cracked and more steel yielded. The specimen continued to deflect with minimal increase in load before reaching the peak load, which averaged 3,191 lbs (14,193 N). The failure occurred suddenly, with no softening of the load observed.

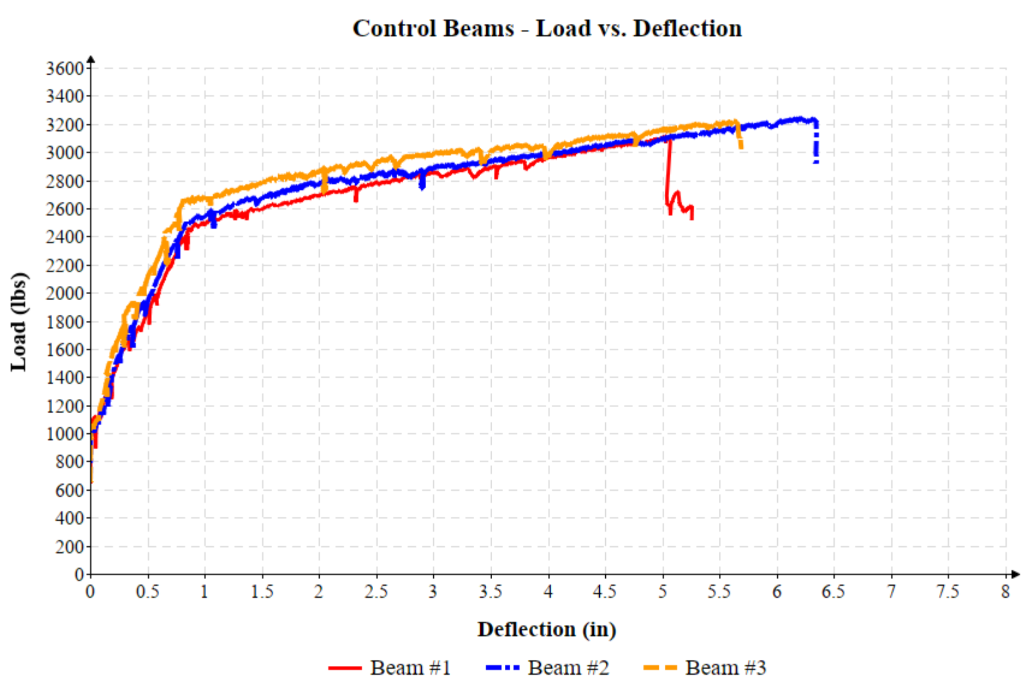

Figure 4-4: Control Beams Load-Deflection Response Graphed

4.4.1.1 Crack Propagation

The control beams displayed typical flexural cracking expected for a simply supported member under four-point bending. Figure 4-5 illustrates the response of Control Beam #3 at various loads as listed in Table 4-12. Initially, when the section first cracked, the cracks were minimal and challenging to discern, and could only be marked once visible. All cracks between the point loads were vertical until the reinforcement yielded. As the load continued to increase, cracks started to form at angles and horizontally at the depth of the tension steel. At each stage of loading, determined based on the compressive strength results in Section 4.3.1, the test was paused, and all visible cracks were marked using a black marker.

As anticipated, cracks outside the constant moment region propagated at approximately a 45-degree angle towards the applied point load. All control beams failed along this 45-degree angle, resulting in a diagonal tension failure attributed to the yielding of reinforcement. Importantly, no concrete crushing occurred for the control beams, and all failures exhibited ductile behavior.

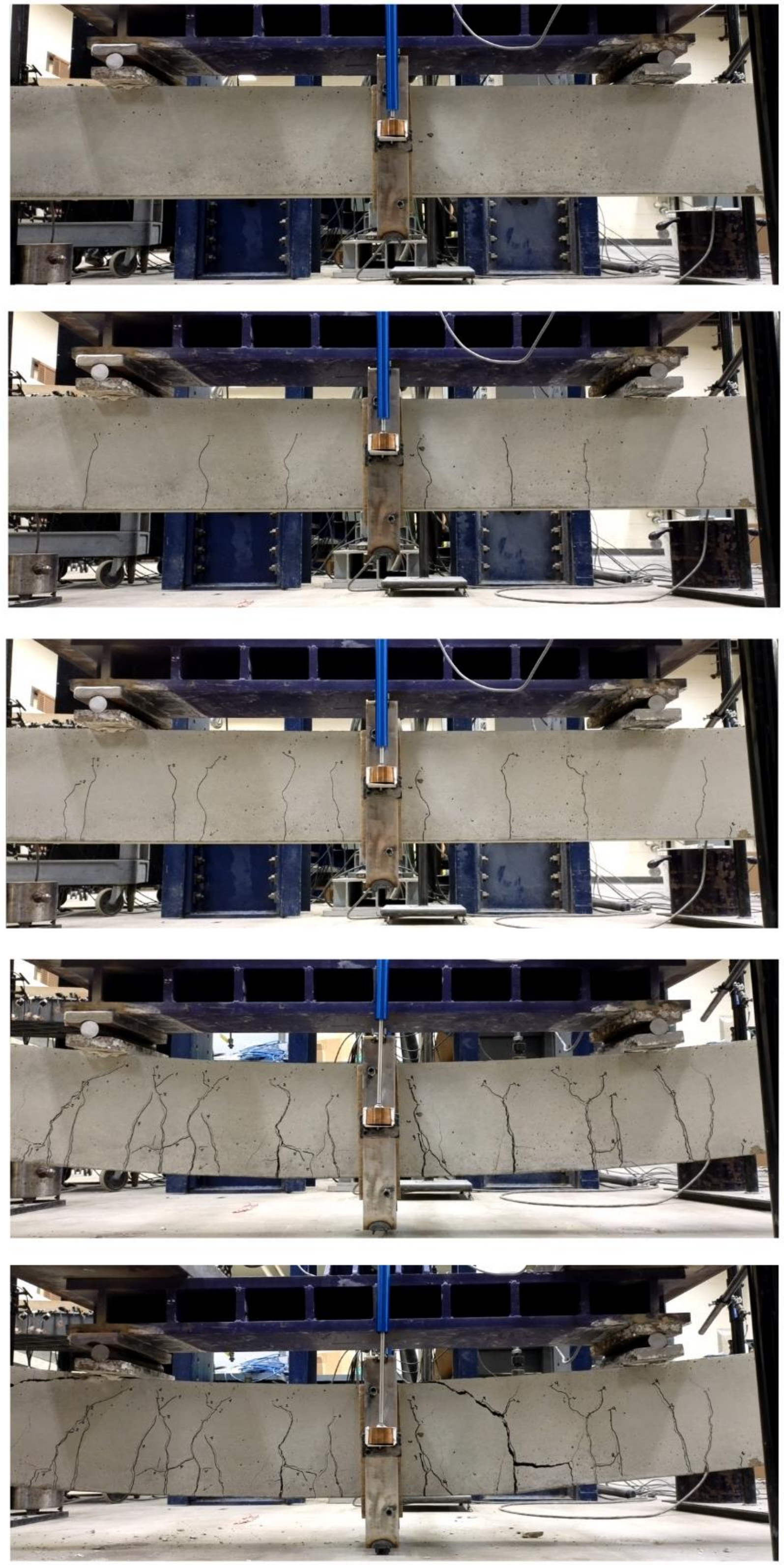

Control beam #3 prior to loading

Control beam #3 just after first crack

Control beam #3 at reinforcement yield

Control beam #3 at peak load

Control beam #3 after failure

Figure 4-5: Control Beam Crack Propagation at Each Stage of Loading

4.4.1.2 Comparison of Effective Moment of Inertia Equations

Section 2.4.6.3 highlighted the American Concrete Institute (ACI) utilization of the effective moment of inertia (I_e) approximation to determine the average stiffness of a structural member between the first crack and the yielding of the tension steel. The effective moment of inertia equations proposed by Branson (1965) and Bischoff (2005), as expressed in Equation 2-37 and Equation 2-39, were compared to experimental results in Figure 4-6, Figure 4-7, and Figure 4-8.

These figures present the load-deflection responses, where experimental results are depicted as a solid black line. The use of Bischoff's (2005) equation to predict deflection based on cracking and yield load is shown in purple with circles, while the use of Branson's (1965) equation for prediction is represented in yellow with squares. The ACI 318-19 method of flexural design, described in Section 2.6, is presented in red with triangles, utilizing experimental values for concrete compressive strength and steel yield strength. Additionally, the green line with crosses illustrates load-deflection results based on ACI 318-19 method of design for flexural members as outlined in Section 2.6 for a typical 4,000 psi (27.6 MPa) mix. The ACI 318-19 method for a typical 4,000 psi (27.6 MPa) mix does not incorporate experimental results; rather, it relies solely on code equations and mechanics of materials. This representation reflects the outcomes expected by practicing structural engineers, and all moment capacities displayed are nominal strengths without the application of safety factors.

The reinforcement ratio (ρ) for the experimental specimens is 0.0046 or 0.46 percent, which is below the 1.0 percent ratio considered adequate by Bischoff (2005) using Branson's (1965) equation. For each of the beams, Branson's (1965) equation closely aligns with the slope of the load-deflection curve after cracking but starts to deviate with an increase in slope quicker than Bischoff's (2005).

For example, Control Beam #1 (Figure 4-6), Bischoff's equation closely predicts the deflection at 0.869 inches (22.1 mm), resulting in a 2.96 percent error compared to the experimental deflection at yield. In contrast, Branson's equation leads to a deflection of 0.580 inches (14.7 mm), representing a negative 31.3 percent error (negative indicating underestimation). Similar trends are observed for Control Beam #2 (Figure 4-7) and Control Beam #3 (Figure 4-8). For Control Beam #2, Bischoff's equation predicts a deflection of 0.909 inches (23.1 mm), with a 7.70 percent error, while Branson's equation leads to a deflection of 0.676 inches (17.2 mm), resulting in a negative 19.9 percent error. Lastly, for Control Beam #3, Bischoff's equation predicts a deflection of 0.972 inches (24.7 mm), with a 17.8 percent error, while Branson's equation leads to a deflection of 0.735 inches (18.7 mm), resulting in a negative 10.9 percent error. Control Beam #3 is an outlier since Branson’s equation predicted the deflection most accurately but still underestimated the deflection at yield.

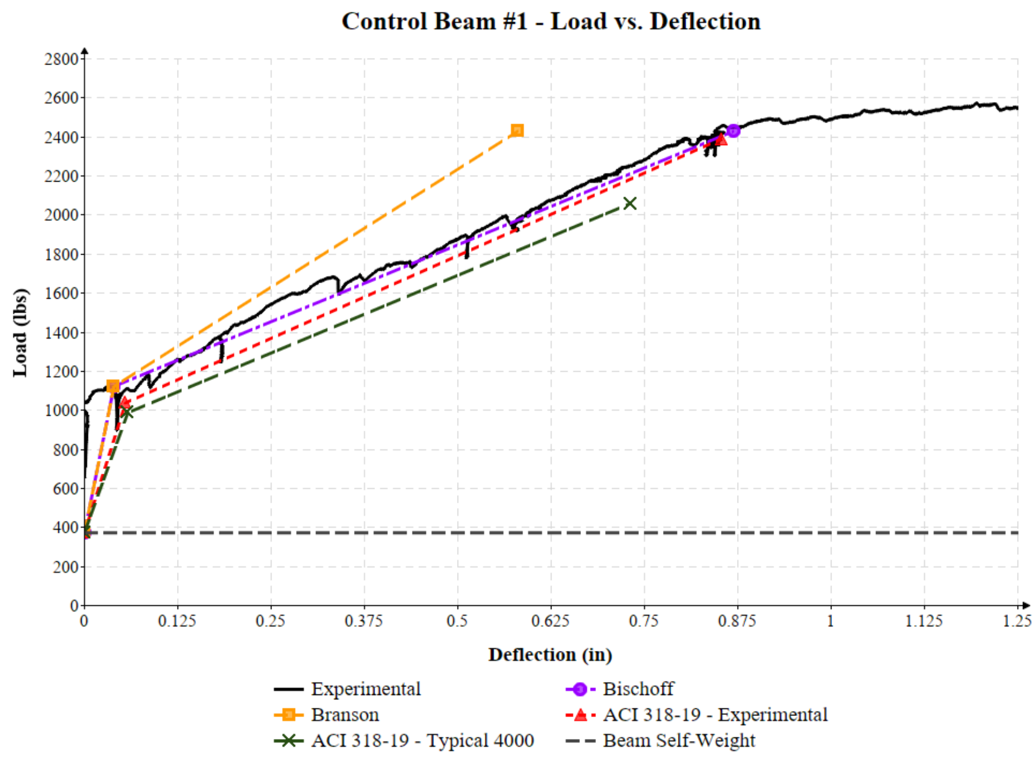

Figure 4-6: Control Beam #1 Comparison of Effective Moment of Inertia Equations

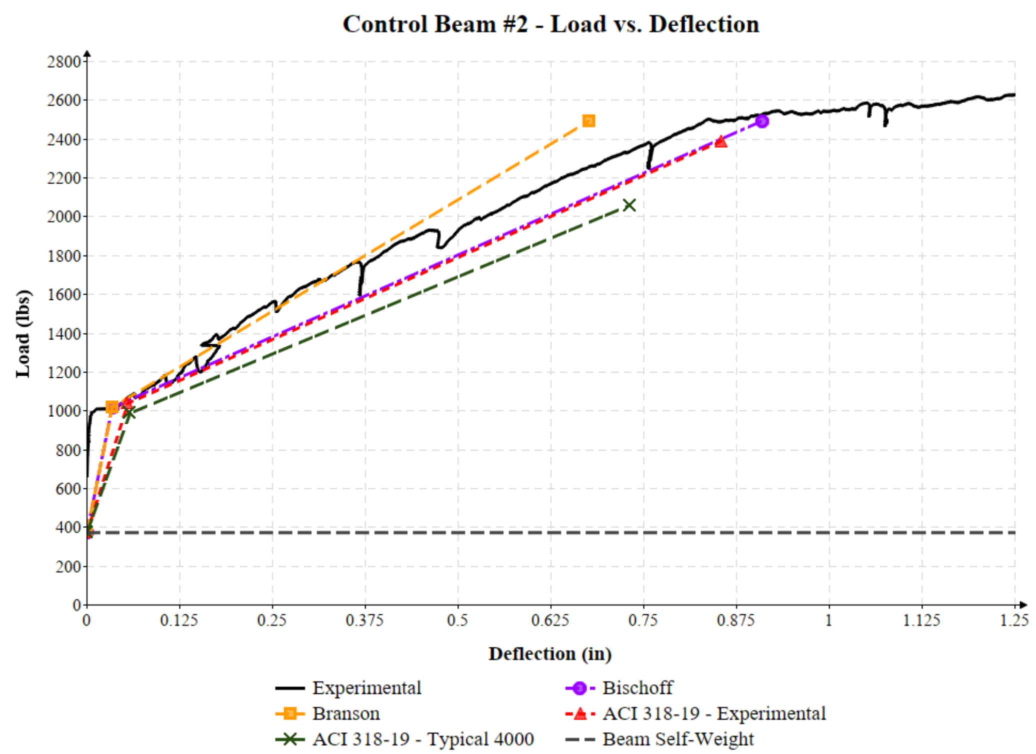

Figure 4-7: Control Beam #2 Comparison of Effective Moment of Inertia Equations

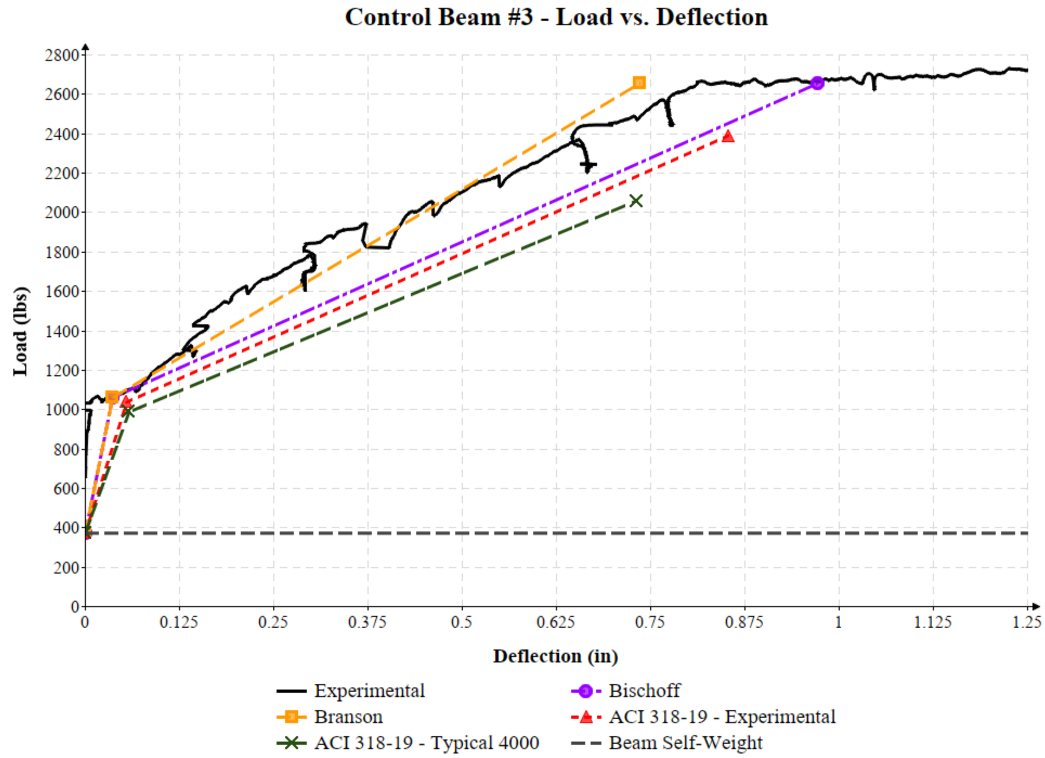

Figure 4-8: Control Beam #3 Comparison of Effective Moment of Inertia Equations

In the case of each beam, the cracking moment determined using ACI 318-19 is consistently lower than the actual cracking moment, aligning with expectations. The experimental ACI 318-19 response and the ACI 318-19 response for a typical 4,000 psi (27.6 MPa) mixture tend to underestimate the deflection and the nominal moment capacity of the control beams. The experimental ACI 318-19 response most accurately predicted the nominal moment capacity due to using the actual compressive strength of the concrete. The average experimental nominal moment capacity was 10.10 kip-ft (13.70 kN-m) while the ACI 318-19 equations predicted a capacity of 9.560 kip-ft (12.96 kN-m) and 8.238 kip-ft (11.17 kN-m) for the experimental and theoretical respectively.

ACI 318-19 Section 21.2 contains strength reduction factors for structural concrete members which is denoted as phi (ϕ). According to Table 21.2.1 of ACI 318-19 the strength reduction factor for structural tension-controlled members subjected to pure flexure is 0.9. The strength reduction factors are required for Load and Resistance Factor Design (LRFD) to decrease the estimated strength of the structural member to account for variability in materials, construction, and design. Upon the application of a safety factor of 0.9 to ACI 318-19 results, the average nominal moment capacity decreases to 8.604 kip-ft (11.67 kN-m) for the experimental ACI 318-19 and 7.414 kip-ft (10.05 kN-m) for the typical 4,000 psi (27.6 MPa) mixture. By applying the safety factor, the predicted moment capacities fall 14.9 and 26.6 percent below the experimental average for the experimental ACI 318 and typical 4,000 psi (27.6 MPa) mixture respectively.

4.4.2 15 Percent Replacement Beam Load-Deflection Results

The outcomes from testing the three 15 percent replacement beam specimens are outlined in Table 4-13, and the corresponding load-deflection data is depicted in Figure 4-9. Table 4-13 provides details regarding the stiffness, MOE, and load and deflection at crack, yield, and ultimate stages for each 15 percent replacement beam, in addition to presenting the average values and the percentage increase from the control beam average load-deflection results. A negative percent change signifies a decrease in the equivalent specimen property compared to the control values.

Table 4-13: 15% Replacement Beam Testing Results Obtained from Load-Deflection

Specimen Properties		Beam #1	Beam #2	Beam #3	Average	% Change
Stiffness, EI	kip/in	18.77	17.81	18.02	18.20	-5.90%
	kN/m	3,287	3,118	3,155	3,187	
MOE, E_c	ksi	3,896	3,690	3,735	3,774	-4.30%
	GPa	26.86	25.44	25.75	26.02	
Load @ Crack, P_{cr}	lbs.	1,237	1,314	1,080	1,210	13.4%
	N	5,500	5,844	4,806	5,383	
Deflection @P_{cr}, Δ_{cr}	in.	0.046	0.053	0.040	0.046	27.3%
	mm	1.168	1.346	1.016	1.177	
Load @ Yield, P_y	lbs.	2,515	2,511	2,488	2,504	-0.90%
	N	11,185	11,169	11,067	11,140	
Deflection @ P_y, Δ_y	in.	0.751	0.689	0.806	0.749	-10.6%
	mm	19.08	17.50	20.47	19.02	
Peak Load, P_u	lbs.	3,209	3,292	3,233	3,245	1.70%
	N	14,273	14,644	14,382	14,433	
Deflection @ P_u, Δ_u	in.	5.30	6.29	6.43	6.01	6.90%
	mm	134.5	159.8	163.3	152.6	

Note: negative percent change signifies a decrease in specimen property compared to control specimens

The stiffness of the 15 percent replacement beams decreased by 5.90 percent compared to the average control beam stiffness, corresponding to a 4.30 percent decrease in the MOE of the concrete. The MOE decreased from 3,945 kip/in² (27.2 GPa) for the control to 3,774 kip/in² (26.0 GPa).

On average, the 15 percent replacement beams experienced their first crack at 1,210 lbs (5,383 N), representing a 13.4 percent increase in load over the control beam average. Additionally, the deflection at the first crack was 0.046 inches (1.177 mm), marking a 27.3 percent increase over the control beams. The theoretical cracking moment was determined to be 6.731 kip-ft (9.126 kN-m), corresponding to a theoretical point load of 1,683 lbs (7,485 N). The theoretical cracking moment is based on the average modulus of rupture (MOR) displayed in Section 4.3.3. On average, the 15 percent replacement beams' first crack, based on the load-deflection curve, was 473 lbs (2,104 N) lower than the theoretical load. The reason the theoretical cracking load is higher than the average experimental cracking load is due to the abnormally high experimental MOR. The actual tensile strength aligns more with the splitting tensile strength testing.

At yield the 15 percent replacement beams experienced inelastic deformation at a faster rate than the control beams due to the increased slope of the load deflection curve over the control. This is due to a significant decrease in stiffness of the member after the tension steel yielded. The compressive strength and MOE of the concrete decreased with the addition of Plazrok leading to this decrease in stiffness and increase in deformation. The specimens continued to deflect with a slight increase in load before reaching the peak load, which averaged 3,245 lbs (14,433 N) which is only 1.70 percent higher than the control beams. The failure occurred suddenly, with no softening of the load observed.

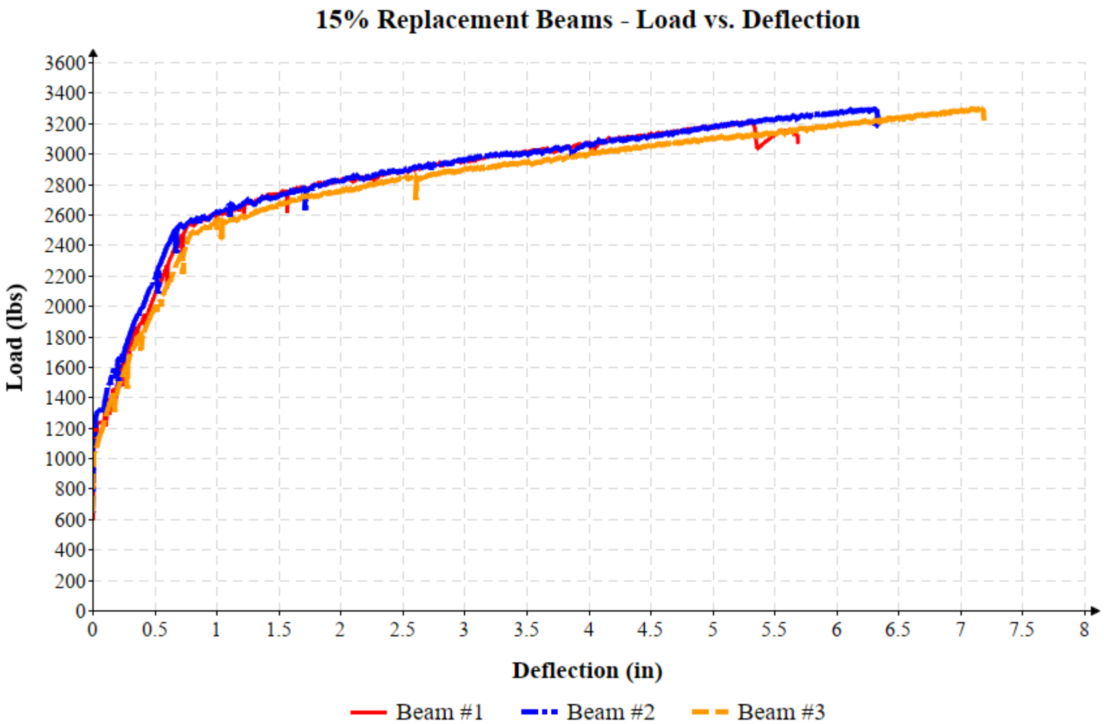

Figure 4-9: 15% Replacement Beams Load-Deflection Response Graphed

4.4.2.1 Crack Propagation

Similar to the control beams, the 15 percent replacement specimens exhibited typical flexural cracking expected for a simply supported member under four-point bending. Figure 4-10 depicts the response of 15 Percent Replacement Beam #3 at various loads as listed in Table 4-13. No discernible difference between the crack patterns of the control and 15 percent replacement members from the first crack to their peak loading was observed. At failure, a notable increase in horizontal cracking around the location of the reinforcing steel occurred compared to the control. Like the control beams, all members experienced diagonal tension failure, with no crushing of the concrete.

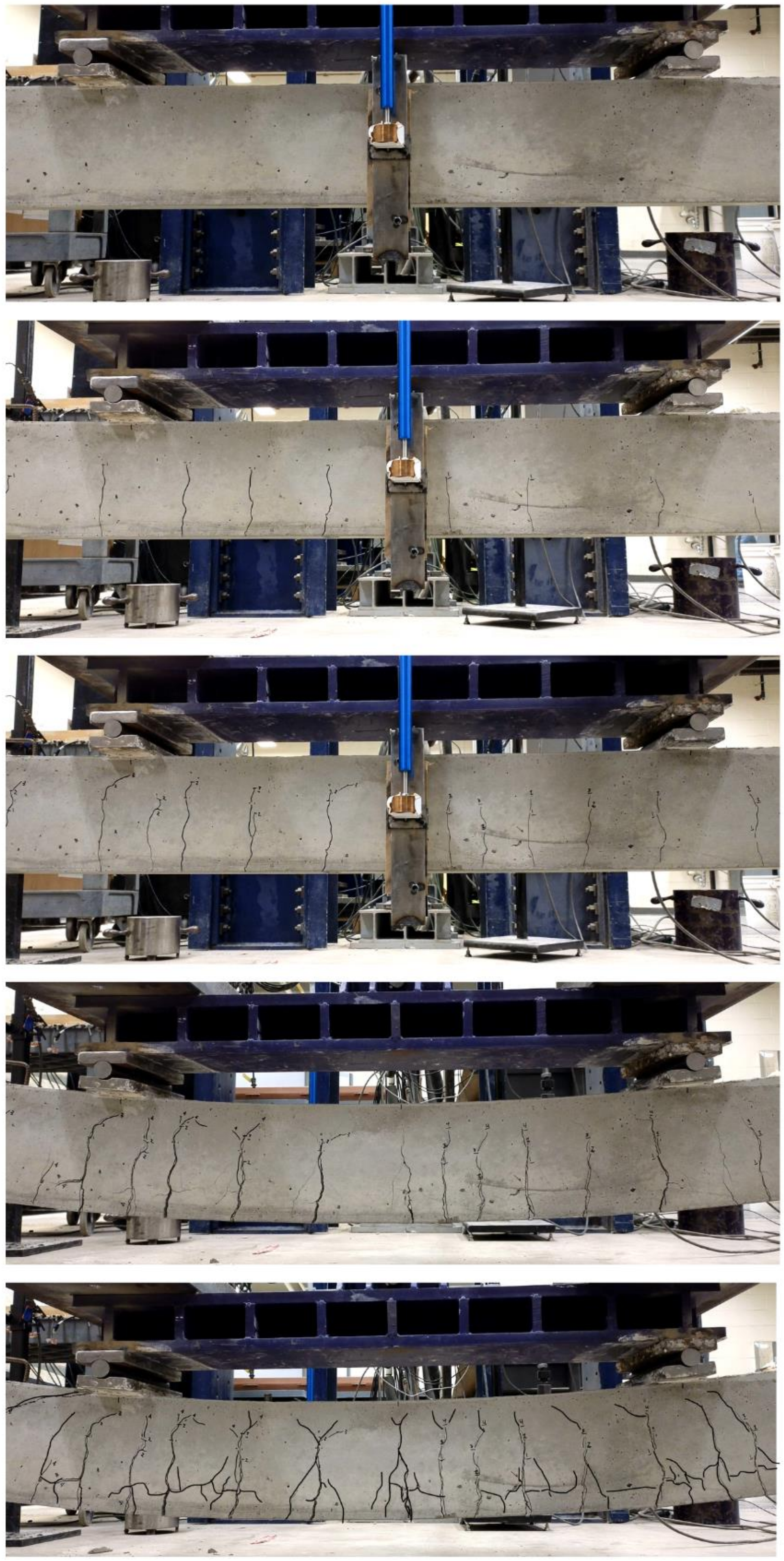

15% replacement beam #3 prior to loading

15% replacement beam #3 just after first crack

15% replacement beam #3 at reinforcement yield

15% replacement beam #3 at peak load

15% replacement beam #3 after failure

Figure 4-10: 15% Replacement Beam Crack Propagation at Each Stage of Loading

4.4.2.2 Comparison of Effective Moment of Inertia Equations

The load-deflection responses for beams with a 15 percent coarse aggregate replacement are individually displayed for beams #1, #2, and #3 in Figure 4-11, Figure 4-12, and Figure 4-13, respectively. As outlined in Section 4.4.1.2, the experimental results are graphically represented by a solid black line. The utilization of Bischoff's (2005) equation for predicting deflection based on cracking and yield load is depicted in purple with circles, while Branson's (1965) equation for prediction is shown in yellow with squares. The ACI 318-19 method of flexural design is presented in red with triangles, incorporating experimental values for concrete compressive strength and steel yield strength. Furthermore, the green line with crosses illustrates load-deflection results based on ACI 318-19 for a typical 4,000 psi (27.6 MPa) mix.

For each of the 15 percent replacement beams, the load-deflection response falls between Bischoff's and Branson's equations. In contrast to the control beams, Bischoff's (2005) equation tends to overestimate the deflection at yield, with values of 0.891, 0.887, and 0.909 inches (22.6, 22.5, and 23.1 mm) for 15 percent replacement beams #1, #2, and #3, respectively. This leads to an overestimation of 19.6 percent on average compared to the experimental 15 percent replacement results. On the other hand, Branson's (1965) equation underestimates the deflection at yield, providing values of 0.560, 0.532, and 0.653 inches (14.2, 13.5, and 16.6 mm) for beams #1, #2, and #3, respectively. Branson’s equation results in a 22.3 percent decrease in the average deflection compared to the experimental 15 percent replacement results. Bischoff's equation is deemed adequate for the 15 percent replacement, as it overestimates deflection instead of underestimating the response like Branson’s equation. The effective moment of inertia equations saw deviations in their ability to predict the deflection at yield compared to the control beams.

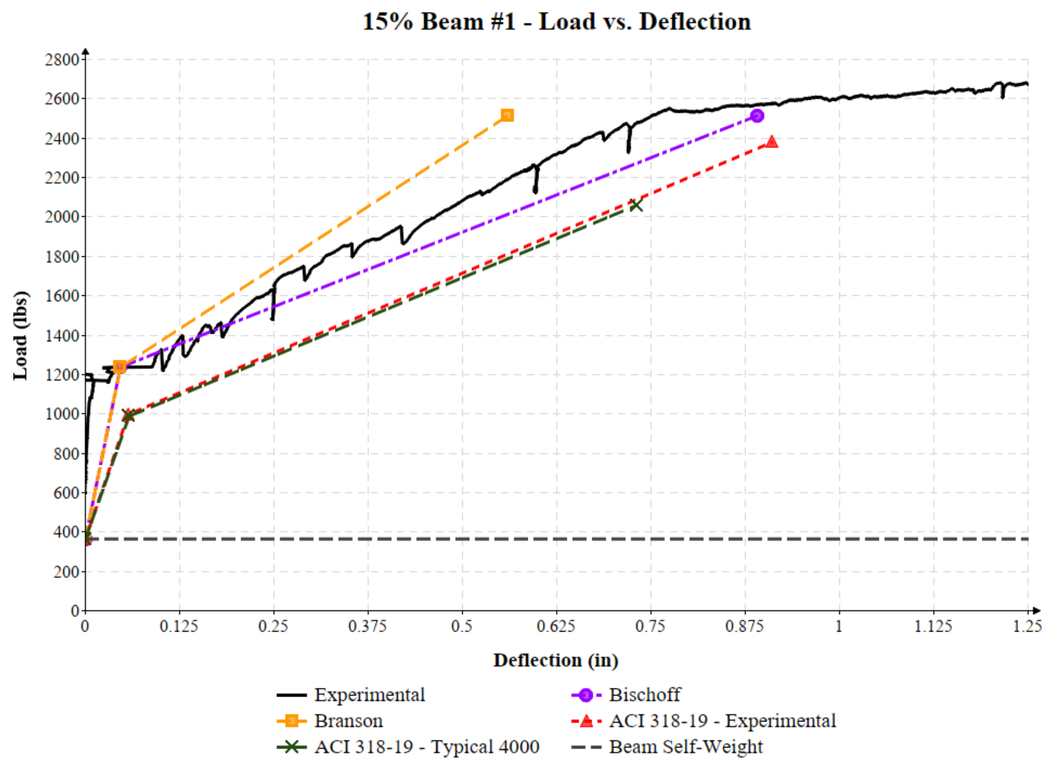

Figure 4-11: 15% Beam #1 Comparison of Effective Moment of Inertia Equations

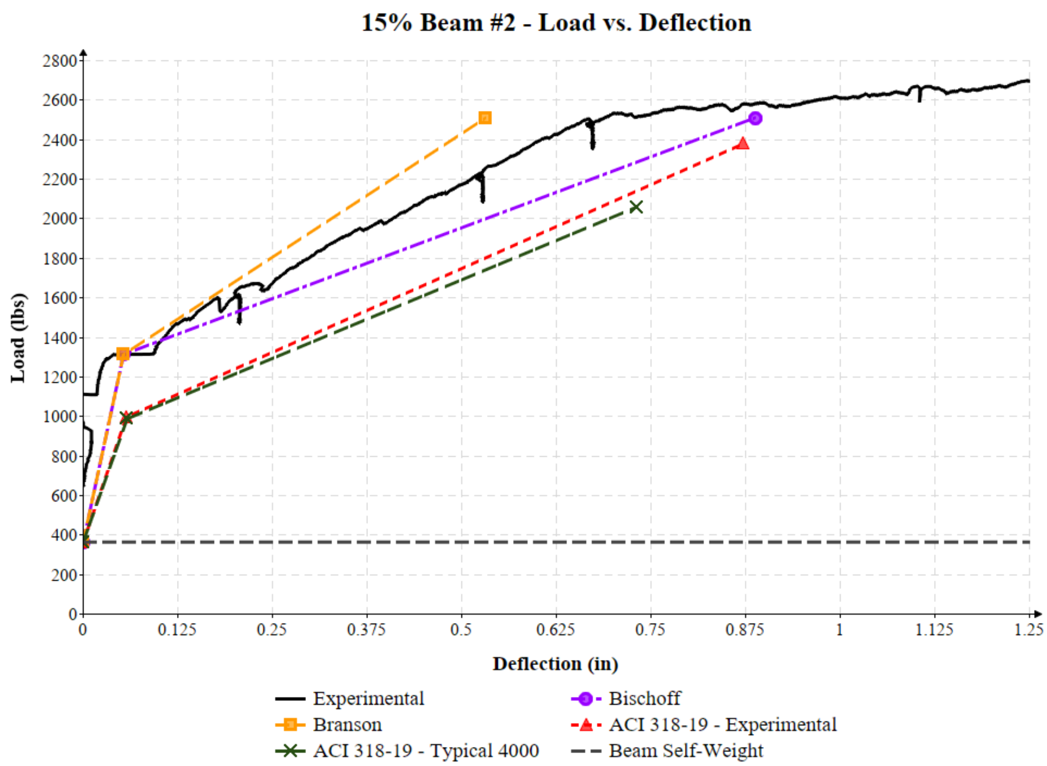

Figure 4-12: 15% Beam #2 Comparison of Effective Moment of Inertia Equations

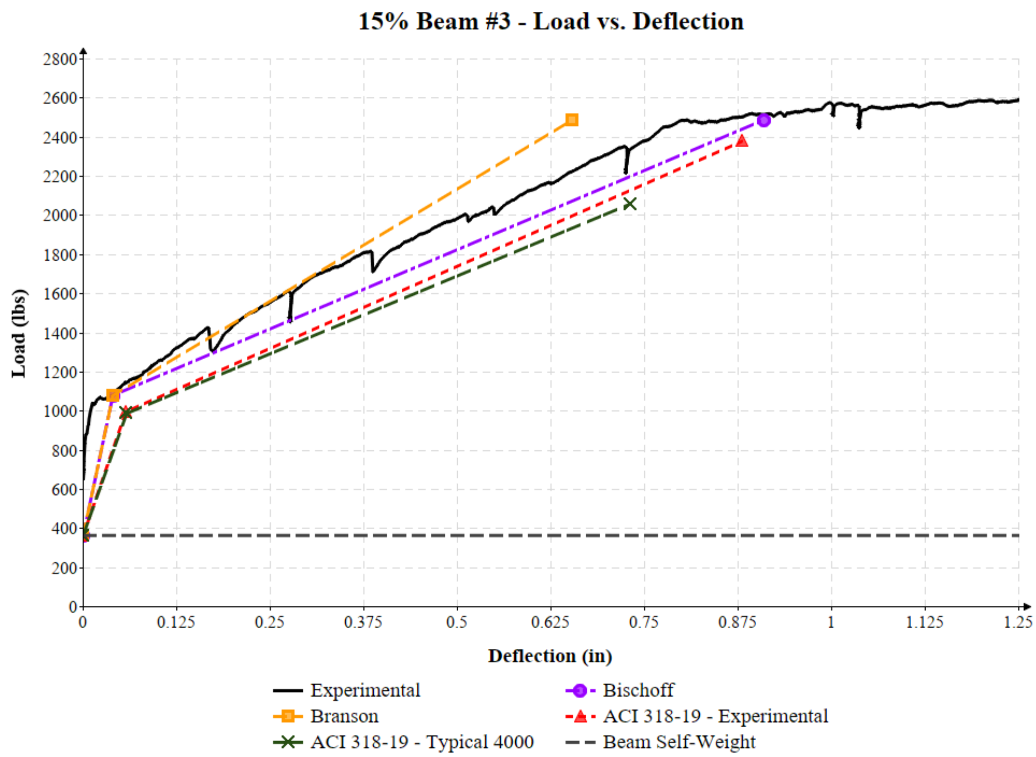

Figure 4-13: 15% Beam #3 Comparison of Effective Moment of Inertia Equations

Unlike the control beams, the cracking moment determined using ACI 318-19 was found to be significantly lower than the actual cracking moment for the 15 percent replacement beams. This is due to the increased experimental MOR compared to the MOR obtained from Equation 2-8. Similarly to the control beams the ACI 318-19 flexural response based on the experimental compressive strength (shown as a red dashed lines with triangles in the figures) better predicted the load deflection curve up to yield. This is due to the use of actual compressive strength of the mixture instead of the theoretical 4,000 psi (27.6 MPa). Using both the experimental and the theoretical compressive strength resulted in nominal moment capacities below the actual beam response for all members. On average the nominal moment capacities based on ACI 318-19 are 9.560 kip-ft (12.91 kN-m) and 8.238 kip-ft (11.17 kN-m) for the experimental and theoretical respectively. Upon incorporating the tension-controlled safety factor, ϕ, of 0.9 in the nominal moment capacity for the ACI equations decrease to 8.571 kip-ft (11.62 kN-m) for the experimental and 7.414 kip-ft (10.05 kN-m) for a typical 4,000 psi (27.6 MPa). The ACI 318-19 theoretical response was closer to the ACI 318-19 experimental response, compared to the control beams, due to the actual compressive strength of the 15 percent replacement mixture being 4,073 psi (28.1 MPa).

4.4.3 30 Percent Replacement Beam Load-Deflection Results

The outcomes from testing the three 30 percent replacement beam specimens are outlined in Table 4-14, and the corresponding load-deflection data is depicted in Figure 4-14. Table 4-14 provides details regarding the stiffness, MOE, and load and deflection at crack, yield, and ultimate stages for each 30 percent replacement beam, in addition to presenting the average values and the percentage increase from the control beam average load-deflection results. A negative percent increase signifies a decrease in the equivalent specimen property compared to the control values.

Table 4-14: 30% Replacement Beam Testing Results Obtained from Load-Deflection

Specimen Properties		Beam #1	Beam #2	Beam #3	Average	% Change
Stiffness, EI	kip/in	16.12	16.12	16.17	16.14	-16.6%
	kN/m	2,822	2,823	2,832	2,826	
MOE, E_c	ksi	3,332	3,333	3,343	3,336	-15.4%
	GPa	22.97	22.98	23.05	23.00	
Load @ Crack, P_{cr}	lbs.	1,065	1,103	793.7	987.1	-7.50%
	N	4,736	4,906	3,531	4,391	
Deflection @P_{cr}, Δ_{cr}	in.	0.044	0.047	0.027	0.039	8.10%
	mm	1.118	1.194	0.686	1.00	
Load @ Yield, P_y	lbs.	2,455	2,455	2,075	2,328	-7.8%
	N	10,919	10,922	9,231	10,357	
Deflection @ P_y, Δ_y	in.	0.901	0.800	0.721	0.807	-3.6%
	mm	22.89	20.32	18.31	20.51	
Peak Load, P_u	lbs.	3,199	3,399	2,909	3,169	-0.70%
	N	14,231	15,117	12,938	14,095	
Deflection @ P_u, Δ_u	in.	7.22	7.49	6.94	7.22	28.5%
	mm	183.5	190.3	176.4	183.4	

Note: negative percent change signifies a decrease in specimen property compared to control specimens

The stiffness of the 30 percent replacement beams demonstrated a decrease of 16.6 percent when compared to the average control beam stiffness. The MOE decreased from 3,945 kip/in^2 (27.2 GPa) for the control to 3,336 kip/in^2 (23.0 GPa). The stiffness and MOE for the 30 percent replacement members decreased by 11.6 and 11.3 percent respectively compared to the 15 percent replacement beams.

On average, the 30 percent replacement beams exhibited their first crack at 987 lbs (4,391 N), representing a 7.50 percent decrease in load compared to the control beam average and a 18.4 percent decrease compared to the 15 percent replacement. The 15 percent replacement specimens cracked before both the control and the 30 percent replacement members, emphasizing that the first crack load is not linear with the replacement of plastic aggregate. Additionally, the deflection at first crack was 0.039 inches (1.00 mm), marking a 8.10 percent increase over the control beams and a decrease of 15.1 percent compared to the 15 percent replacement specimens. The theoretical cracking moment, based on the average modulus of rupture, was determined to be 3.029 kip-ft (4.107 kN-m), corresponding to a theoretical point load of 757 lbs (3,369 N). On average, the 30 percent replacement beams' first crack, based on the load-deflection curve, was 230 lbs (1023 N) higher than the theoretical load.

At yield, the 30 percent replacement beams experienced inelastic deformation at a faster rate than the control and 15 percent replacement beams due to the increased slope of the load-deflection curve. This was a result of a significant decrease in the stiffness of the member after the tension steel yielded. The compressive strength and MOE of the concrete decreased with the addition of Plazrok, leading to this decrease in stiffness and an increase in deformation. The specimens continued to deflect with a slight increase in load before reaching the peak load, averaging 3,169 lbs (14,095 N), which is a 0.7 percent decrease over the control beams and a 2.3

percent decrease from the 15 percent replacement beams. On average, the 30 percent replacement members deflected 28.5 percent more than the control and 20.2 percent more than the 15 percent replacement beams. The failure occurred suddenly, with no softening of the load observed. Compared to the control and 15 percent replacement specimens, the 30 percent replacement showed a decrease in all specimen properties shown in Table 4-14 besides deflection. The significant decrease in stiffness after cracking led the member to increase in deflection quicker than the other two mixtures, resulting in a substantial increase in deflection. The 30 percent specimens were more ductile after the steel yielded due to this increased deflection.

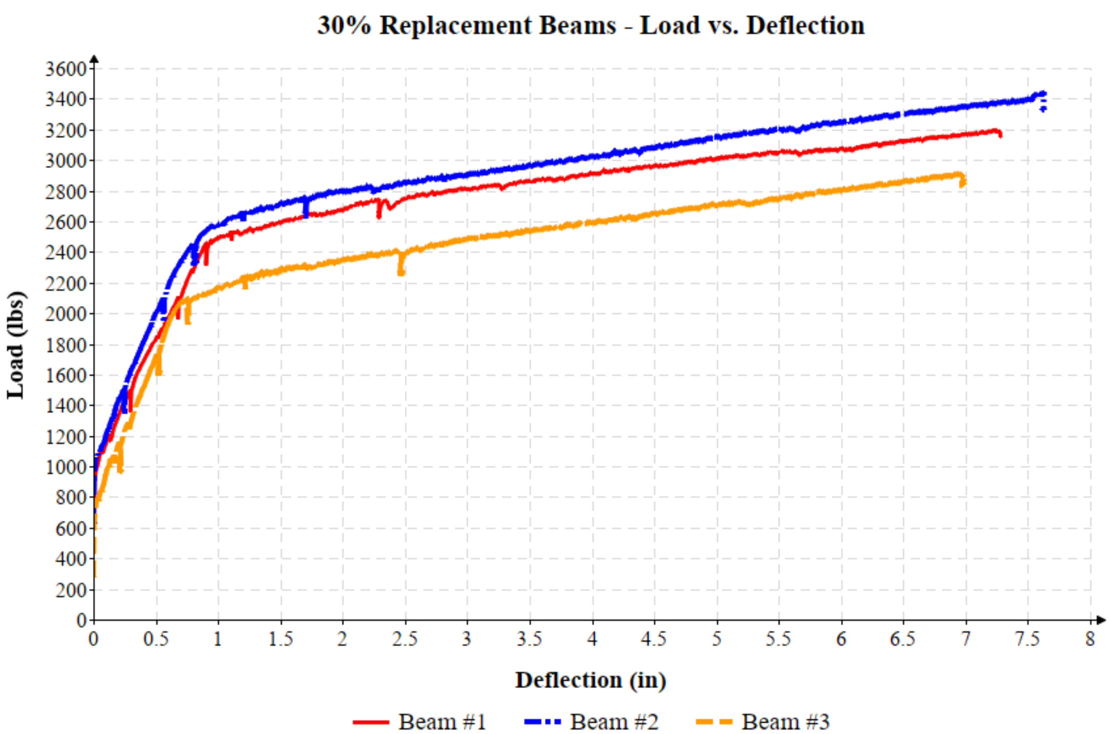

Figure 4-14: 30% Replacement Beams Load-Deflection Response Graphed

4.4.3.1 Crack Propagation

Similar to the control beams and 15 percent replacement specimens, the 30 percent replacement specimens displayed typical flexural cracking expected for a simply supported member under four-point bending. Figure 4-15 illustrates the response of 30 percent replacement beam #1 at various loads as listed in Table 4-14. No discernible difference between the crack patterns of the control, 15 percent replacement, and 30 percent replacement members at first crack and yielding of the reinforcing steel was observed.

At the peak loading experienced by each beam, significantly more cracking occurred in the 30 percent replacement members compared to the control and 15 percent replacement. Spalling of the concrete, in the compression zone, on the 30 percent members happened between the point loads, but the members still experienced diagonal tension failure, similar to all other beam types. If additional coarse aggregate replacement is used, a likelihood of a compression failure occurring due to the significant decrease in the stiffness of the member is possible.

30% replacement beam #1 prior to loading

30% replacement beam #1 just after first crack

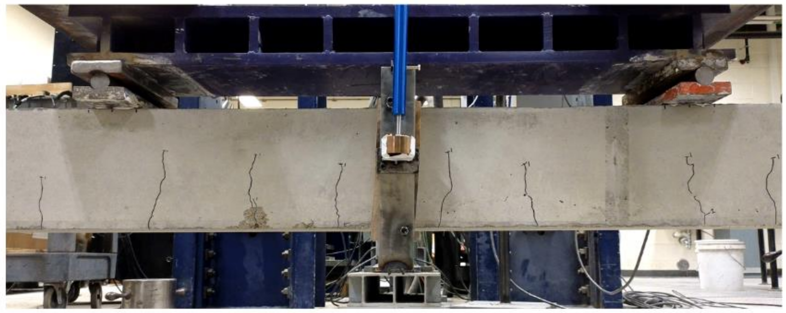

30% replacement beam #1 at reinforcement yield

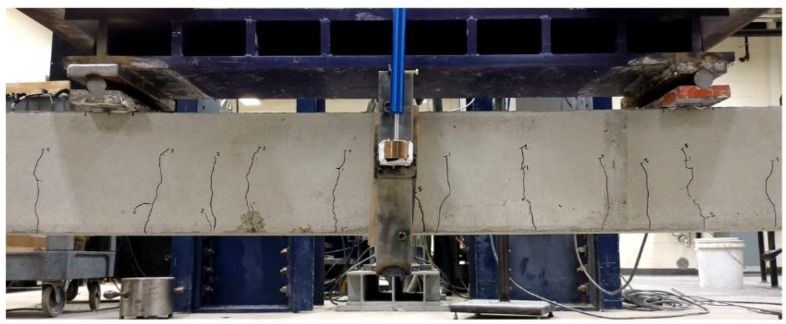

30% replacement beam #1 at peak load

30% replacement beam #1 after failure

Figure 4-15: 30% Replacement Beam Crack Propagation at Each Stage of Loading

4.4.3.2 Comparison of Effective Moment of Inertia Equations

The load-deflection responses for beams subjected to a 30 percent coarse aggregate replacement are individually presented for beams #1, #2, and #3 in Figure 4-16, Figure 4-17, and Figure 4-18, respectively. As detailed in Section 4.4.1.2, the experimental results are visually depicted as solid black lines. Bischoff's (2005) equation for predicting deflection based on cracking and yield load is represented in purple with circles, while Branson's (1965) equation for prediction is shown in yellow with squares. The ACI 318-19 flexural design method is portrayed in red with triangles, incorporating experimental values for concrete compressive strength and steel yield strength. Additionally, the green line with crosses illustrates load-deflection results based on ACI 318-19 for a typical 4,000 psi (27.6 MPa) mix.

Similar to the control and 15 percent replacement beams, Branson's (1965) equation consistently underestimates deflection at yield, providing values of 0.682, 0.660, and 0.638 inches (17.3, 16.8, and 16.2 mm) for 30 Percent Replacement Beams #1, #2, and #3, respectively. On average, Branson's (1965) effective moment of inertia equation results in a deflection 18.2 percent lower than the average 30 percent replacement member. The underestimation of deflection predicted by Branson's equation remains consistent across each mix design with the control beams resulting in 20.8 percent more deflection at yield, and the 15 percent replacement members resulting in 22.3 percent more deflection at yield. As stated in Section 2.5.4, Branson's (1965) equation is not accurate at predicting deflection for lightly reinforced beams ($\rho \leq 1.0\%$).

Alternatively, Bischoff's (2005) effective moment of inertia equation overestimates the deflection at yield with values of 0.918, 0.913, and 0.789 inches (23.3, 23.2, and 20.0 mm) for the 30 Percent Replacement Beams #1, #2, and #3, respectively. This leads to an average overestimation of 8.2 percent compared to the experimental 30 percent replacement results. While neither equation is perfect in predicting the load-deflection response, Bischoff's equation provides the closest results.

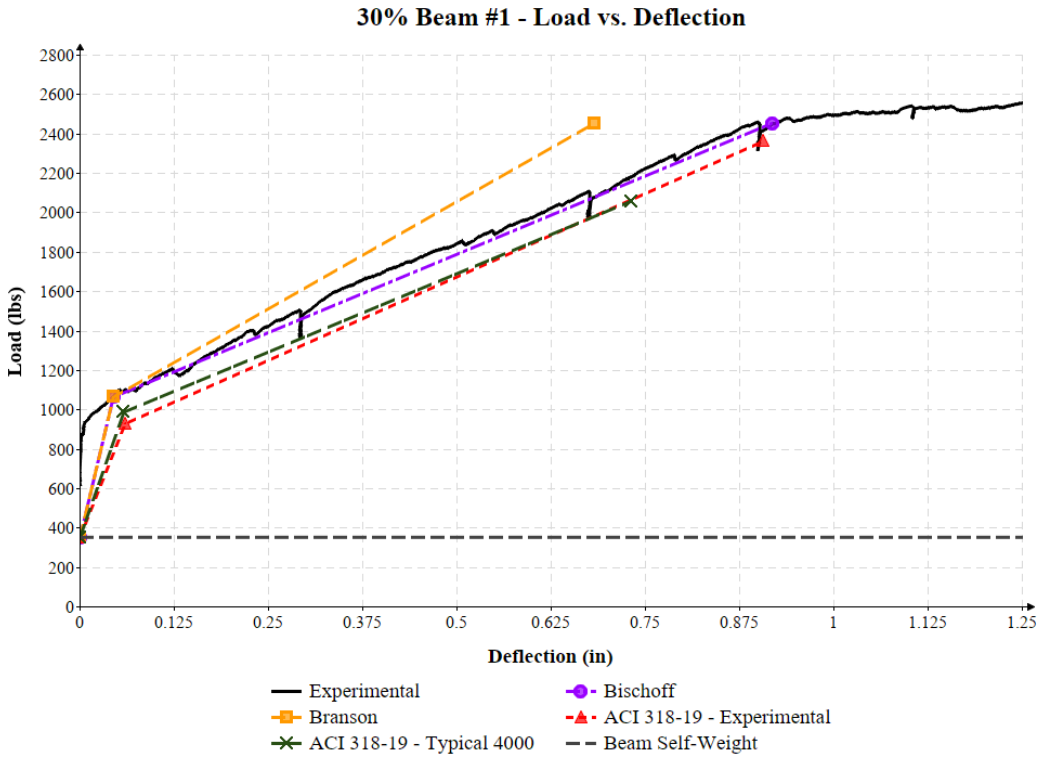

Figure 4-16: 30% Beam #1 Comparison of Effective Moment of Inertia Equations

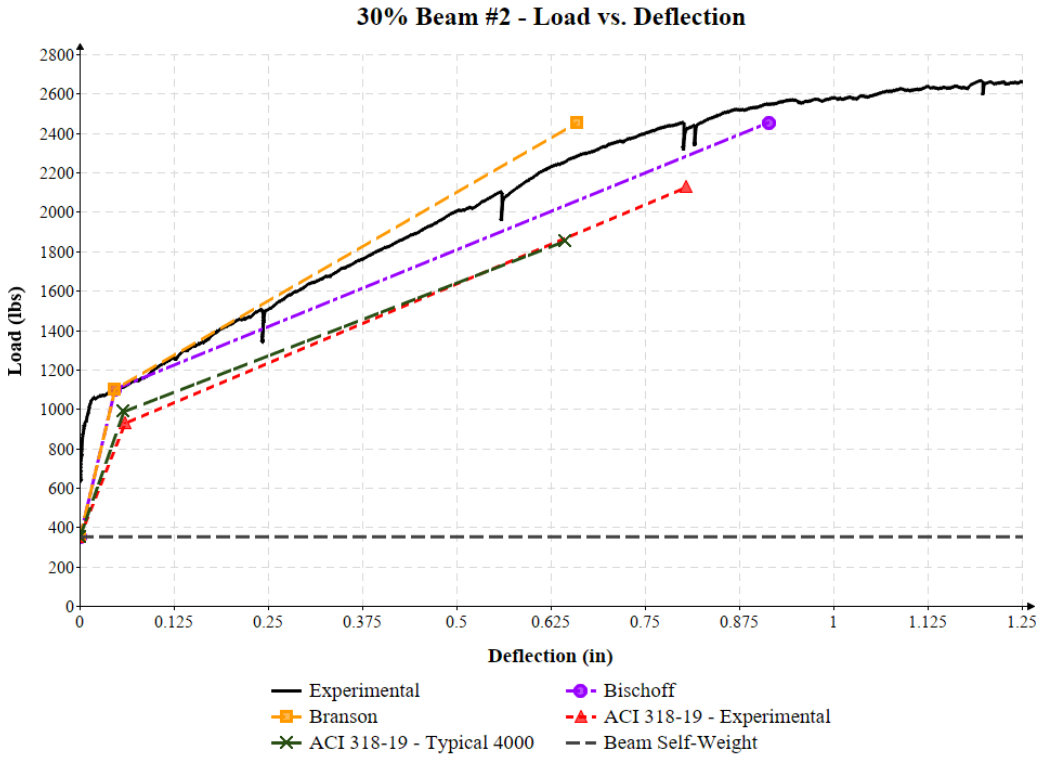

Figure 4-17: 30% Beam #2 Comparison of Effective Moment of Inertia Equations

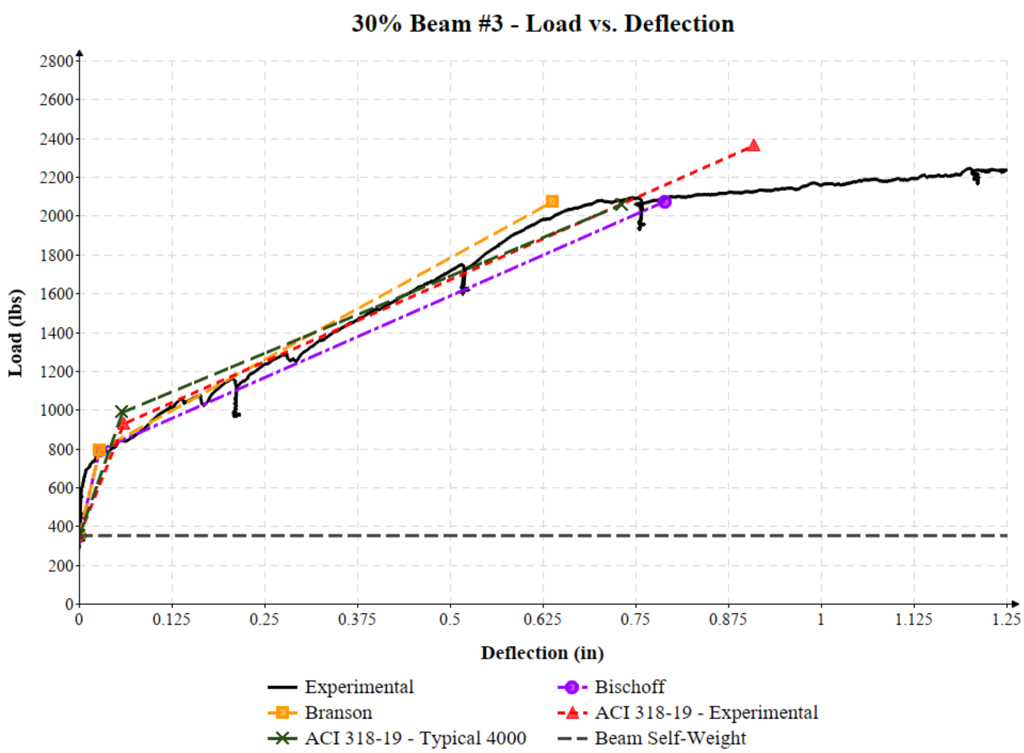

Figure 4-18: 30% Beam #3 Comparison of Effective Moment of Inertia Equations

For 30 Percent Replacement Beams #1 and #2, the observed cracking moments exceeded the ACI 318-19 predicted cracking moment, while for 30 Percent Replacement Beam #3, it was lower than the predicted value. The ACI 318-19 flexural results, both for the experimental values and theoretical 4,000 psi (27.6 MPa) mixture values, yielded lower results for 30 Percent Replacement Beams #1 and #2 while overestimating the capacity of Beam #3.

Upon applying the tension-controlled safety factor, $\phi = 0.9$, the nominal moment capacity for the experimental ACI 318-19 results decreases from 9.452 kip-ft (12.81 kN-m) to 8.507 kip-ft (11.53 kN-m), while the moment capacity for a typical 4,000 psi (27.6 MPa) mix would decrease from 8.238 kip-ft (11.17 kN-m) to 7.414 kip-ft (10.05 kN-m). Each of the ACI predictions are below the average load-deflection results, even with a 20 percent reduction in compressive strength of the concrete. A 30 percent replacement of coarse aggregate with Plazrok is a viable option for tension-controlled simple flexural members.

4.4.4 Stiffness and Modulus of Elasticity

The concrete modulus of elasticity, also known as the secant modulus, was obtained by analyzing the stiffness of the elastic portion derived from the slope of the secant line plotted on the load-deflection graph, extending from the origin to the point of first crack. As strains were not directly measured, the determination of first crack was made visually based on the load-deflection diagram. In Figure 4-19, an illustration showcases an instance of the secant line used to evaluate the stiffness of the beam up to the point of crack initiation.

The visual identification of first crack is associated with a noticeable change in slope on the load-deflection curve, signifying the moment when the beam section starts transferring the tensile load to the tension steel, resulting in a sudden decrease in load and increase in deflection.

Subsequently, following the determination of stiffness, Equation 2-30 was used to calculate the concrete modulus of elasticity.

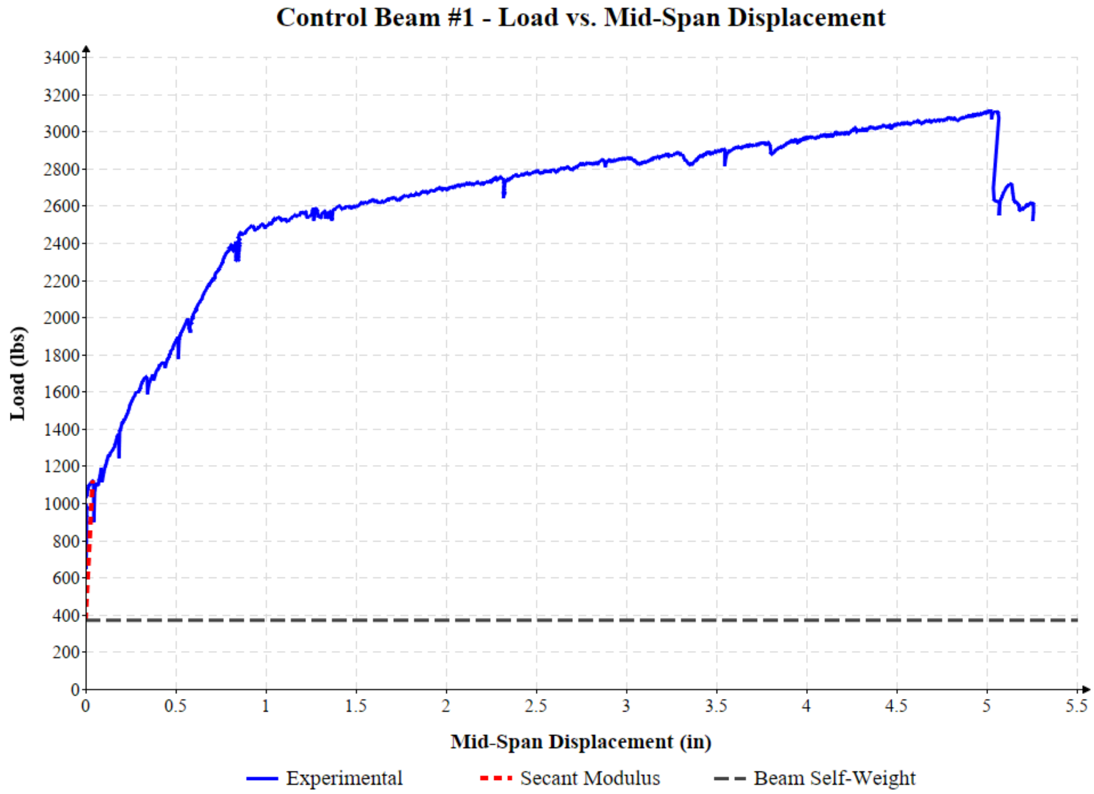

Figure 4-19: Example of Secant Modulus Determination

Table 4-15 presents the average stiffness, modulus of elasticity (MOE), and max deflection obtained from the load-deflection curves in Sections 4.4.1, 4.4.2, and 4.4.3. With the increase in Plazrok replacement for coarse aggregate the average beam stiffness and MOE decrease while the maximum deflection increased. The stiffness decreased by 5.90 and 16.6 percent for the 15 and 30 percent replacement beams respectively compared to the control mix. The MOE decreased by 4.30 and 15.4 percent for the 15 and 30 percent replacement beams respectively compared to the control mix. Since deflection and stiffness are inversely proportional, the maximum deflection increased by 6.90 and 28.5 percent on average for the 15 and 30 percent replacement beams compared to the control.

Table 4-15: Average Stiffness, MOE, and Max Deflection

Beam Type		Property					
		Stiffness, EI		MOE, E_c		Max Deflection, Δ_u	
		kip/in	kN/m	ksi	GPa	in.	mm
Control	**Value**	19.34	3,387	3,945	27.2	5.62	143
	Difference	0.00%		0.00%		0.00%	
15%	**Value**	18.20	3,187	3,774	26.0	6.01	153
	Difference	-5.90%		-4.30%		+6.9%	
30%	**Value**	16.14	2,826	3,336	23.0	7.22	183
	Difference	-16.6%		-15.4%		+28.5%	

Note: Negative percentage denotes decrease compared to control beam results

Section 2.3.2.4 of this Thesis introduces MOE equations obtained from codes around the world for determining the MOE based on the compressive strength of the concrete. Table 4-16 compares the experimental MOE values to the code equations. The average compressive strength obtained during material test (Section 4.3.1) was used to determine the MOE using ACI 318-19 (Equation 2-13 and Equation 2-14), IS 456 (Equation 2-17), EN 1992-1-1 (Equation 2-18), and CAN/CSA A23.3 (Equation 2-19).

In Table 4-16, the percent change column provides a comparison between the code equation results for the MOE and the corresponding experimental values. The most accurate code equation for all three mix designs was ACI 318-19a (Equation 2-13), which is density-based, exhibiting a slight overestimation of 1.23 percent for the control beams and an underestimation of 1.77 and 1.31 percent for the 15 and 30 percent replacement members respectively. According to the results in Table 4-16, the ACI 318-19 code equations exhibited the most consistent performance across the three mix designs. As the percent of coarse aggregate replacement increased the IS 456 (Equation 2-17) and EN 1992-1-1 (Equation 2-18) decreased in accuracy while the CAN/CSA A23.3 (Equation 2-19) and ACI 318-19b (Equation 2-14) increased in accuracy.

Table 4-16: MOE Comparison with Code Equations

Calculation	Control			15%			30%		
	E_c		% Change	E_c		% Change	E_c		% Change
	ksi	GPa		ksi	GPa		ksi	GPa	
Experimental	3,945	27.2	0.00%	3,774	26.0	0.00%	3,336	23.0	0.00%
Equation 2-13 (ACI 318-19a)	3,994	27.5	1.23%	3,708	25.6	-1.77%	3,293	22.7	-1.31%
Equation 2-14 (ACI 318-19b)	3,789	26.1	-4.12%	3,638	25.1	-3.73%	3,390	23.4	1.59%
Equation 2-17 (IS 456)	4,003	27.6	1.45%	3,843	26.5	1.80%	3,582	24.7	6.87%
Equation 2-18 (EN 1992-1-1)	4,772	32.9	17.3%	4,691	32.3	19.6%	4,540	31.3	26.5%
Equation 2-19 (CAN/CSA A23.3)	3,603	24.8	-17.3%	3,459	23.8	-9.1%	3,224	22.2	-3.47%

Note: Negative percentage denotes decrease in MOE compared to experimental results

The experimental data obtained for MOE should be approached with caution, as the MOE was determined based on the load-deflection curve and not through a standard test similar to *ASTM C469/C469M-22 Standard Test Method for Static Modulus of Elasticity and Poisson's Ratio for Concrete in Compression*.

4.4.5 Flexural Capacity

The determination of flexural capacity for reinforced concrete members according to code occurs at the point when the steel yields. Once the steel yields, code equations consider the flexural member as failed, despite its ability to still carry load. The purpose is for the safety of the public. The concrete compressive stress distribution significantly influences the determination of the flexural member, and Section 2.5 of this thesis outlines the three most common and widely accepted stress distribution theories: straight-line theory (Section 2.5.1), parabolic stress theory (Section 2.5.2), and equivalent stress theory (Section 2.5.3). It is important to note that each of these theories assumes that the concrete takes no tensile force after cracking. The moment capacity for each theory is described by Equation 2-22, Equation 2-25, and Equation 2-26 for straight-line, parabolic, and equivalent stress theories, respectively. Table 4-17 presents the nominal moment capacity based on each stress distribution theory compared to the experimental results. The moment equations are derived from the distance between the tensile force and net compressive force.

In parabolic stress distribution, the parameter k_2/k_1k_3 varies based on the magnitude and position of the internal compressive force. Extensive studies by researchers such as Whitney, Hognestad, Jensen, and Gaston have examined these parameters. It has been established through research that this parameter varies significantly between different members failing in tension (Hognestad et al., 1955). The actual stress distribution varies among specimens, even those of the same mix design, making the prediction of nominal moment capacity challenging. Given accepted values for the k_2/k_1k_3 parameter vary between 0.5 to 0.6, each value is presented in Table 4-17.

Following the capacities derived from the parabolic stress theory, the next lines involve the equivalent stress theory as per ACI 318-19. Given that ACI 318-19 uses Whitney's (1937) equivalent stress block, it results in identical outcomes for each nominal moment equation. The moment capacities based on straight line, parabolic, and equivalent stress theories are determined using the experimental compressive strengths established in Section 4.3.1.

Additionally, ACI 318-19 was utilized to predict the nominal moment capacity based on a typical 4,000 psi (27.6 MPa) mix, a process conducted throughout Sections 4.4.1, 4.4.2, and

4.4.3. These results aim to illustrate how a practicing structural engineer would calculate the capacities of the flexural member in practical scenarios.

Table 4-17: Nominal Moment Capacity Comparison with Code Equations

Calculation	Control			15%			30%		
	M_n		% Change	M_n		% Change	M_n		% Change
	kip-ft	kN-m		kip-ft	kN-m		kip-ft	kN-m	
Experimental*	10.1	13.70	0.00%	10.0	13.58	0.00%	9.31	12.63	0.00%
Straight Line Theory*	9.24	12.53	8.51%	9.23	12.51	7.87%	9.19	12.46	1.33%
Parabolic Stress Theory* $k_2/k_1k_3 = 0.5$	9.63	13.05	4.73%	9.59	13.01	4.23%	9.53	12.93	-2.36%
Parabolic Stress Theory* $k_2/k_1k_3 = 0.6$	9.55	12.95	5.46%	9.51	12.90	5.03%	9.44	12.80	-1.37%
Equivalent Stress Theory/ACI 318-19*	9.56	12.96	5.38%	9.52	12.91	4.94%	9.45	12.81	-1.48%
ACI 318-19 Theoretical**	8.24	11.17	18.5%	8.24	11.17	17.8%	8.24	11.17	11.6%

Note: Negative values represent an overestimation based on the experimental results.
*Based on experimental data; **Based on theoretical value of 4,000 psi (27.6 MPa) compressive strength

The parabolic stress theory using a k_2/k_1k_3 parameter set equal to 0.5 exhibited the closest approximation of the flexural capacity of the control and 15 percent specimens at reinforcement yield. The parabolic stress theory would be even more accurate with strain gage data from which the k_2/k_1k_3 parameter could accurately be calculated. Instead, an approximation of the parabolic stress block provides acceptable results. The equivalent stress block, which simplifies the parabolic stress block, produced similar results to the parabolic stress block. The results of the 0.5 parabolic stress block differed by 0.65, 0.71, and negative 0.88 percent compared to the equivalent stress block for the control, 15, and 30 percent replacement beams respectively. The parabolic and equivalent stress distributions overestimated the nominal moment capacity of the 30 percent replacement members but with safety factors the members would be adequate.

As expected, the straight-line theory resulted in the most error, excluding the ACI 318-19 theoretical results. The straight-line theory assumed the material is linear elastic with the stresses proportional to the strains which is only adequate up to first crack.

The final row in Table 4-17 presents the ACI 318-19 results based on a typical 4,000 psi (27.6 MPa) mix, resembling how a practicing engineer would calculate the nominal moment capacity of a flexural member. Given that the actual compressive strength is not known at the design stage, a minimum limit is employed. As indicated in the table, ACI 318-19 predicts the nominal moment capacity below the actual flexural capacity of the member. The predicted capacities were 18.5, 17.8, and 11.6 percent lower for the control, 15, and 30 percent replacement mixtures respectively. The ACI 318-19 theoretical predicted capacities are significantly lower than the rest of the predictions due to the use of a theoretical compressive strength of 4,000 psi (27.6 MPa) and a steel yield strength of 60 ksi (414 MPa). The actual steel yield strength was found to be 69.8 ksi (481 MPa) (in Section 4.3.4) which increased the nominal moment capacity for each beam specimen. The predicted capacity based on ACI 318-19 increased in accuracy with increasing plastic coarse aggregate replacement since the compressive strength of the concrete decreased. If the reinforcing steel was closer to 60 ksi (414 MPa) the ACI 318-19 theoretical capacity would overestimate the capacity of the 30 percent replacement members.

4.4.6 Aggregate Distribution

Concerns arose regarding the uniform distribution of Plazrok throughout the beams due to its low specific gravity and challenges in finishing the beam specimens.

Figure 4-20 displays cross-section samples taken after the beams were tested, offering insights into the distribution of Plazrok. The far-left beam illustrates the 30 percent replacement, the control is on the far right, and the 15 percent replacement is in the center with visible pieces of Plazrok circled.

Initially, the Plazrok appeared to be well-distributed throughout the beams. However, it is crucial to note the accumulation of Plazrok at the top of the beams near the right edge in both the 15 and 30 percent replacements. This phenomenon is likely attributed to the use of a vibrator during concrete consolidation. Costello et al. (2021) observed a uniform dispersion of Plazrok throughout their cylinders when consolidating by hand. In the 30 percent replacement, the buildup of Plazrok around the edges is less pronounced compared to the 15 percent replacement, which exhibits a sizable void with no Plazrok in the center of the member.

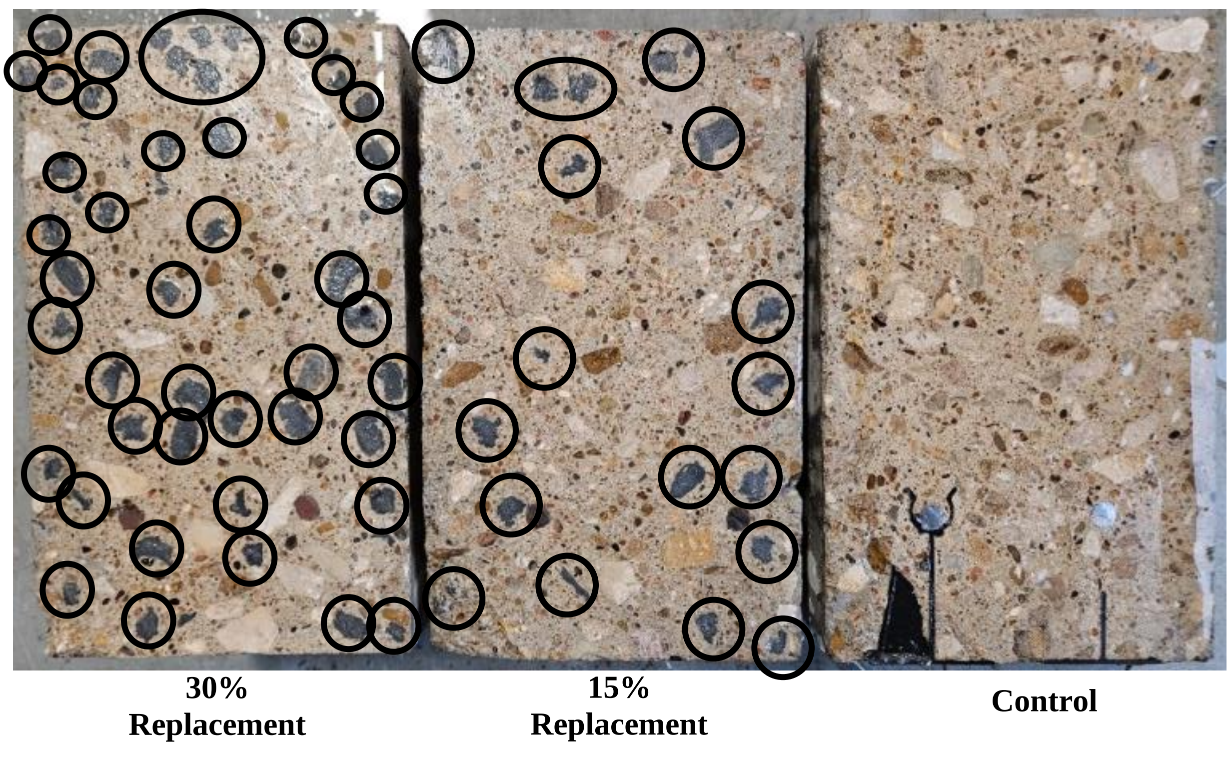

30%
Replacement

15%
Replacement

Control

Figure 4-20: Plazrok Distribution

Chapter 5 - Conclusion and Recommendations

This thesis conducted comprehensive mechanical property tests to assess the characteristics of concrete with an increasing percentage of coarse aggregate replaced using a plastic aggregate known as Plazrok. The mix designs included a control, 15 percent replacement, and 30 percent replacement by volume. Key parameters such as density and water-to-cement (*w/c*) ratio were determined and compared for each mix design. Material strength tests were conducted on both the mixes and reinforcement, including cylinder compression tests, cylinder tensile splitting tests, modulus of rupture flexural tests, and reinforcement tensile tests.

After these material strength tests, flexural tests were performed on six inch (152 mm) wide by 10 inch (254 mm) deep by 12 feet (3.7 m) long reinforced concrete beam specimens, and load-deflection data were meticulously collected from LVDTs (Linear Variable Differential Transformers) for each mix design. Then the stiffness, modulus of elasticity, flexural capacity, and aggregate distribution for each specimen was determined based on the load-deflection results obtained from the flexural testing.

Section 5.1 of this thesis presents the conclusions drawn from the experimental results, highlighting key findings and insights. Following this, Section 5.2 outlines potential avenues for future research, suggesting areas where further investigation could enhance our understanding of the behavior of concrete with plastic aggregate replacements.

5.1 Key Findings

5.1.1 Plastic State and Mechanical Properties

The key findings drawn from the examination of plastic state (fresh concrete) and mechanical properties, as presented in Sections 4.2 and 4.3 of this Thesis, are as follows:

1. The density of concrete decreases with increasing recycled waste plastic aggregate (Plazrok) replacement. This is expected due to the specific gravity of the Plazrok being lower than the naturally occurring coarse aggregate. Even at 30 percent replacement, the mixture was not classified as lightweight concrete according to ACI 318-19.
2. The incorporation of recycled waste plastic aggregate (Plazrok) increases the workability of the mixture, resulting in a reduction in the required water content to achieve a specified slump of 6 inches (152 mm). Notably, the control mixture exhibited a *w/c* ratio of 0.37, whereas the 15 and 30 percent replacement mixtures demonstrated *w/c* ratios of 0.34 and 0.35, respectively. The *w/c* ratios were different than recorded due to excess washout water left in the concrete truck, as discussed in Section 4.2.
3. The compressive strength of the concrete decreases with increased Plazrok replacement. At 15 percent replacement, the compressive strength decreased by 7.8 percent while at 30 percent replacement, the compressive strength decreased by 20.0 percent. A similar decrease was examined by Costello et al. (2021) where at 15, 30, and 45 percent replacement the compressive strength decreased 18.1, 35.6, and 45.3 percent. Costello et al. (2021) results had a known *w/c* ratio while the addition of

washout water in the concrete truck resulted in a higher and unknown *w/c* ratio for each mixture tested in this thesis.

4. The tensile splitting strength increases with the addition of Plazrok replacement. At 15 percent replacement, the splitting strength increased by 38.5 percent and 17.7 percent for 30 percent replacement. The splitting tensile strength seems to peak at 15 percent replacement and beings to decrease back towards the control tensile strength at 30 percent replacement. Costello et al. (2021) saw a decrease in tensile strength with increase replacement unlike the results present in this thesis. A 3.2, 4.2, and 21.9 percent decrease was examined for Costello et al. (2021) 15, 30, and 45 percent replacement mixes respectively.
5. Further investigation and testing are needed for the MOR with coarse aggregate replacement using Plazrok. The MOR calculated in this thesis of 775 psi (5.34 MPa) differs significantly from Costello et al. (2021) maximum MOR of 270 psi (1.86 MPa) for the control mix. The variations in batching methods and mixing environments may contribute to the observed differences.
6. The relationships between compressive strength, tensile splitting strength, and modulus of rupture do not exhibit linear variations for all concrete mixes with coarse aggregate replacement, as suggested by Alkotami and Kramer (2023) and Costello et al. (2021) equations. Additional parameters, including aggregate shape, aggregate type, *w/c* ratio, and percent replacement, should be considered for a more comprehensive understanding of the observed variations.

5.1.2 Load-Deflection and Stiffness

The key findings derived from the comparison of experimental load-deflection curves with ACI 318-19 Theoretical for a 4,000 psi (27.6 MPa) mixture, Branson (1965), and Bischoff (2005), along with the observed decrease in stiffness are summarized as follows:

1. As the coarse aggregate replacement with Plazrok increases, a corresponding decrease in member stiffness occurs. The addition of Plazrok resulted in a flexural stiffness reduction of 5.90 and 16.6 percent for the 15 and 30 percent replacement mixtures, respectively. This decrease in stiffness is indicative of an amplified deflection in comparison to the control members – similar to lightweight concrete.
2. The deflection and physical cracking of the beams increased corresponding to the rise in recycled waste plastic aggregate replacement. This is expected due to the concurrent decrease in flexural stiffness and modulus of elasticity. Specifically, the deflection experienced increments of 6.90 and 28.5 percent for the 15 and 30 percent replacement members, respectively.
3. Aside from the decrease in stiffness, the beam with partial coarse aggregate replacement exhibited the same cracking pattern and flexural failure as the control members. Given that the members were lightly reinforced ($\rho = 0.0046$), and tension controlled as defined by ACI 318-19, the introduction of plastic aggregate replacement did not diminish the strength of the concrete sufficiently to induce crushing of the concrete in the flexural members tested.
4. The 15 percent replacement members exhibited first crack at a load 13.4 percent higher than the control whereas the 30 percent replacement members exhibited first crack at a load 7.5 percent lower than the control. The 15 percent replacement

members ability to carry more load before cracking is due to the increased tensile splitting strength of the mixture.

5. No significant change in the yield or peak load was seen by each of the mixtures. The only significant change was in the deflection at first crack, yield, and at failure where the 15 and 30 percent replacements exhibited a higher deflection at the same load. As the plastic aggregate replacement increases the yield and peak load remain constant with increased deflection.
6. Bischoff (2005) claims that Branson (1965) effective moment of inertia was inadequate for lightly reinforced members ($\rho \leq 1.0\%$) and at higher loads was validated. For each of the mixtures tested, Branson's effective moment of inertia equation, used to predict the deflection of the tested beams, was less than the actual deflection. Whereas using Bischoff's effective moment of inertia equation the tested beams deflection was either overestimated or was close to the actual deflection.
7. The parabolic stress theory using a k_2/k_1k_3 parameter set equal to 0.5 was the closest to predicting the flexural capacity of the specimens at reinforcement yield but using a value of 0.6 or the equivalent stress block yielded similar results. The straight-line theory had the most error as expected since it is best suited for the linear-elastic range. As the natural coarse aggregate replacement increased, the percent error of the nominal moment capacity equations decreases due to the higher strength steel and decreasing compressive strength.
8. The calculated design strength using an equivalent stress block approach, according to ACI 318-19 (Section 2.6), of a typical 4,000 psi (27.6 MPa) concrete mixture yields nominal moment capacities less than the control, 15, and 30 percent

replacement beams. The design nominal moment capacity should be below the actual behavior of the tested beam. Therefore, the ACI 318-19 design approach appears to be adequate for the design of members up to 30 percent replacement with Plazrok.

9. Up to 30 percent replacement is a viable option in tension controlled, lightly reinforced members, but more research is required for mechanical properties and load-deflection behavior. Additionally, while the 30 percent replacement is viable it is not necessary when the 15 percent replacement or lower would make a significant impact on the growing plastic waste problem without a substantial impact to our concrete mechanical properties.

5.2 Recommendations and Future Research

It is recommended to consider a replacement of coarse aggregate with Plazrok up to 30 percent, or lower, as a viable option for lightly reinforced, tension-controlled flexural reinforced concrete members. At 15 and 30 percent replacement, the ACI 318-19 design method for flexural members was proven to be effective by underestimating the strength of the members which is needed in design/consulting profession. At a 30 percent replacement, the mixture experiences a substantial reduction in strength, resulting in decreased stiffness but is deemed adequate. Since beams were tension-controlled, and the actual strength of the reinforcement was higher than the ASTM A615 minimums for Grade 60, 30 percent replacement members exceeded the design flexural strength. The significant decrease in stiffness at 30 percent replacement may pose challenges in meeting code deflection limits resulting in larger members. Although 30 percent replacement was proven to be adequate a more realistic percentage replacement with Plazrok would be 5, 10, and 15 percent replacement. By replacing just 5 percent of coarse aggregate with Plazrok the global plastic waste problem would be significantly impacted without significantly affecting the mechanical properties of the concrete.

Further research is essential for the successful implementation of recycled waste plastic coarse aggregate (Plazrok) replacement in load-carrying structural members, such as beams (flexural members). Adjustment factors are needed to fine-tune the compressive and tensile strength of the concrete based on the percentage replacement of coarse aggregate. Additional testing to understand the impact of Plazrok on the development length of reinforcement and its effect on the bond between deformed bars and concrete with replacement aggregate is needed. Exploring additional flexural testing on varying member sizes and reinforcement ratios is needed. Additionally, testing beams designed to fail in shear would contribute to a more comprehensive understanding. This study underscores that plastic coarse aggregate replacement presents a promising option in reinforced concrete structures, contributing to a more sustainable future.

References

Abrams, D. (1918). Design of Concrete Mixtures. *Structural Materails Research Laboratory, Lewis Institute, Chicago, Bulletin No. 1*, 20.

ACI 318-19 Building Code Requirements for Structural Concrete and Commentary. (2019). American Concrete Institute. https://doi.org/10.14359/51716937

ACI 435R-20 Report on Deflection of Nonprestressed Concrete Structures. (2020). American Concrete Institute. www.concrete.org

Akram, A., Sasidhar, C., & Mehraj Pasha, K. (2015). E-Waste Management by Utilization of E-Plastics in Concrete Mixture as Coarse Aggregate Replacement. *International Journal of Innovative Research in Science, Engineering and Technology*, *04*(07), 5087–5095. https://doi.org/10.15680/IJIRSET.2015.0407008

Alkotami, L., & Kramer, K. (2023). *Mechanical properties of concrete with recycled plastic coarse aggregate partial replacement*. Kansas State University.

Allen, D. E. (1981). Limit States Design: What do we really want? *Canadian Journal of Civil Engineering*, *8*(1), 44–50.

Arafah, A. M. (2000). Factors affecting the reliability of reinforced concrete beams. In *Rish Analysis II* (pp. 379–387). C.A. Brebbia.

ASTM A370-22 Standard Test Methods and Definitions for Mechanical Testing of Steel Products. (2022). ASTM International. https://doi.org/10.1520/A0370-22

ASTM A615/A615M-22 Specification for Deformed and Plain Carbon-Steel Bars for Concrete Reinforcement. (2022). ASTM International. https://doi.org/10.1520/A0615_A0615M-22

ASTM C31/C31M-22 Standard Practice for Making and Curing Concrete Test Specimens in the Field. (2022). ASTM International. https://doi.org/10.1520/C0031_C0031M-22

ASTM C39/C39M-21 Standard Test Method for Compressive Strength of Cylindrical Concrete Specimens. (2021). ASTM International. https://doi.org/10.1520/C0039_C0039M-21

ASTM C78/C78M-22 Standard Test Method for Flexural Strength of Concrete (Using Simple Beam with Third-Point Loading). (2022). ASTM International. http://www.astm.org

ASTM C136/C136M-19 Standard Test Method for Sieve Analysis of Fine and Coarse Aggregates. (2019). ASTM International. https://doi.org/10.1520/C0136_C0136M-19

ASTM C143/C143M-15 Standard Test Method for Slump of Hydraulic-Cement Concrete. (2015). ASTM International. https://doi.org/10.1520/C0143_C0143M

ASTM C469/C469M-22 Standard Test Method for Static Modulus of Elasticity and Poissons Ratio of Concrete in Compression. (2022). ASTM International. https://doi.org/10.1520/C0469_C0469M-22

ASTM C496/C496M-17 Standard Test Method for Splitting Tensile Strength of Cylindrical Concrete Specimens. (2017). ASTM International. https://doi.org/10.1520/C0496_C0496M-17

Bischoff, P. H. (2005). Reevaluation of Deflection Prediction for Concrete Beams Reinforced with Steel and Fiber Reinforced Polymer Bars. *Journal of Structural Engineering*, *131*(5), 752–767. https://doi.org/10.1061/(ASCE)0733-9445(2005)131:5(752)

Bischoff, P. H., & Scanlon, A. (2007). Effective Moment of Inertia for Calculating Deflections of Concrete Members Containing Steel Reinforcement and Fiber-Reinforced Polymer Reinforcement. *ACI Structural Journal*, *104*(1), 68–75. https://doi.org/10.14359/18434

Branson, D. E. (1965). *Instantaneous and Time-Dependent Deflections of Simple and Continuous Reinforced Concrete Beams* (7; pp. 1–78). Alabama Highway Department, U.S. Bureau of Public Roads.

Branson, D. E., & Trost, H. (1982). Unified Procedures for Predicting the Defleciton and Centroidal Axis Location of Partially Cracked Nonprestressed and Prestressed Concrete Members. *ACI Journal*.

Costello, L., Kramer, K., & Loughmiller, K. (2021). *Extruded recycled plastic as a partial coarse aggregate in concrete*. Kansas State University.

Darwin, D., Dolan, C., & Nilson, A. (2015). *Design of Concrete Structures* (15th ed.). McGraw Hill.

De Bortoli, A. (2023). Understanding the environmental impacts of virgin aggregates: Critical literature review and primary comprehensive life cycle assessments. *Journal of Cleaner Production*, *415*. https://doi.org/10.1016/j.jclepro.2023.137629

Elwell, D. J., & Fu, G. (1995). *Compression Testing of Concrete Cylinders vs. Cubes* (FHWA/NY/SR-95/119). New York State Department of Transportation.

EN 12350-2:2019 Testing Fresh Concrete Part 2: Slump Test. (2019). The British Standards Institution.

EN 12390-5:2019 Testing Hardened Concrete Part 5: Flexural Strength of Test Specimens. (2019). The British Standards Institution.

EN 12390-6:2023 Testing Hardened Concrete Part 6: Tensile Splitting Strength of Test Specimens. (2023). The British Standards Institution.

Fakhruddin, Irmawaty, R., Djamaluddin, R., & Rudy, D. A. (2021). Flexural behavior of reinforced concrete beams using PET plastic as partial replacement of coarse aggregate.

IOP Conference Series: Earth and Environmental Science, *871*(1), 012021. https://doi.org/10.1088/1755-1315/871/1/012021

Ford, G. S., & Spiwak, L. J. (2017). The Economic Impact of the Natural Aggregates Industry: A National, State, and County Analysis. *Industry Scorecard*.

Ghaly, A. M., & Gill, S. (2004). Compression and Deformation Performance of Concrete Containing Postconsumer Plastics. *Journal of Materials in Civil Engineering*, 289–296. https://doi.org/10.1061/(ASCE)0899-1561(2004)16:4(289)

Growing global aggregates sustainably. (2021, December 8). Aggregates Business. https://www.aggbusiness.com/feature/growing-global-aggregates-sustainably

Gu, L., & Ozbakkaloglu, T. (2016). Use of recycled plastics in concrete: A critical review. *Waste Management*, *51*, 19–42. https://doi.org/10.1016/j.wasman.2016.03.005

Hashmath, & Meraj. (2015). Experimental study on untilization of waste plastic as aggregate in cement mortar. *International Journal of Engineering Sciences & Research Technology*.

Hognestad, E. (1951). *A Study of Combined Bending and Axial Load in Reinforced Concrete Members* (399; Bulletin Series). University of Illinois.

Hognestad, E. (1952). Fundamental Concepts in Ultimate Load Design of Reinforced Concrete Members. *ACI Journal Proceedings*, *48*(6). https://doi.org/10.14359/11956

Hognestad, E., Hanson, N. W., & McHenry, D. (1955). Concrete Stress Distribution in Ultimate Strength Design. *Journal of the American Concrete Institute*, *27*(4), 455–479.

IS 516-1959: Method of Tests for Strength of Concrete. (1959). Bureau of Indian Standards.

IS 1199-1959: Methods of sampling and analysis of concrete. (1959). Bureau of Indian Standards.

IS 5816-1999: Method of Test Splitting Tensile Strength of Concrete. (1999). Bureau of Indian Standards.

Islam, Md. J., & Shahjalal, Md. (2021). Effect of polypropylene plastic on concrete properties as a partial replacement of stone and brick aggregate. *Case Studies in Construction Materials*, *15*, e00627. https://doi.org/10.1016/j.cscm.2021.e00627

Kansas Department of Transportation Special Provision to the Standard Specifications (90P-266-R2). (1990).

Langer, W. H. (2002). *Managing and Protecting Aggregate Resources* (Open-File Report 02–415; Open-File Report). U.S. Geological Survey.

Manjunath, B. T. A. (2016). Partial Replacement of E-plastic Waste as Coarse-Aggregate in Concrete. *Procedia Environmental Sciences*, *35*, 731–739. https://doi.org/10.1016/j.proenv.2016.07.079

Motra, H. B., Hildebrand, J., & Dimmig-Osburg, A. (2014). Assessment of strain measurement techniques to characterise mechanical properties of structural steel. *Engineering Science and Technology, an International Journal*, *17*(4), 260–269. https://doi.org/10.1016/j.jestch.2014.07.006

Narayanan, S. (2024). Effect of Size and Shape of Test Specimen on Compressive Strength of Concrete. *Concrete International*, *46*, 45–51.

Nemati, M., Nematzadeh, M., & Rahimi, S. (2023). Effect of fresh concrete compression technique on pre- and post-heating compressive behavior of steel fiber-reinforced concrete: Experiments and RSM-based optimization. *Construction and Building Materials*, *400*, 132786. https://doi.org/10.1016/j.conbuildmat.2023.132786

Newman, J. B. (2003). Strength-testing machines for concrete. In *Advanced Concrete Technology* (pp. 1–11). Elsevier. https://doi.org/10.1016/B978-075065686-3/50265-2

O'Keane, T. (2022, May 11). *An eco-friendly alternative*. Waste Management Review. https://wastemanagementreview.com.au/an-eco-friendly-alternative/

Olanike, A. O. (2014). A Comparative Analysis of Modulus of Rupture and Splitting Tensile Strength of Recycled Aggregate Concrete. *American Journal of Engineering Research*, *7*.

Park, R. (2003). Concrete, Reinforced. In *Encyclopedia of Physical Science and Technology* (pp. 583–602). Elsevier. https://doi.org/10.1016/B0-12-227410-5/00134-4

Plastic by the Numbers. (2023, October 18). Plastic Action Centre. https://plasticactioncentre.ca/directory/plastic-by-the-numbers/

Plastic pollution is growing relentlessly as waste management and recycling fall short. (2022, February 22). OECD. https://www.oecd.org/environment/plastic-pollution-is-growing-relentlessly-as-waste-management-and-recycling-fall-short.htm

Plazrok Technology Manufactured Lightweight Composite Aggregates. (2024). Plazrok.Com. https://plazrok.com/

Radhi, M. M., Khalil, W. I., & Shafeeq, S. (2022). Flexural behavior of sustainable reinforced concrete beams containing HDPE plastic waste as coarse aggregate. *Cogent Engineering*, *9*(1), 2127470. https://doi.org/10.1080/23311916.2022.2127470

Rathi, P. J. (1964). *The Comparison of Working Stress Design, Ultimate Strength Design, and Limit Design Theories of Reinforced Concrete*. Virginia Polytechnic Institute.

Recommended Guide Specifications for Batching Equipment and Control Systems in Concrete Batch Plants (102–00; Version 2). (1977).

Resin Identification Codes: What are they? How can they help? (2021, March 10). Cambrian Packaging. https://cambrianpackaging.co.uk/what-are-resin-identification-codes/

Ritchie, H., Samborska, V., & Roser, M. (2023). Plastic Pollution. *Our World in Data*. https://ourworldindata.org/plastic-pollution

Saikia, N., & De Brito, J. (2012). Mechanical properties and abrasion behaviour of concrete containing shredded PET bottle waste as a partial substitution of natural aggregate. *Construction and Building Materials*, *52*, 236–244. https://doi.org/10.1016/j.conbuildmat.2013.11.049

Scanlon, A., & Bischoff, P. H. (2008). Shrinkage Restraint and Loading History Effects on Deflections of Flexural Members. *ACI Structural Journal*, *105*(4), 498–506. https://doi.org/10.14359/19864

Shanmugapriya, M., & Santhi, H. M. (2017). Strength and Chloride Permeable Properties of Concrete with High Density Polyethylene Wastes. *International Journal of Chemical Sciences*, *15*(1). www.tsijournals.com

Statista. (2021). *Annual production of plastics worldwide from 1950 to 2021*. Statista. https://www.statista.com/statistics/282732/global-production-of-plastics-since-1950/

Thermoplastics vs. Thermosetting | History of Plastic Recycling. (2023, May 9). Recycled Plastic. https://www.recycledplastic.com/thermoplastics-vs-thermosetting/

Ugural, A. C., & Fenster, S. K. (2003). *Advanced Strength and Applied Elasticity* (4th ed.). Prentice Hall.

United Nations. (2021, June). *In Images: Plastic is Forever*. United Nations; United Nations. https://www.un.org/en/exhibits/exhibit/in-images-plastic-forever

US EPA. (2023, April 21). *Plastics: Material-Specific Data*. United States Environmental Protection Agency. https://www.epa.gov/facts-and-figures-about-materials-waste-and-recycling/plastics-material-specific-data

Wang, Q., & Quayyum, S. (2023, April). Flexural Design of Reinforced Concrete Beam Sections. *Structure Magazine*. https://www.structuremag.org/?p=23409

Whitney, C. S. (1937). Design Of Reinforced Concrete Members Under Flexure Or Combined Flexure And Direct Compression. *ACI Journal Proceedings*, *33*(3), 483–498. https://doi.org/10.14359/8429

Appendix A - Batched Mixtures

Figure A.1: Control Batched Mix Desgin

MCM MIDWEST CONCRETE MATERIALS, INC.

701 S. 4th Street • P.O. Box 668 • Manhattan, KS 66502
(785) 776-8811 • FAX (785) 776-1816

MANHATTAN • WAMEGO • JUNCTION CITY • ABILENE • SALINA • TOLL FREE (800) 813-5195
LAWRENCE • PERRY • ATCHISON • TOLL FREE (888) 244-2082

"QUALITY AND SERVICE SINCE 1927"

PLANT	TIME	DATE	ACCOUNT	TRUCK	DRIVER	TICKET
06	12:00	03/02/23	KA1230	66	CHRIS WREN	6145037

CUSTOMER NAME	DELIVERY ADDRESS
K.S.U. CIVIL ENGINEERING	925 CARLSON DRIVE

PURCHASE ORDER	SALES ORDER	TAX	CREDIT			SLUMP
CHRIS JONES	613	54				4.00 in

LOAD QTY.	PRODUCT	DESCRIPTION	ORDERED	DELIVERED	UNIT PRICE	AMOUNT
1.00 yd	85531100	4000#	1.00 yd	1.00 yd		
1.00 yd	5000	Short Load Charge	1.00 yd	yd		

WINTER SERVICE

LOADED	ARRIVE JOB SITE	START DISCHARGE	FINISH DISCHARGE	ARRIVE PLANT
11:30				

INSTRUCTIONS
SOUTH OF MCCALL ROAD, ACROSS FROM MENARDS

SUB TOTAL
DISCOUNT
TAX
TOTAL
PREVIOUS TOTAL
GRAND TOTAL

This batch of concrete is mixed with the proper amount of water. If additional water is desired, please instruct the driver.

ADDITIONAL WATER ADDED ON JOB → **GALLONS** 1.5 By

CAUTION: Freshly mixed cement, mortar, grout or concrete may cause skin irritation. Avoid direct contact where possible and wash exposed skin areas promptly with water.

If any cementitious material gets into the eye, rinse immediately and repeatedly with water and get prompt medical attention.

KEEP OUT OF REACH OF CHILDREN

UNLOADING TIME ALLOWED 30 MINUTES PER TRIP
EXTRA CHARGE FOR OVER 30 MINUTES →

RECEIVED IN GOOD CONDITION

By

Purchaser waives all claims for personal or property damage caused by seller's truck when delivery is made beyond street curb line.

If not paid as agreed, this credit agreement provides for your payment of reasonable costs of collection, including, but not limited to, court costs, attorney fees and/or collection agency fees.

Truck	Driver	User	Disp Ticket Num	Ticket ID	Time	Date
66	030	user	6145037	27529	11:29	3/2/23

Load Size	Mix Code	Returned	Qty	Mix Age	Seq	Load ID
1.00 CYDS	85531100				D	27866

Material	Design Qty		Required	Batched		Var	% Var	% Moisture	Actual	Wat
ASHGROVE	564 lb		564 lb	590 lb	+	26	4.61%			
KPSAND	2054 lb		2105 lb	2120 lb		15	0.70%	2.50% M		6 gl
MQCA-5	1094 lb		1099 lb	1120 lb		21	1.87%	0.50% M		1 gl
WATER	30.4 gl		.0 gl	.0 gl		.0				
ADVA140	25.00 oz		25.00 oz	24.00 oz		-1.00	-4.00%			
HOTWATER	100.0 %	#	19.6 gl	18.0 gl		-1.6	-8.06%			18.0 gl

Actual Num Batches: 1

Load 3982 lb Design W/C: 0.449 Water/Cement: 0.429 T Design 30.4 gl Actual 24.9 gl To Add: 5.5 gl
Slump: 4.00 in Water in Truck: 0.0 gl Trim Water: -4.0 gl / CYDS Note: Manual feed occured
Actual W/C Ratio: 0.351 Actual Water: 25 gl Batched Cement: 590 lb Allowable Water: 57 lb

Figure A.2: 15 Percent Replacement Batched Mix Design

MCM | MIDWEST CONCRETE MATERIALS, INC.

701 S. 4th Street • P.O. Box 668 • Manhattan, KS 66502
(785) 776-8811 • FAX (785) 776-1816

MANHATTAN • WAMEGO • JUNCTION CITY • ABILENE • SALINA • TOLL FREE (800) 813-5195
LAWRENCE • PERRY • ATCHISON • TOLL FREE (888) 244-2082

"QUALITY AND SERVICE SINCE 1927"

PLANT	TIME	DATE	ACCOUNT	TRUCK	DRIVER	TICKET
06	15:21	03/06/23	KA1230	66	CHRIS WREN	6145093

CUSTOMER NAME	DELIVERY ADDRESS
K.S.U. CIVIL ENGINEERING	925 CARLSON ROAD 15% REDUCTION CA !!! CA-5 930LBS !!!

PURCHASE ORDER	SALES ORDER	TAX	CREDIT			SLUMP
CHRIS JONES	613	54				4.00 in

LOAD QTY.	PRODUCT	DESCRIPTION	ORDERED	DELIVERED	UNIT PRICE	AMOUNT
1.00 yd	85531100	4000#	1.00 yd	1.00 yd		
1.00 yd	5000	Short Load Charge	1.00 yd	yd		

WINTER SERVICE

LOADED	ARRIVE JOB SITE	START DISCHARGE	FINISH DISCHARGE	ARRIVE PLANT
14:53				

INSTRUCTIONS
SOUTH OF MENARDS

SUB TOTAL
DISCOUNT
TAX
TOTAL
PREVIOUS TOTAL
GRAND TOTAL

This batch of concrete is mixed with the proper amount of water. If additional water is desired, please instruct the driver.

ADDITIONAL WATER ADDED ON JOB → GALLONS 1,5 By

CAUTION: Freshly mixed cement, mortar, grout or concrete may cause skin irritation. Avoid direct contact where possible and wash exposed skin areas promptly with water.

If any cementitious material gets into the eye, rinse immediately and repeatedly with water and get prompt medical attention.

KEEP OUT OF REACH OF CHILDREN

UNLOADING TIME ALLOWED 30 MINUTES PER TRIP
EXTRA CHARGE FOR OVER 30 MINUTES →

RECEIVED IN GOOD CONDITION

By

Purchaser waives all claims for personal or property damage caused by seller's truck when delivery is made beyond street curb line.

If not paid as agreed, this credit agreement provides for your payment of reasonable costs of collection, including, but not limited to, court costs, attorney fees and/or collection agency fees.

Truck	Driver	User	Disp Ticket Num	Ticket ID	Time	Date
66	030	user	6145093	27583	14:51	3/6/23

Load Size	Mix Code	Returned	Qty	Mix Age	Seq	Load ID
1.00 CYDS	85531100				D	27922

Material	Design Qty		Required	Batched		Var	% Var	% Moisture	Actual	Wat
ASHGROVE	564 lb		564 lb	570 lb		6	1.06%			
KPSAND	2054 lb		2105 lb	2120 lb		15	0.70%	2.50% M		6 gl
MQCA-5	930 lb	#	935 lb	940 lb		5	0.57%	0.50% M		1 gl
WATER	30.4 gl		.0 gl	.0 gl		.0				
ADVA140	25.00 oz		25.00 oz	25.00 oz		.00	0.00%			
HOTWATER	100.0 %	#	18.7 gl	15.0 gl	-	-3.7	-19.69%			15.0 gl

Actual Num Batches: 1

Load 3757 lb Design W/C: 0.449 Water/Cement: 0.444 T Design 30.4 gl Actual 21.8 gl To Add: 8.6 gl
Slump: 4.00 in Water in Truck: 0.0 gl Trim Water: -5.0 gl / CYDS Note: Manual feed occured
Actual W/C Ratio: 0.318 Actual Water: 22 gl Batched Cement: 570 lb Allowable Water: 74 lb

Figure A.3: 30 Percent Replacement Batched Mix Design

MCM | MIDWEST CONCRETE MATERIALS, INC.

701 S. 4th Street • P.O. Box 668 • Manhattan, KS 66502
(785) 776-8811 • FAX (785) 776-1816

MANHATTAN • WAMEGO • JUNCTION CITY • ABILENE • SALINA • TOLL FREE (800) 813-5195
LAWRENCE • PERRY • ATCHISON • TOLL FREE (888) 244-2082

"QUALITY AND SERVICE SINCE 1927"

PLANT	TIME	DATE	ACCOUNT	TRUCK	DRIVER	TICKET
06	10:57	03/09/23	KA1230	67	STEPHEN STANHOPE III	6145159

CUSTOMER NAME	DELIVERY ADDRESS
K.S.U. CIVIL ENGINEERING	925 CARLSON ROAD 30% REDUCTION CA5 766?

PURCHASE ORDER	SALES ORDER	TAX	CREDIT			SLUMP
CHRIS JONES	606	54				4.00 in

LOAD QTY.	PRODUCT	DESCRIPTION	ORDERED	DELIVERED	UNIT PRICE	AMOUNT
1.00 yd	85531100	4000#	1.00 yd	1.00 yd		
1.00 yd	5000	Short Load Charge	1.00 yd	yd		

WINTER SERVICE

LOADED	ARRIVE JOB SITE	START DISCHARGE	FINISH DISCHARGE	ARRIVE PLANT
10:28				

INSTRUCTIONS
SOUTH OF MENARDS

SUB TOTAL
DISCOUNT
TAX
TOTAL
PREVIOUS TOTAL
GRAND TOTAL

This batch of concrete is mixed with the proper amount of water. If additional water is desired, please instruct the driver.

ADDITIONAL WATER ADDED ON JOB → GALLONS 1.5 By

CAUTION: Freshly mixed cement, mortar, grout or concrete may cause skin irritation. Avoid direct contact where possible and wash exposed skin areas promptly with water.

If any cementitious material gets into the eye, rinse immediately and repeatedly with water and get prompt medical attention.

KEEP OUT OF REACH OF CHILDREN

UNLOADING TIME ALLOWED 30 MINUTES PER TRIP
EXTRA CHARGE FOR OVER 30 MINUTES →

RECEIVED IN GOOD CONDITION

By

Purchaser waives all claims for personal or property damage caused by seller's truck when delivery is made beyond street curb line.

If not paid as agreed, this credit agreement provides for your payment of reasonable costs of collection, including, but not limited to, court costs, attorney fees and/or collection agency fees.

Truck	Driver	User	Disp Ticket Num	Ticket ID	Time	Date
67	197	user	6145159	27648	10:26	3/9/23

Load Size	Mix Code	Returned	Qty	Mix Age	Seq	Load ID
1.00 CYDS	85531100				D	27987

Material	Design Qty		Required	Batched		Var	% Var	% Moisture	Actual	Wat
ASHGROVE	564 lb		564 lb	560 lb		-4	-0.71%			
KPSAND	2054 lb		2105 lb	2140 lb		35	1.65%	2.50% M		6 gl
MQCA-5	1094 lb		1099 lb	760 lb	-	-339	-30.88%	0.50% M		gl
WATER	30.4 gl		.0 gl	.0 gl		.0				
ADVA140	25.00 oz		25.00 oz	24.00 oz		-1.00	-4.00%			
HOTWATER	100.0 %	#	18.6 gl	15.0 gl	-	-3.6	-19.26%			15.0 gl

Actual Num Batches: 1

Load 3587 lb Design W/C: 0.449 Water/Cement: 0.452 T Design 30.4 gl Actual 21.7 gl To Add: 8.7 gl
Slump: 4.00 in Water in Truck: 0.0 gl Trim Water: -5.0 gl / CYDS Note: Manual feed occured
Actual W/C Ratio: 0.323 Actual Water: 22 gl Batched Cement: 560 lb Allowable Water: 70 lb